Università degli Studi della Calabria

Department of Physics

Bernardino Telesio - Doctorate School of Science and Technique

A thesis submitted for the degree of Doctor of Philosophy in Science and Technology of Mesophases and Molecular Materials

M^3 – XXV Cycle

02/B1

Dielectric Characterization of Different Mesogenic Substances and a Mixture with Non-conventional Gold Nanoparticles

School Director
Prof. Roberto Bartolino

Supervisor
Prof. Nicola Scaramuzza

Curriculum Coordinator
Prof. Carlo Versace

Candidate
Lucia Marino

Academic Year: 2011 - 2012

Table of Contents

ACKNOWLEDGEMENTS

During the past years at the University of Calabria, I had the chance to meet lots of new and interesting people. All of them helped me in a certain way. Therefore, it is impossible to thank every single one personally, nevertheless, a few people deserve a personal thank you.

A special thanks goes to my supervisor, Professor Nicola Scaramuzza. He gave me the opportunity to join the Licryl Group at the University of Calabria. He was always available for scientific advise or help and encouragement. I also want to acknowledge Professors Andrei Ionescu, Carlo Versace, Daniela Pucci, Roberto Bartolino and Doctors: Emanuela Bruno, Maria Penelope De Santo, Federica Ciuchi, Alfredo Mazzulla, Krishna Koduru, Massimo Sposato, Alfredo Pane, Gaetano Nicastro, Giovanni Desiderio, and Salvatore Abate. I want to gratefully mention the collaboration with Prof. Petrov staff at the Bulgarian Institute of Science.

I am grateful to my colleagues and friends: Caterina, Angela, Melissa, Francesco, Alfonso, Claudia, Erminia, Roberta, Tania, Concetta, Rhida, Teresita, Giuseppe, Cristina, Andreea and Loris. Another word of gratitude surely goes to my special "web-friends". Special thanks are due to Ciccio Sciommarella for his kindness and sympathy.

Last but not least the better thank goes to my parents and to my brothers, Antonio, Davide and Salvatore. They gave me a lot of support and helped me to keep my motivation. This work of thesis is dedicated to them.

Lucia Marino
Rende, October 31, 2012

ABSTRACT

The study of liquid-crystalline matter and nano-structured materials is an important and vast field of research with potential implications in the development of new technologies, like sensors and displays. In this work we have analyzed and characterized different systems by dielectric spectroscopy.

The first part of this thesis is devoted to the characterization of an orthoconic liquid-crystalline mixture, W-129, with ferroelectric properties. The analysis of the dielectric response of this material has revealed a plurality of ferroelectric smectic C* subphases; they represent smectic intermediate variants situated between the ferroelectric phase and the antiferroelettric one, known like antiferrielectric phases (SmC_{FI}*, SmC_{FII}*, ...), whose study is still open and is collecting a lot of interest in academic environments.

The same liquid crystalline mixture was then doped with unconventional gold nanoparticles. These nanoparticles are functionalized with a hydrophilic polymer which becomes hydrophobic exceeded 40°C. The nano-composite material obtained by the dispersion of the gold nanoparticles presents interesting characteristics, such as an enhancement of dielectric increments (or strengths) probably due to the molecular interactions between the ferroelectric liquid crystal and the gold nanoparticles, which translates into an increase of the order of the liquid crystal host, in a stabilization of the smectic subphases and in an enhanced memory effect already seen in the pure liquid-crystalline mixture.

The third and last part is devoted to the characterization of a new "banana-shaped" liquid crystal, which exhibits some unusual physical properties during the nematic phase, in particular, the presence of regions of more ordered molecules, organized in a smectic C phase inside a nematic one. The dielectric spectra acquired during the nematic phase show the presence of a relaxation response between 10 and 20 Hz which, with the addition of relatively large values of permittivity, may suggest the presence of a ferroelectric response due to the existence of cybotactic clusters.

ABSTRACT

Lo studio della materia liquido-cristallina e dei materiali nano-strutturati rappresenta un importante e vasto campo di ricerca con probabili risvolti nello sviluppo di nuove tecnologie nell'ambito della sensoristica e dei display. In questo lavoro vengono analizzati e caratterizzati diversi sistemi tramite la spettroscopia dielettrica.

La prima parte di questa tesi è dedicata alla caratterizzazione di una mistura liquido-cristallina ortoconica W-129 con proprietà ferroelettriche. Dall'analisi della risposta dielettrica di questo materiale è emersa una pluralità di sottofasi della fase smettico C* ferroelettrica; esse rappresentano delle varianti smettiche intermedie tra la fase ferroelettrica e la antiferroelettrica, dette ferri-elettriche (SmC_{FI}*, SmC_{FII}*, …), il cui studio è tuttora aperto e riscuote un notevole interesse in ambito accademico.

La stessa mistura liquido-cristallina è stata poi dopata con nanoparticelle d'oro funzionalizzate con un polimero idrofilico che diventa idrofobico superati i 40°C. Il materiale nano-composito ottenuto dalla dispersione delle nanoparticelle d'oro presenta interessanti caratteristiche, quali un aumento dell'incremento dielettrico dovuto a interazioni molecolari tra il cristallo liquido ferroelettrico e le nanoparticelle d'oro che si traduce in un aumento dell'ordine del cristallo liquido ospitante, una stabilizzazione delle sottofasi smettiche e un aumento dell'effetto di memoria che era stato già riscontrato nella mistura liquido-cristallina ospitante.

La terza e ultima parte è dedicata alla caratterizzazione di un nuovo cristallo liquido "banana-shaped" che esibisce alcune proprietà fisiche inusuali durante la fase nematica, in particolare, la presenza di regioni di molecole ordinate in fase smettica C all'interno della fase nematica. Gli spettri dielettrici acquisiti durante la fase nematica mostrano la presenza di una risposta di rilassamento tra 10 e 20 Hz che, unita ai valori relativamente grandi della permittività, potrebbe suggerire la presenza di una risposta ferroelettrica dovuta all'esistenza di clusters cibotattici.

PREFACE

This thesis contains work carried out in the Licryl Laboratory, University of Calabria, during the period 2009 – 2012 under the supervision of Prof. Nicola Scaramuzza. During the Ph.D. course two papers have been published which are listed below with other two papers in preparation.
The two published papers are reported at page 121.

1. L. Marino, E. Bruno, M. P. De Santo, F. Ciuchi, S. Marino, N. Scaramuzza, Dielectric characterization of an orthoconic antiferroelectric liquid crystal mixture. Molecular Crystals and Liquid Crystals 04/2012; 558(1):120
2. L. Marino, A. Ionescu, S. Marino and N. Scaramuzza, Dielectric investigations on a bent-core liquid crystal. In print on Journal of Applied Physics, DOI: 10.1063/1.4767915
3. Evidence of a subphase in an antiferroelectric liquid crystal detected by means of dielectric spectroscopy. In preparation
4. Dielectric characterization of gold nanoparticles/antiferroelectric liquid crystal composites. In preparation

INTRODUCTION

Electric polarization has long been a subject of investigation. In fact as a natural phenomenon, electricity was known in ancient times, but it was not until the eighteenth century that the first experimental studies were undertaken, making it possible to establish a clear distinction between positive and negative electric charges and between conductors and insulators. It was discovered that large quantities of electric charge could be stored in a condensor, an apparatus consisting of two conducting plates separated by insulating materials. Relatively little attention was paid to the properties of the insulating material until 1837, when Faraday published the first numerical results of measurements on this material, which he called the dielectric. The results of Faraday's rather crude measurements indicated that the capacity of a condensor was dependent on the nature of the material separating the conducting surfaces. For the ratio between the capacity of a condensor filled with a dielectric and the capacity of the same condensor when empty, Faraday introduced the term *specific inductive capacity*. This quantity is now generally called the permittivity or the dielectric constant, and denoted by ε [1].

Liquid crystals are dielectrics, i.e. they have low electrical conductivity, but polarize in presence of an electric field $\boldsymbol{E}$. This means that the electric field induces an internal charge reorganization, or distortion, in the material, such a net polarization $\boldsymbol{P}$ appears. The relative dielectric permittivity (or dielectric constant) ε_r, known as a macroscopic material parameter, relates the known external field $\boldsymbol{E}$ to the macroscopic polarization resulting from different microscopic polarization mechanisms (modes) [2].

Dielectric relaxation spectroscopy is a powerful technique useful to study the molecular dynamics and molacular ordering in liquid crystals in general, and in the chiral smectic liquid crystals in particular. In the frequency range 10 Hz to 1 GHz, the technique has the ability to follow the reorientational dipolar motion of collective and non-collective modes. Both types of molecular processes, collective and non-collective (single molecular), exist in chiral and non-chiral phases. Detection of the collective processes in the non-chiral phases is beyond the resolution of the dielectric spectroscopy technique, so collective processes result only visible if we deal with chiral phases. These collective mechanisms, connected with the director fluctuation, are known as the soft mode and the Goldstone mode; the first process is linked to the tilt fluctuation of the director,

a mechanism usually observed in the kHz regime with a strong temperature dependence, the second is due to huge phase fluctuations – in other words the molecules collectively oscillate around the smectic cone in a way roughly similar to the motion of a snake rolling itself on a long tree – with a characteristic frequency which varies between 10 Hz to 1 kHz and with a weak temperature dependence. It is worth pointing out here that these two modes are thermally activated. Both of them can be measured in the planar orientation, i.e. with the smectic layers basically aligned perpendicular to the glass plates [3]. It is important to know that the liquid crystal cell is assumed to be like a condensor filled with a dielectric. The only request, when we are dealing with chiral smectic liquid crystal, is that the cell has to be of the order of the helical pitch because the surface interactions will suppress the helix in order to avoid cancellation of the polarization in the bulk of a sample due to the helical configuration. In this surface-stabilized geometry the helix is intrinsically absent, and such a sample therefore shows ferroelectric properties, i.e. in the absence of a field it will exhibit a non-zero macroscopic polarization which could be switched between two stable states. This can easily be verified since any ferroelectric sample will spontaneously form domains of polarization up and polarization down [2].

References

1. C. J. F. Böttcher, Theory of Electric Polarization, Volume 1, Elsevier Scientific Publishing Company, Amsterdam (1973)
2. J. P. F. Lagerwall, Phase Characterization of Polar Liquid Crystals using Dielectric Spectroscopy, Institutionen för mikroelektronik och nanovetenskap, Göteborg (2000)
3. F. M. Gouda, Dielectric Relaxation Spectroscopy of Chiral Smectic Liquid Crystals, Chalmers University of Technology, Göteborg (1992)

List of Figures

List of Tables

Chapter 1

Liquid Crystals

1.1 Liquid crystals: a brief history

Liquid crystals are partially ordered, anisotropic fluids, thermodynamically located between the three dimensionally ordered solid state crystal and the isotropic liquid.

The history of liquid crystals (LCs) began in the mid-nineteenth century, when several European scientists observed unusual behaviour while passing polarized light through liquid-like biological materials [1]. Rudolph Virchow, C. Mettenheimer, and G. Valentin were among the first that observed LC properties. They reported interesting anisotropic fluid behaviours in some biological materials; however, none of them realized that they were actually observing a different phase of matter [2]. The earliest, but still useful tools for the characterization of LCs, the polarizing microscope and heat stage, were first used by Otto Lehmann [2] to study these strange transitions. In 1888, Friedrich Reinitzer (credited as the discoverer of LCs) working with cholesteryl benzoate, observed two melting points and similar interactions with polarized light as observed by others [2]. This and his later works, generated a larger interest into the study of materials which would later be referred to as LCs. Using his polarizing microscope, Otto Lehmann became a leading figure in the study of these new materials and was the first to label them as “Liquid Crystals” [2]. In 1922, Georges Freidel established much of the nomenclature such as nematic, smectic, and cholesteric, which are still used today [2]. Since these early days, the interest in LCs has exploded on both experimental and theoretical fronts. While the experimental side has been motivated by the characterization and discovery of new phases and materials, the theoretical side has attempted to understand the connection between the basic molecular interactions and the resulting phase structures and macroscopic properties.

1.2 Liquid crystal phases

When a crystal is melted, in most cases, it becomes an isotropic liquid in which no preferential orientation or long range positional order can be distinguished. But for some substances a number of extra phases occur between solid and liquid. A crystal has positional order (meaning there is a regular "grid" on which all molecules reside) and orientational order (if there is a shape asymmetry in the molecule, then they are all directed the same way), whereas a liquid has neither forms of order.
Some compounds do not lose their order completely at the melting temperature. For example, in liquid crystals the long range positional order disappears: molecules remain oriented the same way, but are (more or less) randomly distributed throughout the space. Of course this simple picture of a liquid crystal needs to be refined and extended to account for the tens of different liquid crystalline phases that have been discovered during the twentieth century; all of them with different combinations of orientational and positional order [3].
A general classification of liquid crystal phases is known:

Lyotropic liquid crystals. Here molecules are mixed with a solvent. Apart from the temperature, the concentration is the important parameter. A typical example is a surfactant mixed in a polar solvent like water. Such a surfactant has a polar head and an apolar tail (or more than one head or tail). The heads mix with the water, but the tails do not and stick together.
This way micelles can be formed, droplets of surfactants with the polar heads directed outwards and the tails inside. At higher concentrations cylindrical or layered structures can be formed. [2].

Thermotropic liquid crystals. Here the pure compound forms the liquid crystalline phases, due to a pronounced shape asymmetry. Based on this asymmetry a further division is often made in
- calamitic liquid crystals, where the molecule has a rod-like shape;
- discotic liquid crystals, where the molecule has the shape of disc.
- bent or banana shaped liquid crystals (Paragraph 1.7 will be devoted to a description of this kind of mesogen molecules).

Apart from this mainly shape-based classification, another parameter is important for the liquid crystalline behaviour. Some molecules do not have mirror symmetry: the mirror image cannot be translated or rotated onto the

original molecule. This property, called chirality, gives in a number of liquid crystalline phases rise to supramolecular structures, for example helices.

For their potential implications in the development of new technologies due to the presence of ferroelectric properties, results on bent-core liquid crystals and on chiral smectic liquid crystals will be discussed in this work of thesis.

1.3 The nematic phase

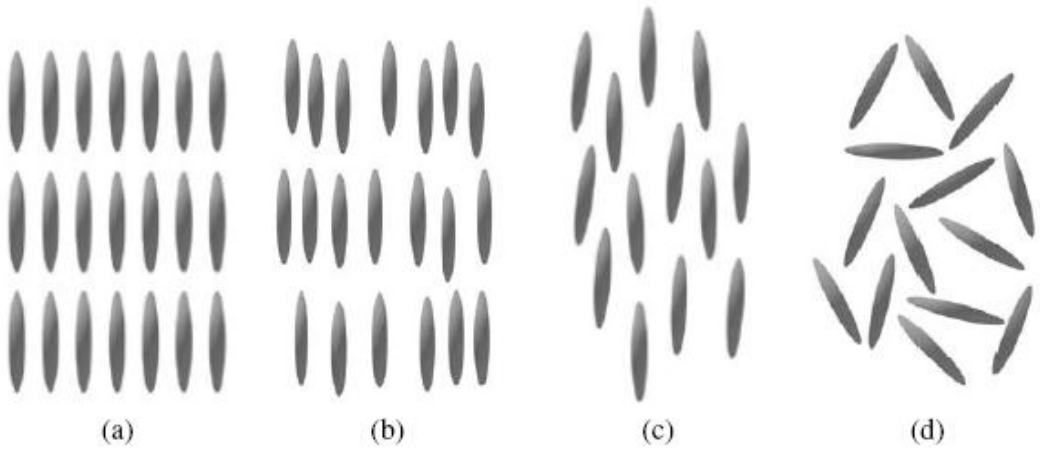

Figure 1.1: Some common liquid crystalline phases, in order of increasing temperature. (a) Crystal phase; (b) Smectic A phase; (c) Nematic phase; (d) Isotropic phase.

The nematic phase (N) is about the most common liquid crystalline phase. In this case, positional order is totally absent: the molecules are free to flow and their center of mass positions are randomly distributed as in a liquid. Yet long-range orientational order is still present: the long axes of the molecules are on average all parallel to an axis called the director **n**.
The ordered structure of a liquid crystalline phase is described by an order parameter. For the nematic phase the choice is simple: the order can be quantified as the deviation of the molecules from the director. If ϑ is the angle between the director **n** and the long axis of the molecule, the nematic order parameter S can be defined as:

$$S = \frac{1}{2}\left\langle 3\cos^2 \vartheta - 1 \right\rangle \tag{1.1}$$

where $\langle\ \rangle$ denotes an averaging over the ensemble of molecules [3].

1.4 The smectic phase

The smectic phase is the generic term for a whole class of phases. Their common property is the presence of a layered structure. The differences are the structure inside the layers and the correlation between the layers. Smectic phases are distinguished by letters (A, B, C,…) and until today 12 different variations have been identified [4].

The smectic A phase consists of layers of liquid crystal molecules, but inside the layers there is only orientational order. One can look at the SmA phase as stacking of layers of a two dimensional oriented liquid or as the nematic phase with layered order. However the ordering is strong enough to give rise to Bragg reflections in X-rays. Since there are two types of order present, one-dimensional positional order and orientational order, the smectic order parameter should have two components: u that denotes the displacement of the layers from their equilibrium position and k_0 that indicates the wave number of the density wave. The order parameter is then given by [4]:

$$\psi = |\psi| e^{ik_0 u}. \tag{1.2}$$

1.5 The cholesteric or chiral nematic phase

The cholesteric phase is the equivalent of the nematic phase for chiral molecules (i.e. they lack mirror simmetry), and it was first observed in the liquid crystalline derivatives of cholesterol. The local molecular ordering is that of the nematic structure, but the important difference is that the director is not a constant vector, but rotates in a direction perpendicular to the long axes of the molecules. This means that a helical structure is formed, and one introduces the pitch of the cholesteric phase as half of the length of this helix. It is half of the length because it does not matter in which direction the director points out of two opposite ones. Thus after half a rotation of the helix, the situation is physically the same. Typical lengths of the pitches range from a few hundred nm to infinity for an ordinary nematic phase. The structure of this phase is depicted in figure 1.2. The main consequence of this helical structure is the strong influence on the polarization of the light that passes through it. A property that made this chiral nematic systems useful for display applications.

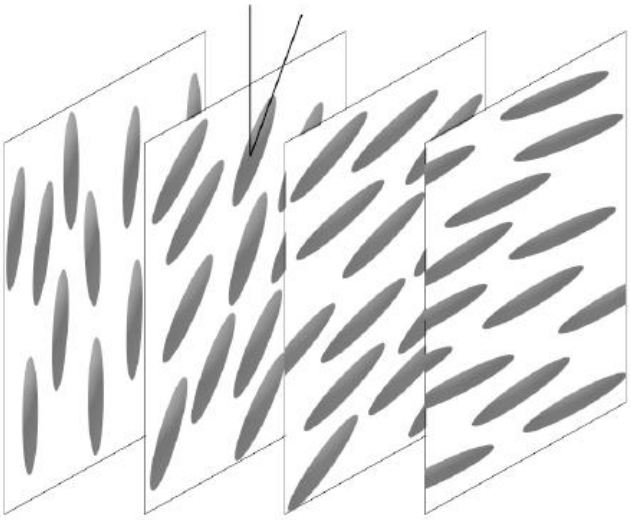

Figure 1.2: The structure of the chiral nematic phase with the rotating director. Over this four pictures the director rotates over 90°.

1.6 Chiral smectic liquid crystals

When liquid crystal molecules are chiral, the macroscopic behaviour of the phase could radically change. Such a phase is therefore differentiated from the achiral one by adding a star after the letter, for example SmC*, SmA*, etc. The molecular arrangement of the chiral phase may be completely similar to the achiral version (as in SmA and SmA*) or distinctly different (as in SmC and SmC*), but the physical properties of the chiral phases are always different from those of the achiral ones [5].

1.6.1 The SmC phase*

The SmC* phase is a tilted phase, in fact all molecules are inclined of an average temperature dependent angle θ (called the tilt-angle) relative to the layer normal. However, the star in the name indicates that the molecules (or at least some of them) are chiral. In general, this phase will also tend to form a macroscopic helical structure. As a helix within the layer plane is incompatible with a layered structure[1], the helix axis must be oriented along the layer normal. The variable that changes along the helix axis is the phase-angle (often denoted φ), *i.e.* the angle describing the direction towards which the molecules in a specific layer tilt (see Figure 1.3). Instead of the phase-angle (or azimuthal

[1] An in-layer helix would break the layers, and therefore such a helix-structure is incompatible with the layered structure.

angle as it is also called) one sometimes prefers to speak of the c-director, which is simply the projection of the director onto the layer plane.

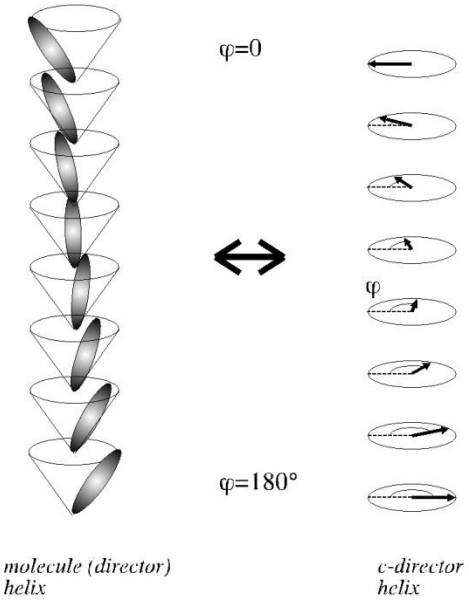

Figure 1.3: The chiral smectic C* phase features a helical director configuration, where the helix axis is parallel to the layer normal. The tilt-angle is constant throughout the sample, but the phase-angle changes continuously from layer to layer. Sometimes one prefers to describe the SmC* structure using the concept of the c-director, which is simply the projection of the director onto the layer plane (right part).

The periodicity of the helix, called the pitch, often increases with increasing temperature, but the variation might be very complex and varies from compound to compound. In some materials there is even a helix inversion, meaning that the pitch first increases to infinity and then decreases, within the SmC* phase. A helix inversion is easily observed by looking at a quasi-homeotropic sample through a polarizing microscope. In the vicinity of the inversion temperature the texture becomes very unstable and a large schlieren constantly appears and disappears. If one studies the optical rotation on different sides of the helix inversion one will also see that the sign has changed, reflecting the change of helix handedness [5].

The helical structure gives the material interesting optical properties. First of all, the medium gets an unusually strong optical activity, i.e. it will strongly rotate the polarization plane of linearly polarized light passing through the medium along the helix axis. Secondly, one may see selective reflections in a quasi-homeotropically aligned sample; circularly polarized light with a wavelength equal to the pitch of the helix, and with the same handedness as the helix, cannot propagate through the medium but will be completely reflected

(Bragg-reflected).
One of the most interesting properties of the SmC* phase is that its symmetry permits the presence of a spontaneous polarization P_s, within the layer plane and perpendicular to the director [6]. However, because of the steric coupling between the director and P_s, the helical director configuration will lead to a cancellation of polarization in bulk samples, but in specific geometries the helix may be suppressed and then the SmC* liquid crystal will exhibit a macroscopic spontaneous polarization which may be switched between two stable states [7]. It thus fulfils the requirements to be called ferroelectric, and this is extremely interesting for numerous applications.

1.6.2 The smCa phase*

During the latter part of the 1970's and throughout the 1980's, reports on a new chiral tilted smectic phase, with unusual behaviour became more and more common [8]. It was not until 1989 ([9] and [10]) that it was made totally clear that the new phase was an antiferroelectric liquid crystal, called SmC_a*. It is clear from the name that the phase can be regarded as a subphase of SmC*. It is a chiral tilted smectic phase with no in-plane ordering and it also features the helical arrangement of the molecules described above, and this leads to similar optical effects. The important difference is that the SmC_a* phase is anticlinic as opposed to the SmC* phase which is synclinic. This particular structure gives to the phase antiferroelectric properties.
The index in a SmC_a* is often taken to be short for antiferroelectric, which was perfectly adequate in the beginning when only chiral SmC_a* compounds existed. However, in the last few years several examples of achiral SmC_a liquid crystals have been reported [7] and these cannot be antiferroelectric. A better interpretation of the subscript is therefore "a stands for anticlinic" or "a stands for alternating tilt", since these two properties are common to both the chiral and achiral versions of the phase.

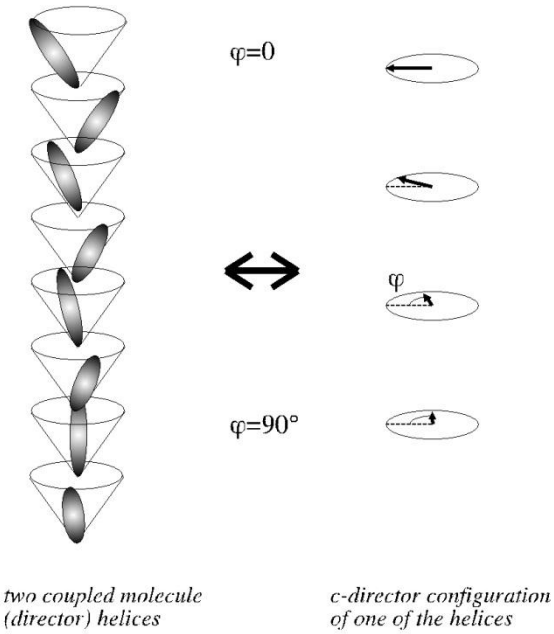

Figure 1.4: The chiral smectic C_a* phase features a combination of an anticlinic structure and a helical director configuration. Such a structure can be obtained by coupling two helices, with a fix phase-angle difference of slightly more than 180° (it cannot be exactly 180° since the phase-angle shift on going between two neighboring layers should be constant).

1.6.3 SmC subphases: SmC_α*, $SmC_{1/3}$* (= SmC_γ*) and $SmC_{1/4}$**

After recognition of the anticlinic order it became obvious that SmC* liquid crystals could have not only synclinic and anticlinic structures, but also intermediates. In one of the first antiferroelectric compounds properly characterized, MHPOBC, observations indicated a subphase called SmCα*, situated between the SmA* and the SmC* phases, and another subphase called SmCγ* (also known like SmC F_{I1}* or $SmC_{1/3}$*) between the SmC* and SmCa* [11]. Later, several other subphases have been reported, but it is doubtful whether all observations really correspond to new thermodynamically stable phases or to other effects such as helix inversions or surface-induced effects. At present, five different chiral tilted smectic phases without in-plane positional order (i.e. of the chiral smectic C family, or smectic C* family for short), including the SmC* and SmCa*, have been experimentally confirmed by resonant X-ray scattering [12].

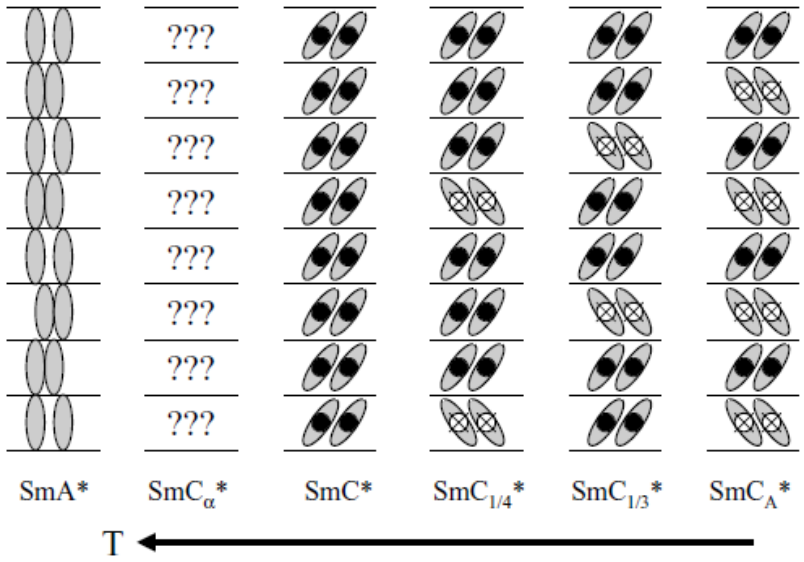

Figure 1.5: Schematic overview of the non-helical local model structures of the chiral fluid smectic phases.

This family of liquid crystal phases is important both for theoretical reasons (the phases show ferroelectric, antiferroelectric, and ferrielectriclike properties without long-range order) and also experimentally in fact if commercially viable compounds and mixtures can be developed then the subsequent new materials could potentially provide a significant leap forward in the functionality of the now ubiquitous liquid crystal display.

The different smectic liquid crystal phases are each composed of similar layered arrangements of molecules, with fluidlike ordering in the plane of the layer. Each variant phase is distinguished by the orientation of the molecules within a certain layer with respect to that in the adjacent layers. One can describe the structure of each Sm*C** subphase by the use of the diagrams presented in Fig. 1.6. A single molecule can be represented as lying on the side of an imaginary cone (Fig. 1.6 (e)), the axis of the cone being parallel to the layer normal $\hat{n}$. The azimuthal angle φ changes differently from layer to layer in each phase and this is illustrated in Figs. 1.6 (a) – 1.6 (d). Notice how in addition to the layer to layer changes there is also an overall precession in φ due to the chirality of the phase. This slow precession gives rise to the macroscopic pitch of the material. Experiments have shown that the Sm*C*FI1* (SmC_γ* or SmC$_{1/3}$*) phase is a chiral liquid crystal phase with a three-layer clock structure, while the Sm*C*FI2* phase exhibits a four-layer clock structure [12].

Because these two subphases appear between SmC* and SmCa* in compounds exhibiting the full AFLC phase sequence, it was natural to assume that they in some way are intermediate between synclinic and anticlinic (or between ferroelectric and antiferroelectric) organization [13]. Since there is no simple intermediate structure between synclinicity and anticlinicity this would give the phases a frustrated character.

The last type of chiral smectic-C phase which with certainty has been identified is the SmC_α* phase (incommensurate varying from three to eight layers), which essentially is an extreme short-pitch version of SmC*. Although the properties of the different phases in the family can differ quite drastically, in particular regarding their polar nature and the dimensions and handedness of their helical superstructures, the enthalpies of the first-order transitions between these phases are extremely small, suggesting that the structural changes taking place are very subtle. The different types of correlation in tilting directions across smectic layer boundaries which distinguish the phases from each other are not yet fully understood [14].

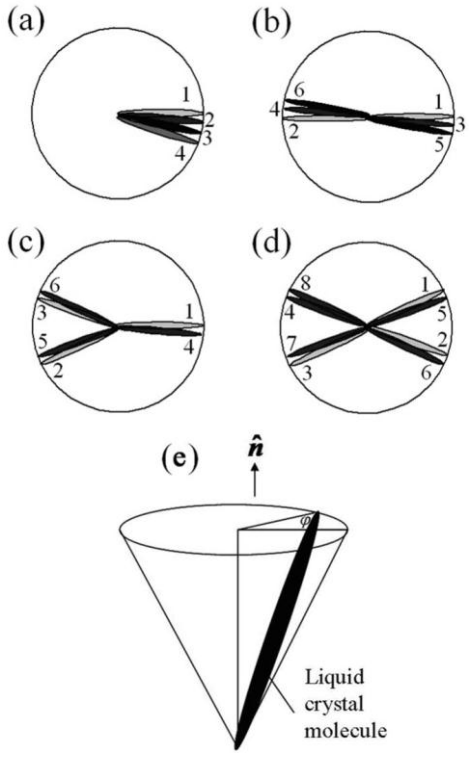

Figure 1.6: Cartoon illustrating the periodic clock structures of the (a) Sm*C**, (b) Sm*Ca**, (c) Sm*C*FI1*, (d) Sm*C*FI2* phases and (e) a schematic showing the geometry of a single liquid crystal molecule.

1.7 Bent Core liquid crystals

It is known that not only rod-shape (calamitic) or discotic mesogens can form liquid crystals, but bent-core (bow-like or banana-shape) mesogens do, too [15] Although the first synthesis of bent-core liquid crystals (BCLC) was reported more than sixty years ago by Vorländer [16], they have not attracted much interest until the synthetic work of Matsunaga et al.[15] in the early 1990s.

The discovery of the interesting properties of these mesogens has opened up a major new and exciting dimension in the science of thermotropic LCs. Seminal findings, having broad implications for the general field of soft matter physics including the observations of ferroelectricity and spontaneous breaking of chiral symmetry in smectic phases composed of achiral mesogens [17]. In the following sections, we will discuss the microscopic structures and interactions between bent-core mesogens.

As for the classical mesogens, the bent-core mesogens consist of a rigid, highly conjugated core, and flexible hydrocarbon tails. Bent-core mesogens are typically composed of five aromatic rings with a meta-substituted central ring, various side linkages to the core, and terminal chains at one or both ends. The meta-substitution of the central ring gives an opening angle (bending angle) of approximately 120° and typically they are about 5 nm long and 0.5 nm wide. These mesogens may be symmetric or asymmetric, and the linkages between the aromatic rings may vary in position and size [18].

One of the major interactions between the bent-core mesogens is their steric close packing, which attempts to fill the space as effectively as possible. This steric requirement when coupled to the bent-shape of the mesogens immediately implies two important features. When translating a bent-core mesogen in the “sea” of the other mesogens, it experiences a periodic interaction due to their molecular kink. This results in a translational symmetry breaking along the long axis of the mesogens (the average direction connecting to the ends of the mesogens) forming temporary smectic-like aggregates. In the case of the nematic phase, this suggests that nematic order is only valid at length scales much larger than these clusters as illustrated in Figure 1.7 [18]. The other important feature resulting from close packing is the formation of polar order along the kink direction. Provided that the mesogens have a dipole moment along this direction, then this polar order results in the formation of a spontaneous polarization which is inherently different from that of the SmC* phase where molecular chirality must be coupled to the director tilt as first shown by R.B. Meyer [19].

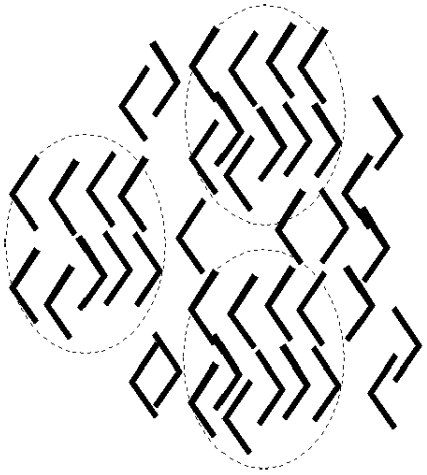

Figure 1.7: Sketch of hypothetical nematic phase of bent-core mesogens.

This effect is best illustrated in the SmAP phase (Figure 1.8) which is a non-tilted smectic phase with a spontaneous polarization which has only been observed in bent-core LCs [18].

Due to the previously described shape and close packing requirements of bent-core mesogens, it is convenient to define three orthogonal unit vectors $\hat{n}$, $\hat{m}$, and $\hat{p}$.

The vector $\hat{n}$ is the unit vector along the long axis (the director), $\hat{m}$ is normal to the molecular plane, and $\hat{p}$ is along the kink direction which is parallel to the polarization $\vec{P}$.

Figure 1.8 shows the situations when $\hat{n}$ is parallel to the smectic layer normal $\hat{k}$.

This is similar to the SmA phase of calamitic liquid crystals, except that now the layers are polar. This difference is designated by adding the letter P (for polar) to SmA. In this case one can have two distinct situations, the layer polarization $\vec{P}$ can be either parallel or antiparallel in the subsequent layers corresponding to ferroelectric (SmAPS) or antiferroelectric (SmAPA) subphases [17].

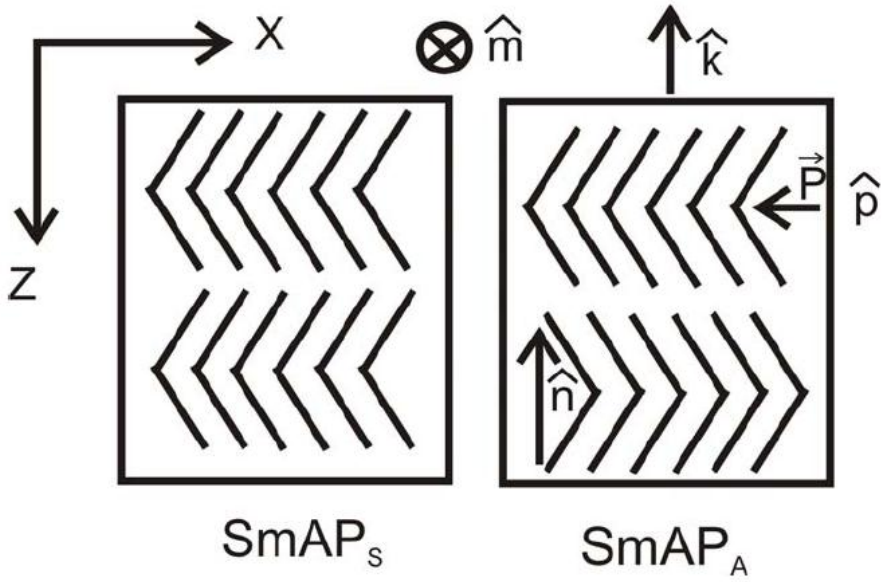

Figure 1.8: Schematic structure of the ferroelectric SmAPS and the antiferroelectric SmAPA phases.

Here we denote the same polarization directions by the subscript S for synchronous and the alternating directions by the subscript A.

The situations when the molecular planes are tilted with respect to the layer normal, i.e., when $\hat{m}$ is not perpendicular to $\hat{k}$, are shown in the upper row of Figure 1.9. In this figure, we show the plane determined by the polarization $\vec{P}$ and the layer normal $\hat{k}$ (polar plane), in which case the tilt is illustrated by a bar that is stuck on the end of the mesogen which is closest to the observer. Depending on whether the tilt directions between subsequent layers are parallel or antiparallel, one can describe them as being synclinic and anticlinic, respectively. By using the same nomenclature for the SmAP phases we can define two more subscripts to describe the tilt between layers the synclinic (S) or anticlinic (A) configurations.

Combining these tilt descriptions with the ferroelectric and antiferroelectric packing configurations discussed earlier, we can arrive at the following four subphases: SmCSPS, SmCAPA, SmCSPA and SmCAPS. Such a notation with some variations was introduced by Link et. al.[20] and is widely used in the literature.

In principle, we can also envision that only the director $\hat{n}$ and $\hat{p}$ are tilted (or leaning) with respect to the layer normal $\hat{k}$. Similarly, the successive smectic

layers can be either ferroelectric (with the same direction of polar order) or antiferroelectric (with opposite directions). Likewise, successive layers can be either synclinic (with the same direction of molecular tilt) or anticlinic (with opposite tilt directions). Those situations are illustrated in the bottom row of Figure 1.9. To distinguish from the tilt of the molecular plane (which is denoted by the symbol C to express "clinic"), the tilt of the long axis will be called "leaning" and will be labeled with L. Just as in the SmCP cases, there exists four distinct sub-phases SmLSPA , SmLAPS , SmLAPA and SmLSPS depending on the subsequent tilt and polarization direction combinations.

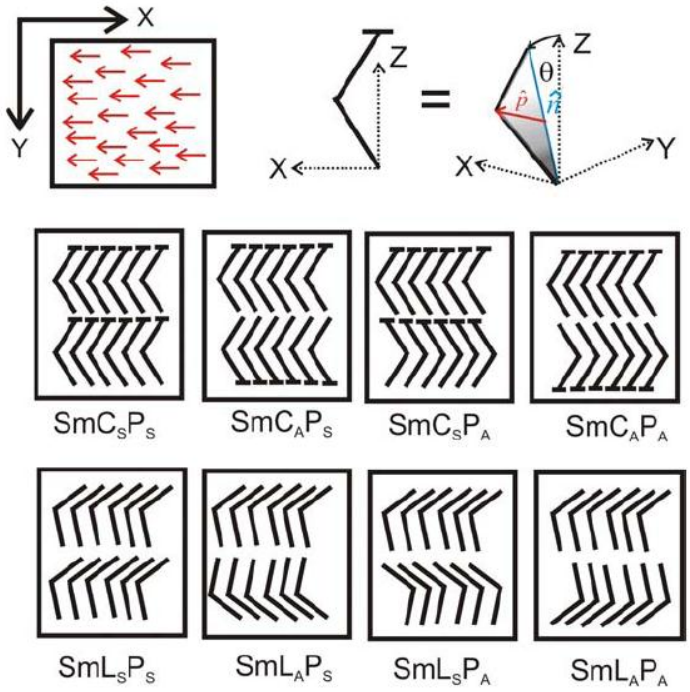

Figure 1.9: The possible single tilted bent-core smectic structures. Top row: Illustration of the fluid in plane order of the layer polarization, and three dimensional explanation of tilt. Middle row: two dimensional illustration of the four possible situations when only the molecular plane is tilted with respect to the layer normal; Bottom row: two dimensional illustration of the four possible situations when only the long axis is tilted (leaned) with respect to the layer normal.

While the proposed structures in this section are not the only possible phases which are allowed by symmetry, they coincide well with most of the experimentally observed phases. Many of the observations of the smectic and columnar phases of bent-core liquid crystal phases were pioneered by groups in Tokyo [21], Boulder [22], Berlin [23], Halle [24], Budapest [25], and several other places [26, 27]. In the last several years the research has quickly

broadened with very intensive experimental studies carried out all around the world. Activities of this field have been recently reviewed in several papers [27].

In the first few years of experimental studies seven different bent-core liquid crystal textures were documented and labeled as B1,…, B7 according to the chronological order of their observations [28]. The list of these phases, based on textural observations and X-ray measurements, are summarized in Table 1.1.

Table 1.1: List of several observed bent core liquid crystals.

Name	**Structure**	**Polarity**	**Director tilt**
B_1	Columnar	non-polar	non- tilted
B_2 (SmCP)	smectic with no in-layer order	polar	Tilted
B_3 (SmIP)	smectic with hexagonal in-layer order	Polar?	Tilted
B_4	optically active solid	Polar?	non-tilted
B_5	highly viscous SmCP	polar	Tilted
B_6	interdigitated layers	non-polar	non-tilted
B_7	Columnar	polar	Tilted
$B_{7'}$	modulated layer structure SmCP or SmCG	polar	Tilted

References

1. P.J. Collings and M. Hird, Introduction to Liquid Crystals, Taylor & Francis, (1997)

2. P.J. Collings, Liquid Crystals: Nature's Delicate State of Matter, Princeton University Press, (1990)

3. P.G. De Gennes and J. Prost, The Physics of Liquid Crystals, 2nd Ed., Oxford University Press, Oxford, New York, (1993)

4. A. Jakli and A. Saupe, One- and Two-Dimensional Fluids; Properties of Smectic, Lamellar, and Columnar Liquid Crystals, Taylor and Francis, Boca Raton, FL, (2006)

5. J. P. F. Lagerwall, Phase Characterization of Polar Liquid Crystals using Dielectric Spectroscopy, Institutionen för mikroelektronik och nanovetenskap, Göteborg, (2000)

6. R. B. Meyer, L. Liebert, L. Strzelecki, P. Keller, J. Physique Lett., 36, pp. L69-71 (1975)

7. N. A. Clark, S. T. Lagerwall, Appl. Phys. Lett., 36, 11, pp. 899-901 (1980)

8. S. T. Lagerwall, "Ferroelectric and Antiferroelectric Liquid Crystals", Wiley-VCH, (1999)

9.Y. Galerne, L. Liebert, Oral Presentation at the FLC'89 conference, Göteborg, Sweden (1989)

10. H. Takezoe, A. D. L. Chandani, J. Lee, E. Gorecka, Y. Ouchi, A. Fukuda, Oral Presentation at the FLC'89 conference, Göteborg, Sweden (1989)

11. K. Hiraoka, A. Taguchi, Y. Ouchi, H. Takezoe, A. Fukuda, Jpn. J. Appl. Phys., 29,1, pp. L103-106 (1990)

12. P. Mach, R. Pindak, A.-M. Levelut, P. Baroit, H. T. Nguyen, H. Baltes, M. Hird, K. Toyne, A. Seed, J. W. Goodby, C. C. Huang, L. Furenlid, Phys. Rev. E, 60, 6, pp. 6793-6802 (1999); L.S. Hirst, S.J. Watson, H.F. Gleeson, P. Cluzeau, P. Barois, R. Pindak, J. Pitney, A. Cady, A.M. Levelut, P.M. Johnson,

C.C. Huang, G. Srajer, J. Pollmann, W. Caliebe, A. Seed, M.R. Herbert, J.W. Goodby, M. Hird, Phys. Rev. E 65 (2003) 041705 (1)

13. E. Gorecka, A. D. L. Chandani, Y. Ouchi, H. Takezoe, and A. Fukuda, Jpn. J. Appl. Phys., Part 1 29, 131 s1990d

14. J. Kirchhoff and L. S. Hirst, Phys. Rev. E 76, 051704 (2007)

15. Y. Matsunaga, S. Miyamoto, Mol. Cryst. Liq. Cryst., 237, 311-317, (1993); H. Matsuzaki, Y. Matsunaga, Liq. Cryst., 14, 105-120, (1993)

16. D . Vorländer, A. Apel, "Die Richtung der Kohlenstoff-Valenzen in Benzolabkömmlingen (II.)." Berichte der Deutschen Chemischen Gesellschaft, 1101 - 1109 (1932)

17. T. Niori, T. Sekine, J. Watanabe, T. Furukawa, H. Takezoe, , J. Mater. Chem. 6(7), 1231-1233, (1996); T. Sekine, T. Niori, M. Sone, J. Watanabe, S.W. Choi, Y. Takanishi, H. Takezoe, Jpn. J. Appl. Phys., 36, 6455 (1997); D.R. Link, G. Natale, R. Shao, J.E. Maclennan, N.A. Clark, E. Körblova, D.M. Walba, Science 278, 1924-1927 (1997)

18. C.A. Bailey, Structure and Rheology of Some Bent Core Liquid Crystals, Kent State University (2008)

19. R.B. Meyer, L. Liebert, L. Strzelecki, P. Keller, J. Phys. (France) 36, L69-L74 (1975)

20. D.R. Link, G. Natale, R. Shao, J.E. Maclennan, N.A. Clark, E. Körblova, D.M. Walba, Science 278, 1924-1927 (1997)

21. Niori, T., Sekine, T., Watanabe, J., Furukawa, T., Takezoe, H., J. Mater. Chem. 6(7), 1231-1233, (1996); Sekine, T., Niori, T., Sone, M., Watanabe, J., Choi, S.W., Takanishi, Y., Takezoe, H., Jpn. J. Appl. Phys., 36, 6455 (1997)

22. G. Heppke, A. Jákli, D. Krüerke, C. Löhning, D. Lötzsch, S. Paus, R. Rauch, K. Sharma, ECLC'97 Abstract book, 34 (1997); Macdonald, R., Kentischer, F., Warnick, P., Heppke, G., Phys. Rev. Lett., 81, 4408 (1998)

23. Weissflog, W., Lischka, C., Scharf, T, Pelzl, G, Diele, S., Kurth, H., Proc. Spie: Int. Soc. Opt. Eng., 3319, 14 (1998), Diele, S., Grande, S., Kurth, H., Lischka, C., Pelzl, G., Weissflog, W., Wirth, I., Ferroelectrics, 212, 169 (1998); Pelzl, G., Diele, S., Grande, S., Jákli, A., Lischka, C., Kresse, H., Schmalfuss,

H., Wirth, I., Weissflog, W., Liq. Cryst., 26, 401 (1999) ; G. Pelzl, S. Diele, A. Jákli, CH. Lischka, I. Wirth, W. Weissflog, Liquid Crystals, 26, 135-139 (1999)

24. A. Jákli, S. Rauch, D. Lötzsch and G. Heppke, Phys. Rev. E, 57, 6737-6740 (1998), A. Jákli, Ch. Lischka, W. Weissflog, S. Rauch, G. Heppke, Mol. Cryst. Liq. Cryst, 328, 299-307 (1999)

25. H.R. Brand, P.E. Cladis, H. Pleiner, Eur. Phys. J. B, 6, 347 (1998); P.E. Cladis, H.R. Brand, H. Pleiner, Liquid Crystals Today, 9, 1 (1999)

26. Nguyen, H.T., Rouillon, J.C., Marcerou, J.P., Bedel, J.P., Barois, P., Sarmento, S., Mol. Cryst. Liq. Cryst., 328, 177 (1999)

27. R. Amaranatha Reddy, C. Tschierske, J. Mater. Chem. (2006); preprint DOI: 10.1039/b504400f; M.B. Ros, J.L. Serrano, M. R. de la Fuente, C. L. Folcia, J. Mater. Chem., 15, 5093 (2005)

28. G. Pelzl, S. Diele, W. Weissflog, Adv. Mater., 11, 707-724 (1999)

Chapter 2

Dielectric Spectroscopy

2.1 Introduction

Dielectric spectroscopy (DS) is a robust and versatile measurement technique with numerous applications in fundamental science and engineering field. The principle which is the basis of this measurement technique (DS) is the correlation between the dielectric behavior of a substance subjected to a time variable electric field, and its microscopic properties. Among its main advantages are its wide frequency range, in fact the modern DS technique may work on frequencies from 10^{-6} to 10^{12} Hz, and the (relative) simplicity of conducting measurements in different conditions of temperature (-170°C to 500°C) and, sometimes, pressure. Dielectric spectroscopy measures the time or frequency dependent response of current and voltage of a sample to a changing electric field. It is especially sensitive to intermolecular interactions and is able to monitor cooperative processes at the molecular level [1].

The outcome of an experiment is typically given in the form of a dimensionless quantity ε^*, the complex dielectric permittivity, which depends on parameters like frequency, temperature, and pressure.

Experiments can be conducted in the time domain as well as in the frequency domain. In case of a frequency domain experiment a sinusoidal voltage with a fixed angular frequency ω_0 is applied and the response for that frequency is obtained, and consequently also $\varepsilon^*(\omega_0)$. Variation of the frequency ω_0 then gives the full spectrum.

2.2 The static electric polarization

Consider two conducting parallel plates in vacuum as depicted in figure 1.1 (a), each carrying an equal charge of opposite sign, $+Q$ and $-Q$ respectively. The plates have a surface area *A* and are separated by a distance *d*. The capacitance C_0 of this parallel plate capacitor is then by definition given by

$$C_0 = \frac{Q}{V}, \tag{2.1}$$

where V is the voltage over the plates. Using the basic formulas from electrostatics [2] and supposing that $d \ll \sqrt{A}$, C_0 can be rewritten as

$$C_0 = \frac{Q}{V} = \frac{Q}{Ed} = \frac{Q}{\frac{Q}{\varepsilon_0 A}d} = \frac{\varepsilon_0 A}{d}, \tag{2.2}$$

where E is the electric field between the plates and ε_0 the electrical permittivity of vacuum. The last equality describes the capacitance of a parallel plate capacitor in terms of its geometry.

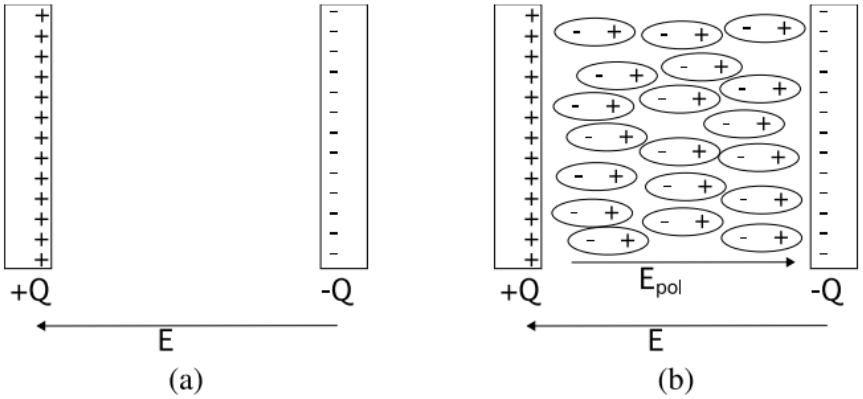

Figure 2.1: (a) A charged parallel plate capacitor in vacuum; (b) a parallel plate capacitor with a dielectric between the plates.

If the capacitor is now filled with a non-conducting[1] material, the positive charges in the material will be attracted towards the plate carrying $-Q$ and likewise the negative charges towards $+Q$.
When stabilized, the system will be in the state shown in figure 2.1(b). For the calculation of C in geometrical terms, the electric field E must now include the surface charge of the material. To do this, a quantity P is introduced, the polarization, which quantifies the way a material reacts to an applied electric field. P is the dipole moment per unit volume and therefore has the dimension of a surface charge density and in the linear approximation is given by

$$P = \chi \varepsilon_0 E\ . \tag{2.3}$$

[1] Suppose an ideal non-conducting material, thus without any free charges, only with dipoles that can rotate but cannot move. We don't want a shortcut, since +Q and−Q would cancelled in that case.

χ is the dielectric susceptibility, a dimensionless quantity that quantifies the response of permanent and induced dipoles in a material to an applied frequency dependent electric field[2]. This allows to calculate the total electric field E_{tot} and the capacitance C. The total field is the sum of the original electric field between the plates and the field emerging from the surface charge on the dielectric, E_{pol}. The former is given by $Q/A\varepsilon_0$, like in the case of the empty capacitor. The latter field is given by the polarization, which is now emerging from the total field. One gets for the electric field that

$$E_{tot} = \frac{\frac{Q}{A} - P}{\varepsilon_0} = \frac{\frac{Q}{A} - \chi\varepsilon_0 E_{tot}}{\varepsilon_0} = \frac{Q}{A\varepsilon_0} - \chi E_{tot} \,. \tag{2.4}$$

Solving this equation for E_{tot} gives that

$$E_{tot} = \frac{Q}{A\varepsilon_0(1+\chi)} = \frac{E}{1+\chi} \,. \tag{2.5}$$

This is the electric field that should be used to calculate the new capacitance C of the filled capacitor.

$$C = \frac{Q}{E_{tot}d} = \frac{Q}{\frac{Q}{A\varepsilon_0(1+\chi)}d} = \varepsilon_0(1+\chi)\frac{A}{d} \,. \tag{2.6}$$

Now ε_r is defined as $1+\chi$ and called the relative permittivity. The last equation is then rewritten as

$$C = \varepsilon_r C_0 \,. \tag{2.7}$$

since there is no material known for which the negative charges of the dipoles move towards the negatively charged plate, χ is always positive. This means that the capacitance of a filled capacitor is always larger than that of an empty one. The result can be easily extended to the general case, where $\boldsymbol{E}$ and $\boldsymbol{P}$ are vectors and χ and ε_r, in the case of anisotropic medium, become tensors.

$$P_i = \varepsilon_0 \chi_{ik} E_k \,, \tag{2.8}$$

[2] Equation 2.3 can be extended to include higher order terms:

$$P = \chi\varepsilon_0 E + \xi_1\varepsilon_0 E^2 + \xi_2\varepsilon_0 E^3 + \ldots$$

This is only necessary if the applied field is large.

where χ_{ik} is the tensor of the dielectric susceptibility. Here we refer to the literature [3], where the complete derivation starting from Maxwell's equations can be found.

2.3 Mechanism for polarization

Any material can be polarized by an external electric field. Numerous mechanisms can contribute to the polarization, in fact the macroscopic polarization is a result of different microscopic polarization mechanisms (modes) that can be divided in three categories.

- **Deformation polarization or charge displacement.** The electric field moves the electric charges slightly away from their equilibrium positions, but without causing a real current although. It can be divided into two independent types:

    - **Electron polarization**: This includes the displacement of the electron cloud relative to the core of an atom, movement of the core itself from its equilibrium position in a crystal, and shifts of bonding electron pairs. In this case a dipole moment is induced. Because electrons are very light, they have a rapid response to the field changes; they may even follow the field at optical frequencies.

    - **Atomic polarization:** the displacement of atoms or atom groups in the molecule under the influence of an external electric field [1].

- **Orientational polarization.** Here dipoles move to new equilibrium orientations. Essentially molecules with an induced or permanent dipole moment, thus caused by some charge distribution in the molecule, reorient themselves to align their dipole moment with the electric field. The rotation is counteracted by the thermal motion of the molecules. Therefore, the orientation polarization is strongly dependent on the frequency of the applied electric field and on the temperature.

- **Redistribution of free charges or ionic polarization.** In a real material, conducting as well as non-conducting, there are always free

charges present. These charges will also move through the material under influence of the field and accumulate at the edges of the material, or eventually at internal interfaces in heterogenous systems [2]. This kind of polarization demonstrates only weak temperature dependence and is determined mostly by the nature of the interface where the ions can accumulate. Many cooperative processes in heterogeneous systems are connected with ionic polarization [1].

Each of these classes has a typical time scale related to it. The larger the unit to be moved and the distance to be bridged, the longer the related time scale.

Charge displacement takes place at time scales of 10^{-14} s. The displacement of electrons is about one or two orders of magnitude faster than that of the cores of the atoms. Actually, in dielectric experiments it is usually considered an instantaneous process. The electronic polarizability contributes at optical frequencies and is usually considered in terms of the refractive index.

The **orientational polarization** covers a broad range of time scales. Factors influencing the speed at which a molecule or a part of it can reorient are, among others, the size of molecule and the intermolecular potentials to overcome. Also the degree of cooperativity is important: some processes involve lots of molecules and thus can be very slow. Typical values are 10^{-9}s for the reorientation of a small molecule to 10^{-2} s for certain cooperative reorientations in liquid crystals or motions in polymers.

The redistribution of free charges is generally the slowest process, since it involves the movement of the charge carrier through the material. Thus it will depend on material parameters like the viscosity and on the size of the charge carrier [2].

2.4 A model for the static permittivity in isotropic systems

There exist a lot of theories describing the static permittivity. As an illustration, the calculation of one of the simplest models is given here, further examples can be found in books like [3].

In general one can split the polarization in two parts:

$$\boldsymbol{P} = \boldsymbol{P}_{in} + \boldsymbol{P}_{or} \,, \tag{2.9}$$

where $\boldsymbol{P}_{in}$ is the contribution of induced dipoles and $\boldsymbol{P}_{or}$ the contribution of the orientational polarization.

$\boldsymbol{P}_{in}$ can be written as

$$\boldsymbol{P}_{in} = N\alpha\boldsymbol{E}_i \,, \tag{2.10}$$

Where N denotes the number of molecules per m^3 and α the polarizability of the molecule. $\boldsymbol{E}_i$ is the internal field acting on the molecules; this field can be different from the applied field.
The calculation of the second part is somewhat more extensive. A molecule with a permanent dipole moment $\boldsymbol{\mu}$ contributes to the polarization if an external field $\boldsymbol{E}$ is applied. Apart from the electric field, also thermal agitation is influencing the orientational polarization, which is thus written as:

$$\boldsymbol{P}_{or} = N\langle\boldsymbol{\mu}\rangle \,. \tag{2.11}$$

$\langle\boldsymbol{\mu}\rangle$ is an average over all possible orientations for $\boldsymbol{\mu}$, considering in this average the energy of the dipole in the electric field and the thermal energy. A dipole in an electric field has an energy

$$W = -\mu \cdot \boldsymbol{E}_d = -\mu E_d cos\theta \,, \tag{2.12}$$

where $\boldsymbol{E}_d$ is the field felt by the dipole (generally different from the applied field) and θ is the angle between $\boldsymbol{E}_d$ and the dipole moment $\boldsymbol{\mu}$. Using the Boltzmann expression for averaging, $\langle\boldsymbol{\mu}\rangle$ can now be calculated, essentially by considering [3]

$$\frac{\langle\boldsymbol{\mu}\rangle}{\mu} = \langle\cos\theta\rangle = \frac{1}{3}\frac{\mu E_d}{KT} - \frac{1}{45}\left(\frac{\mu E_d}{KT}\right)^3 + \cdots \tag{2.13}$$

$$\approx \frac{1}{3}\frac{\mu E_d}{KT} \tag{2.14}$$

The approximation essentially states that the electric field is small. Inserting this back in equation 2.11 gives

$$\boldsymbol{P}_{or} = N\frac{\mu^2}{3kT}\boldsymbol{E}_d \,. \tag{2.15}$$

To be able to write a final expression, the electrical fields E_i and E_d still need to be calculated in function of the applied electrical field. This is not a simple problem, and many models have been proposed. One of these is the so-called Lorentz field, calculated for the situation where a dipole is placed in a cavity,

surrounded by a material that is homogenously polarized. The field acting on the dipole is

$$E_L = \frac{\varepsilon+2}{3} E \ . \tag{2.16}$$

Debye supposed that both E_i and E_d are equal to E_L, resulting in a polarization of the form:

$$\boldsymbol{P} = \frac{\varepsilon+2}{3} N \left(\alpha + \frac{\mu^2}{3kT}\right) \boldsymbol{E} \ . \tag{2.17}$$

Inserting this equation in 2.3 and also replacing χ with *(ε - 1)* gives

$$\frac{\varepsilon-1}{\varepsilon+2} = \frac{N}{3\varepsilon_0}\left(\alpha + \frac{\mu^2}{3KT}\right) . \tag{2.18}$$

The Debye equation describes in theory the behavior of isotropic systems with polar molecules, but in reality only applies to gasses at ordinary pressures. This is of course a consequence of the approximations and assumptions underlying this expression. More sophisticated models have been introduced [3, 4].

2.5 Dielectrics in time-dependent electric fields

The theory of dynamic dielectric response can be based on that for the static case [5]. Suppose that $\boldsymbol{E}(t)$ is a time-dependent electric field that changes such that the polarization $\boldsymbol{P}(t)$ is always in equilibrium with the field. Then we can write, formally extending the equations for the static case to a quasi-static case, so

$$\boldsymbol{D}(t) = \varepsilon_0 \boldsymbol{E}(t) + \boldsymbol{P}(t) = \varepsilon_0 \boldsymbol{E}(t) + \chi \varepsilon_0 \boldsymbol{E}(t) = (1+\chi)\varepsilon_0 \boldsymbol{E}(t)$$
$$= \varepsilon_r \varepsilon_0 \boldsymbol{E}(t), \tag{2.19}$$

Where the susceptibility χ depends on the temperature, pressure, and composition of the dielectric, but not on time. The relative permittivity ε_r is given as $1 + \chi$.

The dynamic case is most easily studied with the help of harmonic, i.e. sinusoidally varying electric fields. The time dependence of the electric field strength is given by:

$$\boldsymbol{E}(t) = \boldsymbol{E}_0 \cos \omega t \ , \tag{2.20}$$

where $\boldsymbol{E}_0$ is the amplitude and ω the angular frequency of the sinusoidal variation. The dielectric displacement **D**(t) (which is equivalent to the free surface charge) in the case of a linear and isotropic dielectric can be written as

$$\boldsymbol{D}(t) = \boldsymbol{D}_0 \cos(\omega t - \delta) \, . \tag{2.21}$$

δ is the phase difference between the driving field and the polarization and $\boldsymbol{D}_0$ is the amplitude of the sinusoidal variation. This phase difference expresses that the response of the dielectric can lag behind the driving electric field. The linearity of the system gives that the frequencies are the same and that $\boldsymbol{D}_0$ and $\boldsymbol{E}_0$ have the same direction. $\boldsymbol{D}(t)$ is split into orthogonal parts:

$$\boldsymbol{D}(t) = \boldsymbol{D}_0 \cos\delta \cos\omega t + \boldsymbol{D}_0 \sin\delta \sin\omega t \, . \tag{2.22}$$

Introduction of two new quantities leads to a more familiar form. If we write

$$\varepsilon^{I}(\omega) = \cos\delta(\omega) \frac{D_0}{\varepsilon_0 E_0} \tag{2.23}$$

$$\varepsilon^{II}(\omega) = \sin\delta(\omega) \frac{D_0}{\varepsilon_0 E_0} \, , \tag{2.24}$$

We get that

$$\boldsymbol{D}(t) = \varepsilon^{I}(\omega)\varepsilon_0 \boldsymbol{E}_0 \cos\omega t + \varepsilon^{II}(\omega)\varepsilon_0 \boldsymbol{E}_0 \sin\omega t. \tag{2.25}$$

Equivalently this relation can be written as

$$\boldsymbol{D}(t) = \varepsilon^{*}\varepsilon_0 \boldsymbol{E}(t) \, , \tag{2.26}$$

Where

$$\varepsilon^{*} = \varepsilon^{I} - i\varepsilon^{II} \, . \tag{2.27}$$

Thus the response of a dielectric to an electric field is given by a complex quantity ε^{*}, the complex dielectric permittivity, a material property that depends on time or frequency, pressure, temperature, etc.

2.6 The Kramers - Kronig relations

The equations 2.28 and 2.29 are the Kramers - Kronig relations. They describe how the real and imaginary part of $\varepsilon^{*}(\omega)$ are related to each other. The

consequence is that it suffices to know the imaginary part to know the full complex ε^*, since the real part can be calculated from the imaginary, and of course vice versa. A derivation of these relations can be found in the classic book *Theory of Electric Polarization, vol. 2* of Böttcher and Bordewijk [5].
In short, it is shown, based on the superposition principle, that $\varepsilon^*(\omega)$ can be expressed as the Laplace transformation of a pulse response function with certain properties. Complex integration allows to derive the Kramers - Kronig relations:

$$\varepsilon^I(\omega_0) = 1 + \frac{2}{\pi} P \int_0^\infty \frac{\omega \varepsilon^{II}}{\omega^2 - \omega_0^2} d\omega \tag{2.28}$$

$$\varepsilon^{II}(\omega_0) = \frac{2}{\pi} P \int_0^\infty \frac{\omega_0 \varepsilon^I}{\omega^2 - \omega_0^2} d\omega \tag{2.29}$$

in which the symbol *P* denotes the *Cauchy principal value integral*, that is, the integral is evaluated by excluding singular points like $\omega = \omega_0$ where the integral would diverge. In practice, one uses the Kramers - Kronig relations implicitly when limiting the analysis of a dielectric spectrum to the imaginary part. This is usually the easiest method to analyze spectra and in virtue of these relations, it still contains the full relaxation information.
Equations 2.28 and 2.29 were derived supposing that all polarization processes take place in a finite time. But, as mentioned in section 2.3, the charge displacements are a lot faster than the orientational polarization that is the main subject of dielectric spectroscopy. This means that it makes sense, from a pragmatic point of view, to develop the formalism again, but now supposing that a part of polarization is instantaneous.

The idea is that the polarization $\boldsymbol{P}$(t) is now considered as the sum of the instantaneous polarization $\boldsymbol{P}_{\text{in}}$(t) and the remaining polarization from the slower processes (mainly orientational), denoted $\boldsymbol{P}_{\text{or}}$:

$$\boldsymbol{P}(t) = \boldsymbol{P}_{in}(t) + \boldsymbol{P}_{or}(t) \, . \tag{2.30}$$

Since it does not take time to build up $\boldsymbol{P}_{in}$, the expression for the static case, equation 2.3, can be used, replacing χ by χ_∞, the susceptibility for the instantaneous polarization. Thus

$$\boldsymbol{P}_{in} = \chi_\infty \varepsilon_0 \boldsymbol{E}(t) = (\varepsilon_\infty - 1)\varepsilon_0 \boldsymbol{E}(t) \, , \tag{2.31}$$

Introducing ε_∞ as the dielectric constant for induced polarization.
In the same way, also new forms for the Kramers – Kronig relations can be derived. Only the first one, for the real part, actually changes, but they are given both for completeness.

$$\varepsilon^I(\omega_0) = \varepsilon_\infty + \frac{2}{\pi} P \int_0^\infty \frac{\omega \varepsilon^{II}}{\omega^2 - \omega_0^2} d\omega \tag{2.32}$$

$$\varepsilon^{II}(\omega_0) = \frac{2}{\pi} P \int_0^\infty \frac{\omega_0 \varepsilon^I}{\omega^2 - \omega_0^2} d\omega \tag{2.33}$$

2.7 Some physical interpretation

A lot of the quantities introduced in the previous sections have a physical meaning, and we will give them here for some.

• It is possible to correlate $\varepsilon^{II}(\omega)$ to the energy loss in a dielectric. If $\dot{W}$ denotes the average energy dissipation per unit of time, it can be shown that [5]:

$$\dot{W} = \frac{\omega (E_0)^2}{8\pi} \varepsilon^{II} \,. \tag{2.34}$$

Therefore ε^{II} is usually termed the dielectric loss.

• It can also be shown [5] that

$$\dot{W} \prec \sin\delta \,,$$

where δ is the same quantity introduced in equation 2.21. Therefore δ is also called the loss angle.

Making the connection between the polarization and the actual behaviour of the molecules and their related dipole is an important and extended area of the dielectric work and theory. We will not go deep into this subject, but limit ourselves to a simple intuitive description. To contribute to the polarization, a dipole (and thus also the molecule or part of the molecule it belongs to) has to be able to reorient itself to align with applied electric field. This aligning serves of course the purpose of minimizing the energy of the dipole. The dipole has to overcome certain forces, like Van der Waals forces or hydrogen bonds with neighbouring molecules and steric constraints, there has to be room for the new position. Thus it takes some typical time for a dipole to reorient, say τ, the

relaxation time. If an oscillating field is applied with a frequency that is substantially larger than $1/\tau$, all dipoles can reorient themselves and contribute to the polarization. This changes if the field frequency raises to a level similar as $1/\tau$: not all molecules can contributed anymore, thus the polarization and consequently the (real part of the) dielectric permittivity decreases. This is the step in ε^I and the peak in ε^{II}. Finally, when the field frequency rises above $1/\tau$ no molecules can catch up with the electric field anymore and the contribution of this dipole motion to the polarization ceases to exist. ε^I is flat again and ε^{II} has returned to zero.

This already explains the form of the dielectric data curves, which can be described by model function as shown in the next sections, but it does not give any clue which molecular motion gives raise to the relaxation step. In fact this question goes beyond the field of dielectric spectroscopy and can usually only be solved with the help of theoretical models and other measurement techniques.

2.8 The Debye relaxation function

The Debye relaxation function can be introduced in multiple ways. In the following paragraphs we elaborate slightly on two approaches that give some insight on the background of this relaxation function. The first approach is based on the assumption that the time dependence of the polarization of the sample decays exponentially. In the second approach one tries to calculate the rotation of a dipole in an electric field with a friction term.

Yet another way is assuming an electrical circuit consisting of an ideal capacitor in parallel with an ideal resistor with alternating current. Some basic calculations then also lead to equation

$$\varepsilon^*(\omega) = \varepsilon_\infty + \frac{\varepsilon - \varepsilon_\infty}{1 + i\omega\tau}, \tag{2.35}$$

this is the expression for the Debye relaxation function.

2.9 From a macroscopic point of view

When an external field is applied to a dielectric, polarization of the material reaches its equilibrium value, not instantaneously but rather over a period of time. By analogy, when the field is suddenly removed, the polarization decay,

caused by thermal motion, follows the same law as the relaxation or decay function of dielectric polarization $\varphi(t)$:

$$\varphi(t) = \frac{\boldsymbol{P}(t)}{\boldsymbol{P}(0)}, \tag{2.36}$$

where $\boldsymbol{P}(t)$ is the time-dependent polarization vector. The relationship for the dielectric displacement vector $\boldsymbol{D}(t)$ for time-dependent fields may be written as follows [1, 5]:

$$\boldsymbol{D}(t) = \varepsilon_0 \left[\varepsilon_\infty \boldsymbol{E}(t) + \int_{-\infty}^{t} \dot{\phi}\,(t^I)\boldsymbol{E}(t - t^I)dt^I\right]. \tag{2.37}$$

In 2.37 $\boldsymbol{D}(t) = \varepsilon_0 \boldsymbol{E}(t) + \boldsymbol{P}(t)$, and $\phi(t)$ is the dielectric response function

$$\phi(t) = (\varepsilon_s - \varepsilon_\infty)\,[1 - \varphi(t)], \tag{2.38}$$

where ε_s and ε_∞ are the low- and high-frequency limits of the dielectric permittivity, respectively. The complex dielectric permittivity $\varepsilon^*(\omega)$ (where ω is the angular frequency) is connected with the relaxation function by a very simple relationship [1, 5]:

$$\frac{\varepsilon^*(\omega) - \varepsilon_\infty}{\varepsilon_s - \varepsilon_\infty} = \hat{L}\left[-\frac{d}{dt}\varphi(t)\right] \tag{2.39}$$

in which $\hat{L}$ is the Laplace transform operator, which is defined for an arbitrary time dependent function $f(t)$ as

$$\hat{L}[f(t)] \equiv F(\omega) = \int_0^\infty e^{-pt} f(t)dt \tag{2.40}$$

$p = x + i\omega$, where $x \to 0$ and i is an imaginary unit

Relation 2.39 gives equivalent information on dielectric relaxation properties of the sample being tested both in frequency and in time domain. Therefore the dielectric response might be measured experimentally as a function of either frequency or time, providing data in the form of a dielectric spectrum $\varepsilon^*(\omega)$ or the macroscopic relaxation function $\varphi(t)$.
For example, when a macroscopic relaxation function obeys the simple exponential law

$$\varphi(t) = \exp(-t/\tau_m) \tag{2.41}$$

where τ_m represents the characteristic relaxation time. The well-known Debye formula for the frequency-dependent dielectric permittivity can be obtained by substitution of (2.41) into (2.40) [1, 5]

$$\frac{\varepsilon^*(\omega)-\varepsilon_\infty}{\varepsilon_s-\varepsilon_\infty} = \frac{1}{1+i\omega\tau_m}\,. \tag{2.42}$$

Finally the expression for the Debye relaxation function looks like:

$$\varepsilon^*(\omega) = \varepsilon_\infty + \frac{\varepsilon_s-\varepsilon_\infty}{1+i\omega\tau_m}\,. \tag{2.43}$$

For many of the systems being studied, the relationship above does not sufficiently describe the experimental results. The Debye conjecture is simple and elegant. It enables us to understand the nature of dielectric dispersion. However, for most of the systems being studied, the relationship above does not sufficiently describe the experimental results. The experimental data are better described by non-exponential relaxation laws. This necessitates empirical relationships, which formally take into account the distribution of relaxation times.

2.10 From a microscopic point of view

The Debye equation can also be derived from a molecular model. Debye supposed that the rotation of a molecule in an electric field is interrupted by collisions with the neighbours. This obstruction can be described by a resistive couple proportional to the angular velocity of the molecule [4, 7]. We refer to the literature for the derivation.

2.11 A more empirical approach

In practice the analysis of a dielectric spectrum is based on the determination of the distribution of the relaxation times of the processes that are seen in the spectrum. Although a number of approaches are possible, the presence of computers with some special programs makes it now possible to easily perform non-linear fits to model functions. In the following parts, a number of model functions, will be presented. The collection given here is based on the Debye function, that has been extended empirically to account for certain types of broadening of the spectra.

2.11.1 The Debye relaxation function

In Figure 2.2, the Debye function introduced in the previous section, is plotted, splitted in his real and imaginary part. The real part shows a step down, and the half height of this step is found at $\omega = \tau^{-1}$. For the imaginary part, the top of the peak corresponds to this frequency. Here we see that the function is symmetric around $\omega = \tau^{-1}$ and that the half-width is 1.14 decades.

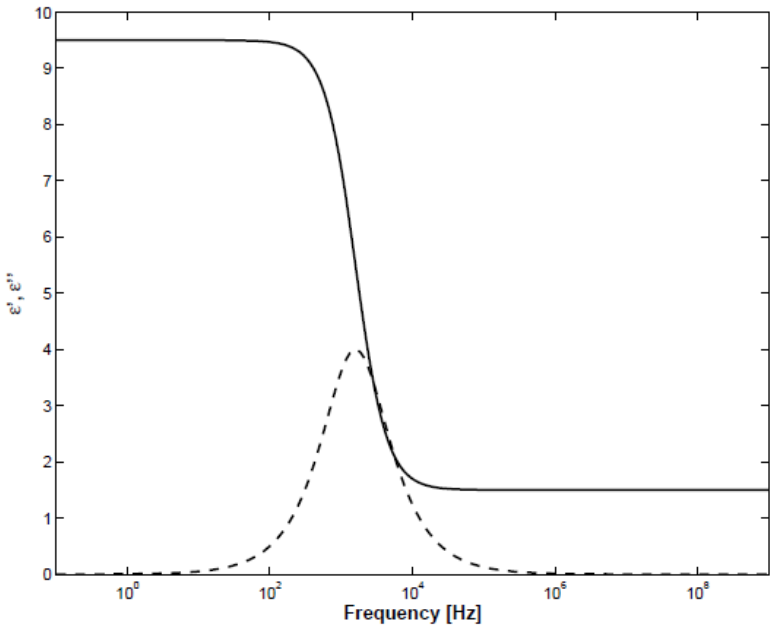

Figure 2.2: The Debye relaxation function. The full line is the real part ε^{I} and the dashed line is the imaginary part ε^{II}. Plotted for $\varepsilon_{\infty} = 1.5$, $\varepsilon_{s} = 9.5$ and $\tau = 10^{-4} s$.

2.11.2 The Cole-Cole relaxation function

Since in reality a perfect Debye relaxation is rare, some empirical modifications have been made, resulting in broadened peaks in the imaginary parts and smeared out steps in the real part. The Cole–Cole function is aimed at the description of a symmetric broadening of the peak [8]. This is done by changing equation 2.43 to

$$\varepsilon^{*}(\omega) = \varepsilon_{\infty} + \frac{\varepsilon_{S} - \varepsilon_{\infty}}{1 + (i\omega\tau_{m})^{\alpha}} \quad . \tag{2.44}$$

The distribution or shape parameter α, which lies between 0 and 1, describes the broadening: $\alpha = 1$ corresponds to the situation of no broadening (the Debye function) and with decreasing α the peak becomes lower and broader.

Sometimes one uses $1-\alpha$ instead of α. In Figure 2.3 real and imaginary part for some values of α are plotted. The maximum of the peak is located at $\omega = \tau^{-1}$.

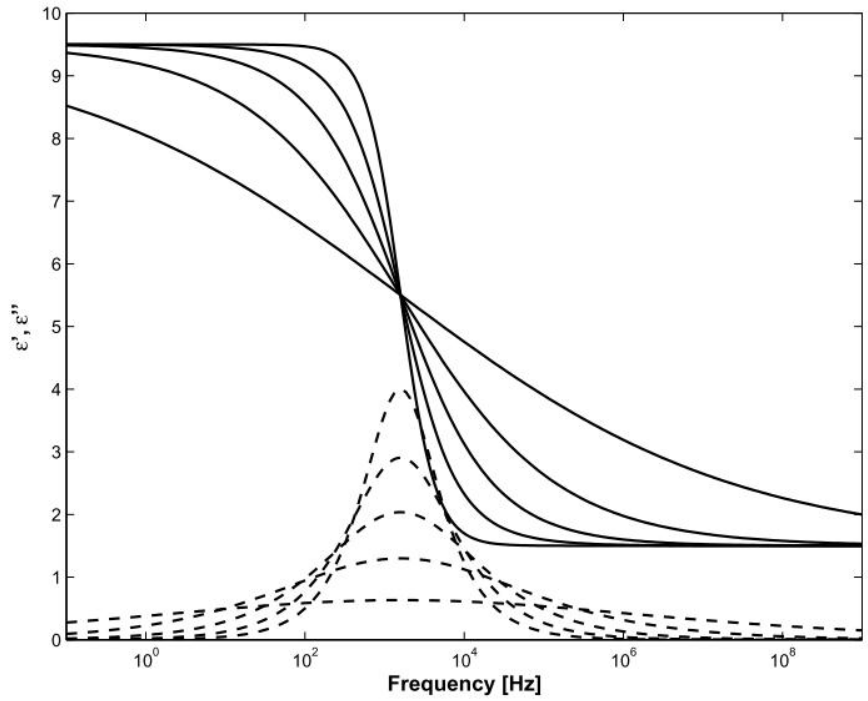

Figure 2.3: The Cole–Cole relaxation function. The full lines are the real parts $\boldsymbol{\varepsilon^{I}}$ and the dashed lines are the imaginary parts $\boldsymbol{\varepsilon^{II}}$. Curves are plotted for α = 1, α = 0.8, α = 0.6, α = 0.4 and α = 0.2.

2.11.3 The Cole-Davidson relaxation function

When the relaxation peak is only broadened at the high frequency side, the Cole–Davidson function can be used [9, 10]. In this case a shape parameter β is introduced, resulting in the expression

$$\varepsilon^*(\omega) = \varepsilon_\infty + \frac{\varepsilon_S - \varepsilon_\infty}{(1+i\omega\tau_m)^\beta}\,. \qquad (2.45)$$

For $\beta = 1$ this expression reduces to the Debye function. β takes values between 0 and 1. Plots of the Cole–Davidson function for some values of β are given in figure 2.4.

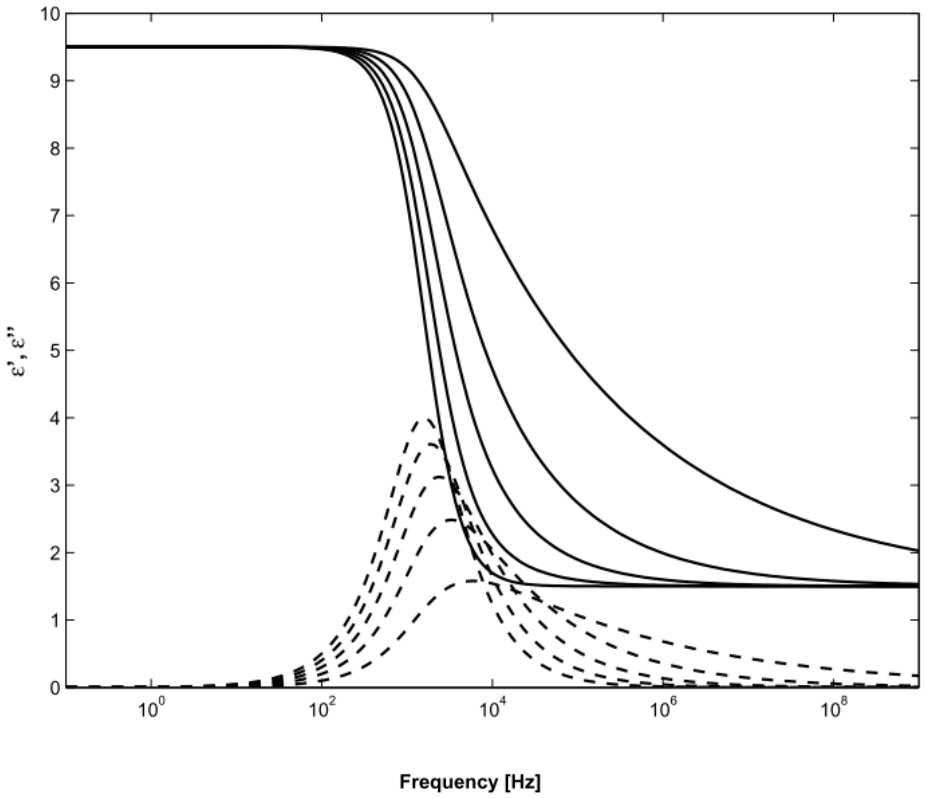

Figure 2.4: The Cole–Davidson relaxation function. The full lines are the real parts $\boldsymbol{\varepsilon^{I}}$ and the dashed lines are the imaginary parts $\boldsymbol{\varepsilon^{II}}$. Curves are plotted for β = 1, β = 0.8, β = 0.6, β = 0.4 and β = 0.2.

2.11.4 The Havriliak-Negami relaxation function

The Havriliak–Negami function [11, 12] is the natural combination of the Cole–Cole and Cole–Davidson functions: it describes the combined symmetric and asymmetric broadening by two shape parameters α and β both between 0 and 1.

$$\varepsilon^*(\omega) = \varepsilon_\infty + \frac{\varepsilon_S - \varepsilon_\infty}{(1+(i\omega\tau_m)^\alpha)^\beta}\,. \tag{2.46}$$

2.12 Additions of other phenomena

The expressions given in the previous paragraphs describe the orientational polarization. The polarization at high frequencies or short timescales is summarized by a dielectric constant ε_∞.

The only additions to be made are at low frequencies or long timescales. In this regime, the movement of charge carriers through the samples becomes important and it can be observed in the dielectric spectra.
The first phenomenon is electrical conduction. This simple movement of charge carriers leads typically to a response that is the same as of an ohmic conductor. It shows only in the imaginary part of the dielectric permittivity. When analysing a dielectric spectrum, it is accounted for by a term of the form

$$-\frac{-i\sigma}{\varepsilon_0 \omega^s}. \tag{2.47}$$

σ is the DC electrical conductivity and the exponent *s* is a fitting parameter that has a value of 1 for pure ohmic conduction. Note again that because of its purely imaginary character this term only contributes to imaginary part ε^{II}.

Electrode polarization can be seen as a large rise of ε^I for low frequencies. The explanation is that for slowly varying fields, the mobile charge carriers can reach the electrodes. Because they cannot leave the sample they build up a charged layer. This layer masks the electric field in the bulk of the actual sample and gives rise to the increased ε^I. Since electrode polarization does not tell much about the sample (actually mainly that it contains free charges), the part with the electrode polarization is often excluded from the analysis. If for some reason it is necessary to include this part, it is fitted with a power law in the real part:

$$A\omega^{\lambda}. \tag{2.48}$$

The exponent λ takes values typically in the order of -1.5 to -2. A consequence of electrode polarization is that the power law of the conductivity contribution changes, and that a second power law for the conductivity is necessary.

The Maxwell–Wagner effect [14, 15] is equivalent to electrode polarization, but in this case the charges accumulate at the internal boundaries of a heterogeneous sample. In the dielectric spectra this shows up as an ordinary relaxation process. In a formulation with equivalent electrical circuits, it can be shown that a Maxwell–Wagner process appears when a sample consists of two parts with different dielectric permittivity and electrical conductivity [16].

2.13 The temperature dependence of the relaxation times

Once the relaxation times have been determined with the procedures described in the previous section, the temperature dependence of the relaxation times can be determined. In practice two expressions are commonly used to express the temperature dependence. The first one is the Arrhenius equation, originally introduced to describe chemical reactions. The second one is the Vogel–Fulcher–Tamman (VFT) dependence, introduced to describe the non-Arrhenius dependence in many glass-forming systems.

2.13.1 Arrhenius dependence

A derivation of this relation was made by Eyring (see [3] for calculations and reference), based on an analogy between chemical reactions and the rotation of a dipole that has to overcome a potential barrier.

Suppose a chemical reaction where two components A and B form a new compound C. Eyring supposed that first an "activated complex" AB* must be formed, requiring a certain amount of energy. One can then identify A + B and C as the initial and final states of the dipole and AB* as the state in which the dipole has enough energy to cross the potential barrier. Eyring finds that

$$\tau = A\exp\left(\frac{\Delta E}{RT}\right), \tag{2.49}$$

where A is a temperature independent factor and ΔE, the activation energy, does not depend on temperature either.

The Arrhenius equation describes the temperature dependence of the relaxation times of a process where a temperature-independent potential barrier has to be crossed.

Linearization of this equation shows that an Arrhenius process shows up as a straight line when the relaxation times are plotted versus the inverse temperature, and the slope of this line is the activation energy. Therefore the relaxation time data in this work will mainly be presented in such a so-called Arrhenius plot.

2.13.2 VFT

The VFT equation was introduced as a fitting function for the curved relaxation time behaviour for glass-forming liquids. Later it received some theoretical

foundation, mainly based on free volume theories. It will lead us too far to go into this subject. A recent review concerning
relaxation in glass-formers can be found in [17], with further references to the literature.
The VFT equation is usually given in the form

$$\tau = \tau_\infty \exp\left(\frac{B}{T - T_0}\right), \tag{2.50}$$

where τ_∞ is the high temperature limit of the relaxation time, B is related to the fragility of the glass-former and T_0 is the Vogel temperature. When T_0 = 0, this equation reduces to the Arrhenius equation.

2.14 Basic concepts of measurement technique

There are a number of possibilities to determine ε^*. A first classification to make is between time - domain ($\varepsilon^*(t)$) and frequency - domain techniques ($\varepsilon^*(f)$). Since in this work time-domain techniques have not been used, all our attention will go to frequency-domain technique.
The basis of any measurement of $\varepsilon^*(f)$ is essentially a determination of the impedance *Z* of the sample. It then requires some simple calculation to arrive at a value for ε^*. In the simplest case, that of a pure capacitor, the value of the impedance is given by

$$Z_c = \frac{1}{\omega C}, \tag{2.51}$$

where $\omega = 2\pi f$. For the case of a dielectric sample cell, one can use either a measured value of the vacuum capacitance C_0 or the equation for the geometrical capacitance, for example equation 2.2 in the case of a parallel plate capacitor. One gets

$$\varepsilon = \frac{C}{C_0}. \tag{2.52}$$

In reality the impedance is a complex number and the complex form of Z_c is:

$$Z_c^* = \frac{1}{i\omega C}. \tag{2.53}$$

This means that also the phase information must be measured, to allow for the determination of both real and imaginary part of ε^*. Suppose that a sinusoidal voltage is applied to the sample and the voltage over and current through the sample are determined, including the phase information. This gives:

$$V(t) = V_0 \exp(i\omega t), \tag{2.54}$$

$$I(t) = I_0 \exp(i\omega t + i\phi) \tag{2.55}$$

so the complex impedance becomes

$$Z^* = \frac{V_0}{I_0}\exp(i\phi), \tag{2.56}$$

and the complex permittivity looks like

$$\varepsilon^* = \frac{-i}{\omega Z^*}\frac{1}{C_0} \tag{2.57}$$

The value obtained for ε^* is that corresponding to the frequency of the applied field.

The present discussion could be considered very short but we can justify it considering that modern dielectric equipment is like a black box that when operated correctly gives the right value of complex permittivity [2,13].

References

1. Y. Feldman, Fractals, Diffusion, and Relaxation in Disordered Complex Systems: A Special Volume of Advances in Chemical Physics, vol. 133 (John Wiley & Sons, Hoboken, 2006)

2. J. Leys, PhD Thesis, University of Leuven, Belgium, Broadband dielectric spectroscopy of confined liquid crystals and hydrogen bonded liquids, 2007

3. C. J. F. Böttcher, Theory of Electric Polarization, vol. 1 (Elsevier Science, Amsterdam, 1973), 2nd ed.

4. N. E. Hill, W. E. Vaughan, A. H. Price, and M. Davies, Dielectric properties and molecular behaviour (Van Nostrand Reinhold Company, London, 1969)

5. C. J. F. Böttcher and P. Bordewijk, Theory of Electric Polarization, vol. 2 (Elsevier Science, Amsterdam, 1978)

6. G. Williams and D. K. Thomas, Phenomenological and molecular theories of dielectric and Electrical relaxation of materials, Novocontrol Application Note Dielectrics nr. 3 (1998)

7. P. Debye, Polar Molecules (Dover, New York, 1929)

8. K. S. Cole and R. H. Cole, J. Chem. Phys. 9, 341 (1941)

9. D. W. Davidson and R. H. Cole, J. Chem. Phys. 18, 1417 (1950)

10. D. W. Davidson and R. H. Cole, J. Chem. Phys. 19, 1484 (1950)

11. S. Havriliak and S. Negami, J. Polymer Sci. C 14, 99 (1966)

12. S. Havriliak and S. Negami, Polymer 8, 101 (1967)

13. F. Kremer and A. Schönhals, eds., Broadband Dielectric Spectroscopy (Springer Verlag, Berlin, 2003)

14. J. C. Maxwell, Electricity and magnetism, vol. 1 (Clarendon, Oxford, 1892)

15. K. W. Wagner, Arch. Electrotech. 2, 317 (1914)

16. J. Thoen and T. K. Bose, Handbook of Low and High Dielectric Constant Materials and Their Applications (Academic Press, San Diego, 1999), vol.

1,chap. Dielectric Behavior in Liquids: Critical Mixtures and Liquid Crystals, pp. 501–561

17. J. C. Dyre, Rev. Mod. Phys.78, 953 (2006)

Chapter 3

Dielectric Characterization of an Orthoconic Antiferroelectric Liquid Crystal Mixture

3.1 Introduction

It is well known that tilted chiral structures in smectic liquid crystal phases exhibit spontaneous polarization and if the structure is synclinic the liquid crystal is called ferroelectric liquid crystal (FLC) while if the structure is anticlinic (the director is tilted in opposite direction in alternate layers) the liquid crystal is an antiferroelectric liquid crystals (AFLC).

The study of FLCs and AFLCs is important for different aspects: the interesting physical properties and their application in electro-optical devices. Moreover, due to their fast response time, they can be employed in visual display applications [1, 2].

Dielectric spectroscopy is a useful tool for characterizing liquid crystals phases which allows a temperature dependent analysis of their physical properties. The electro-optical response of a liquid crystal cell is related to dielectric modes observed in liquid crystals phases. In fact if the dielectric relaxation mode is fast, the electrooptical switching related to this mode can be fast as well [3].

If a smectic C* (SmC*) phase is present in the Liquid Crystal (LC) phase diagram, the dielectric response would be a result of two relaxation modes [4 – 7]. The first, Goldstone mode, due to the phase fluctuation in the azimuthal orientation of the director, is usually observed in the low frequency range. The second is the soft mode that corresponds to fluctuations in the tilt-angle of the director and appears in the SmC* and in the SmA* phases becoming more evident near SmC* to SmA* phase transition. Antiferroelectric liquid crystals show not only antiferroelectric and ferroelectric phases, but frequently, as we have just seen in the first chapter, they show also the smectic chiral subphases.

In this chapter, dielectric spectroscopy is used to investigate the high-tilted chiral smectic phases of the antiferroelectric liquid crystal W-129. This material exhibits an high spontaneous polarization at room temperature (300 nC/cm^2) in virtue of its tilted chiral structure (the tilt angle is 45° at room temperature). The Cole-Cole function has been used to determine the dependence of distribution parameter, dielectric increment (also called dielectric strength) and relaxation frequency as a function of temperature.

3.2 Materials and Techniques

W-129 has been synthesized from R. Dabrowski group at the Military University of Technology, in Warsav, Poland. It is a smectic liquid crystalline mixture which presents both ferroelectric and antiferroelectric smectic C phases. The phase sequence of this material is the following:

Cr - 13/15°C – SmCa* - 84.5°C – SmC* - 102.3°C – SmA* - 117/125.2°C -Iso, obtained from DSC measurements. The study of electro-optical properties of W-129 has been already done in the past as detailed in Ref. [8]. A Japanese commercial cell (EHC Ltd, Tokyo, Japan) with a thickness of (2.0 ± 0.2) μm and a ITO resistance of 100 Ω/□ has been used. The cell was filled by capillary method in the isotropic phase [9].

The dielectric measurements have been carried out using an EG&G 273A galvanostat / potentiostat – impedentiometer in the frequency range 10 mHz–100 kHz with a maximum applied voltage of 0.5 V (RMS) and no bias field was applied. In order to perform dielectric measurements as a function of temperature the sample has been placed in a CaLCTec FB150 programmable temperature hot stage.

3.3 Results and discussion

The real part of the dielectric permittivity (ε') is almost constant in the SmA* phase and for frequencies from 0.1 to 10 Hz (see Fig. 3.1). For these frequencies, ε' is also almost constant in the SmC* phase. For the other frequencies the real part of the permittivity decreases gradually with decreasing temperature until the SmA* - SmC* transition temperature is reached, then it increases slowly for frequencies equal to 100 Hz and 10 kHz and increases rapidly for frequency equal to 1 kHz. In this last region the soft ferroelectric mode contributes to the increase of the dielectric constant.

Further cooling the sample, below the SmC*- SmCa* transition, the dielectric constant decreases slowly till the temperature of 70°C is reached, then decreases very rapidly. The measurements performed at 10 kHz show an opposite behaviour.

The frequency dependence of the real and imaginary parts of the dielectric constant, respectively called, dispersion and absorption or dielectric loss curve, shows different relaxation responses (see Fig. 3.2 (a), (b)). The dielectric loss curve (Fig. 3.2(b)) shows a very high relaxation peak, probably due to the ionization diffusion in the limit of zero mobility of slow ions at room

temperature (20/25°C) and at very low frequencies (~0.1 Hz). The Goldstone mode results more evident in the region from 10 to 102 Hz and for temperatures from 85°C to 110°C.

For a complete overiew of experimental data, dispersion/absorption spectra are shown together with the Cole-Cole plots obtained for every fixed temperature. All parameters were obtained from fitting the experimental dielectric constant data with the Cole-Cole modification of the Debye equation [10],

$$\varepsilon^* = \varepsilon_\infty + \frac{\varepsilon(0) - \varepsilon_\infty}{1 + (i2\pi f\tau)^{1-\alpha}} \tag{3.1}$$

where f is the frequency, $\varepsilon(0)$ is the static dielectric constant, ε_∞ is the high frequency dielectric constant, τ ($=1/(2\pi f_a)$) is the dielectric relaxation time, f_a is the absorption peak frequency and α is the distribution parameter for a particular relaxation process that varies between 0 and 1. If α is very small (eq. 1), it satisfies the Debye equation while if α is more than 0.5 there could be more than one relaxation process.

The real and imaginary part of the dielectric constant are shown together with the Cole-Cole plots at 25°C and 90°C respectively (see Fig. 3.3 and Fig. 3.4).

The relaxation response of W-129 at 25°C (Fig. 3.3(b)) is typical of the antiferroelectric phase. Two relaxation processes are evident: the relaxation process (2) corresponds to Anti-phase mode (PHM), the other process (1) corresponds to In-phase mode (PLM). In the Cole-Cole plot, obtained at 90°C (Fig. 3.4(b)), the Goldstone mode is well clear (1), while the Soft mode (2) is weakly detected. The large value of distribution parameters evalueted for both processes at 25°C (see Table 1) makes the Cole-Cole plot far from being a overlapping of two semi-circles. The same result has been obtained for process (1) at 90°C (see Table 2) where an unusually large value of dielectric increment has been revealed. The very small value of the distribution parameter for process (2) (Table 2) makes the Cole-Cole mode very close to be a semi-circle, reducing it to a Debye response [11].

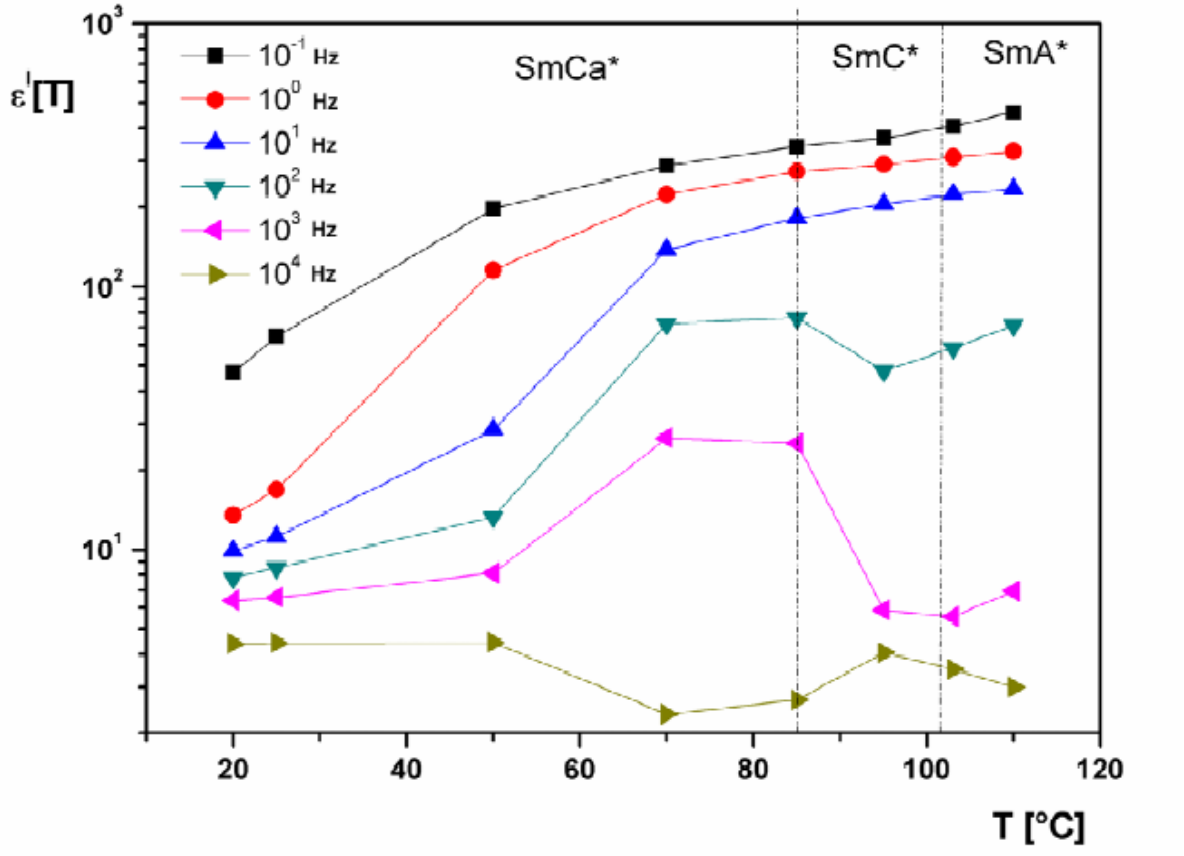

Figure 3.1: Temperature dependence of the real part of the dielectric constant at different fixed frequencies.

Table 3.1. Fitting parameters for the two relaxation processes shown in Fig. 3 for SmCa* phase of W-129.

T = 25°C						
Process	f_a	ε (0)	τ [s]	α	ε (∞)	$\Delta\varepsilon$
1	63.47	11.84	2.51 · E ^−3	0.31	6.78	5.06
2	2.38 · E ^+4	6.79	6.68 · E ^−6	0.49	1.59	5.20

Table 3.2. Fitting parameters for the two relaxation processes shown in Fig. 4 for SmC* phase of W-129.

T = 90°C						
Process	f_a	ε (0)	τ [s]	α	ε (∞)	$\Delta\varepsilon_i$
1	24.42	287.42	6.52 · E ^−3	0.45	0.67	286.75
2	2.28 · E ^+4	5.05	6.98 · E ^−6	0.08	0.12	4.93

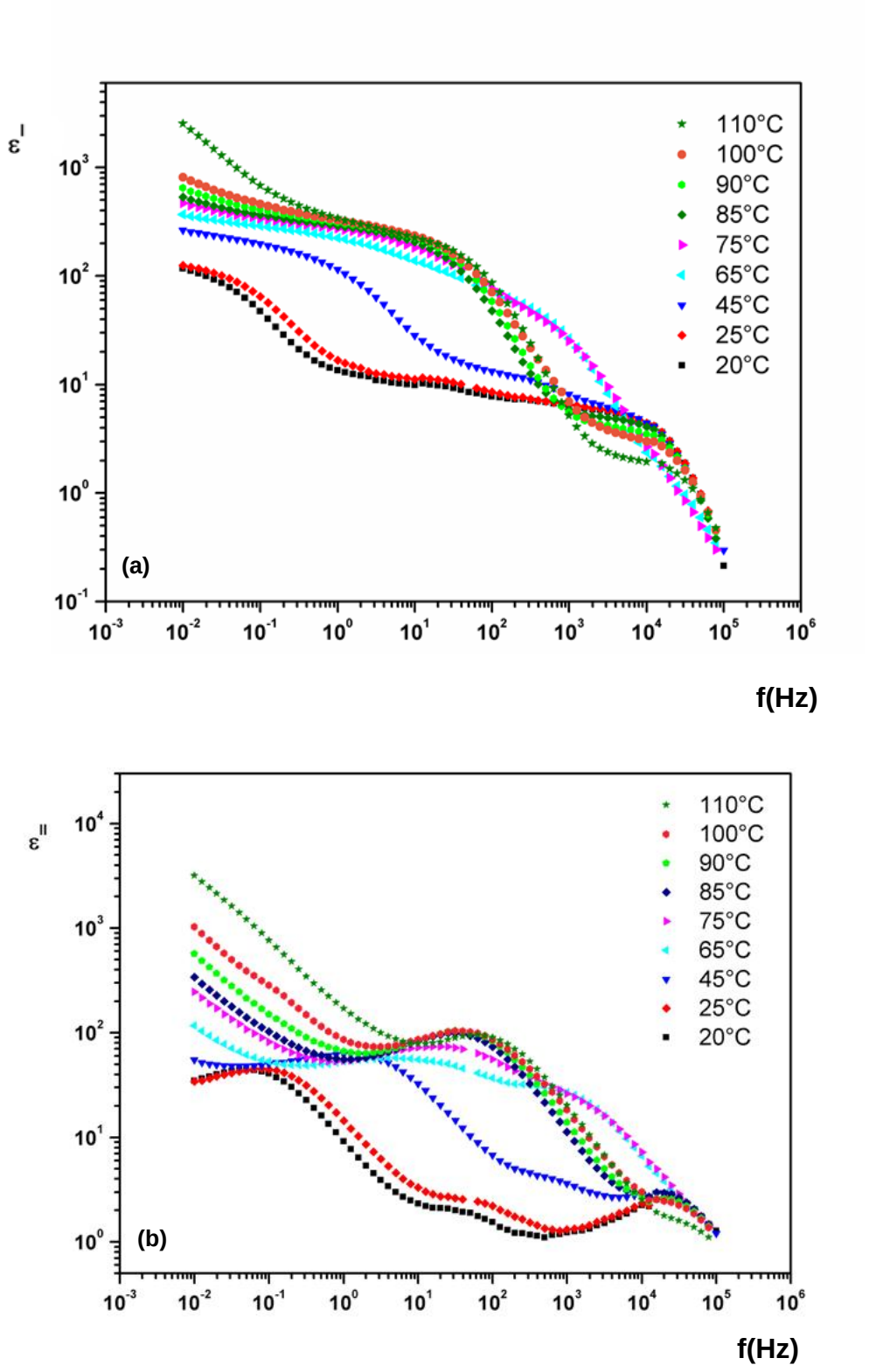

Figure 3.2: Dispersion (a) and absorption (b) curves of the dielectric spectra acquired for W-129 at different temperatures.

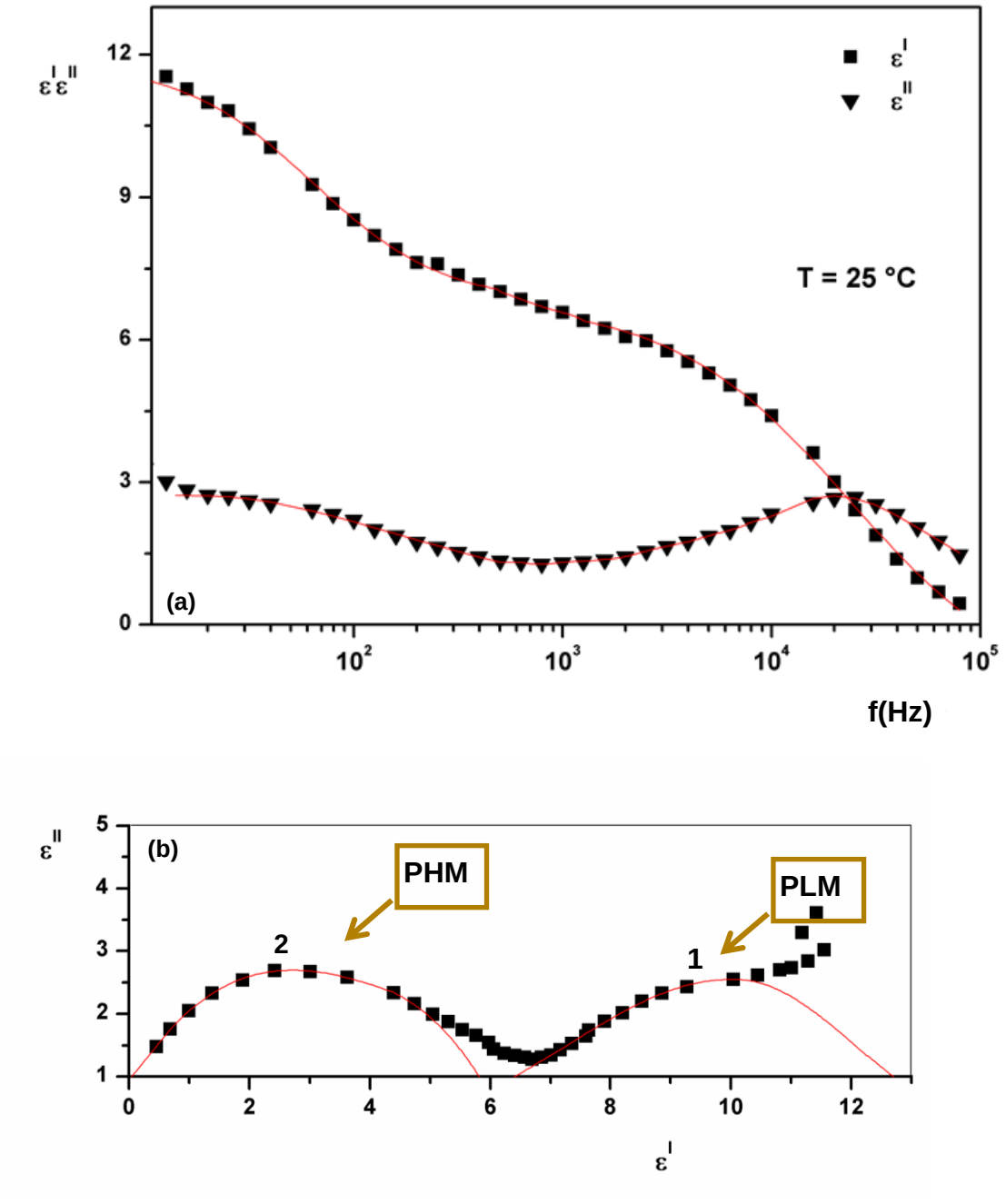

Figure 3.3: Dispersion and absorption curves (a) and Cole-Cole plot (b) of the dielectric spectra acquired for W-129 at 25°C. The solid red line shows the best theoretical fit of the Cole–Cole equation into experimental data.

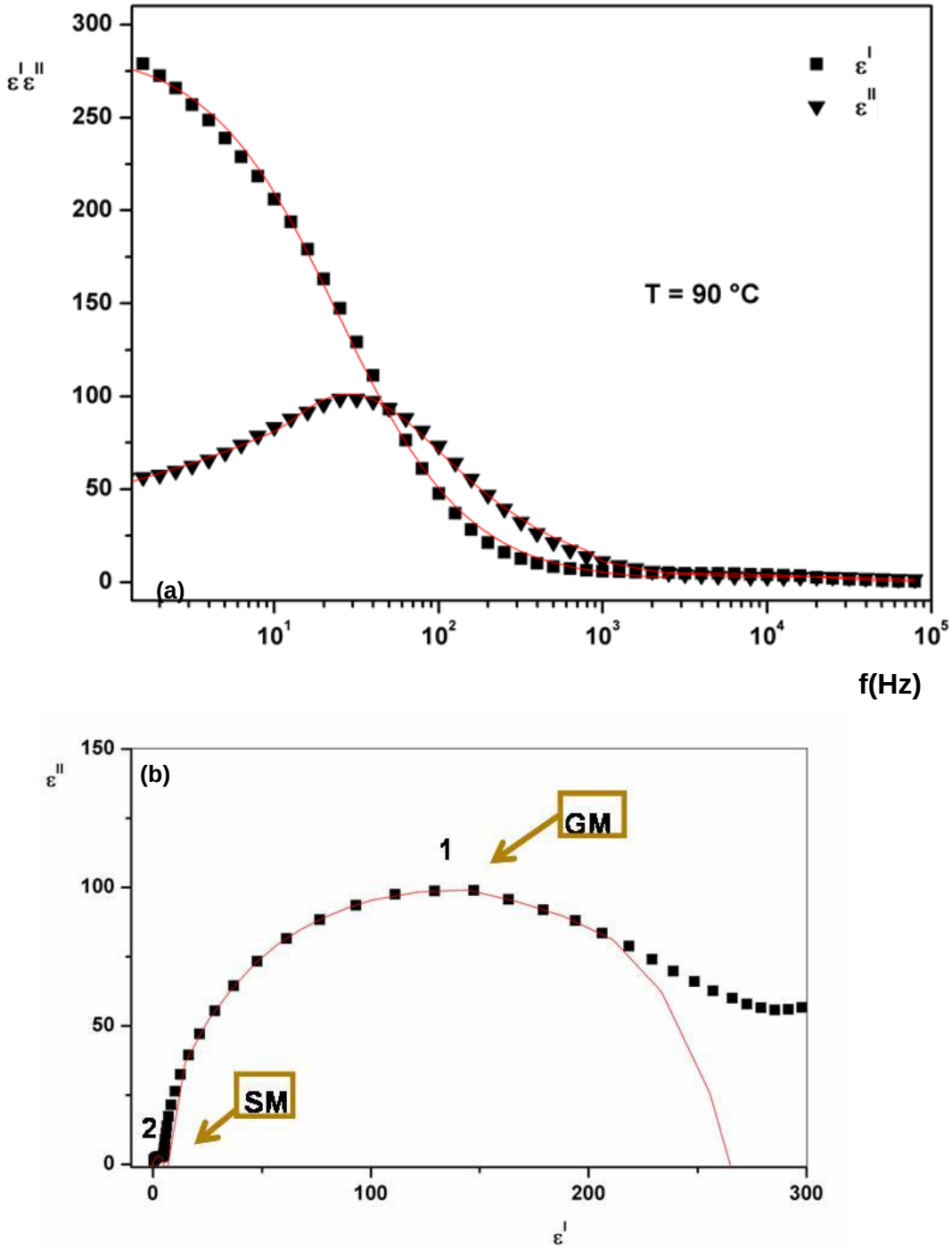

Figure 3.4: Dispersion and absorption curves (a) and Cole-Cole plot (b) of the dielectric spectra acquired for W-129 at 90°C. The solid red line shows the best theoretical fit of the Cole–Cole equation into experimental data[1].

[1] L. Marino et al., Molecular Crystals and Liquid Crystals 04/2012; 558(1):120.

The EFM (Electrostatic Force Microscopy) technique has proven effective to bring out a visual image of antiferroelectric phase in W-129. Applying a voltage the material orients itself in a particular way, assuming this aspect:

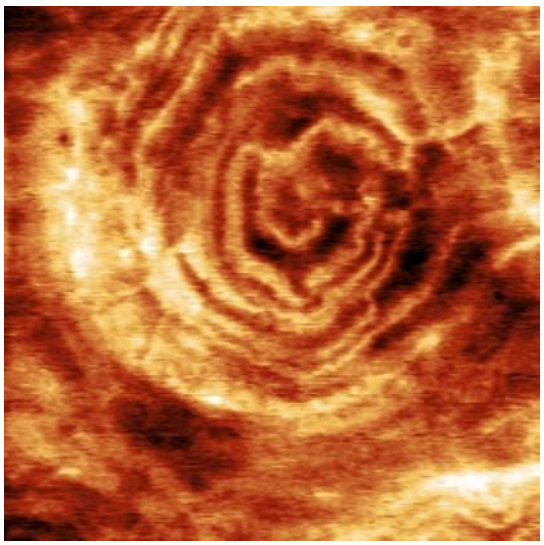

Figure 3.5: EFM (1.5 Vpp AC; -7 V DC) W-129 on ITO.

In the second EFM image (Fig. 3.6) we see that changing the sign of the applied voltage the material reorients itself. Dark and light areas appear inverted respect to the first EFM image (Fig. 3.5).

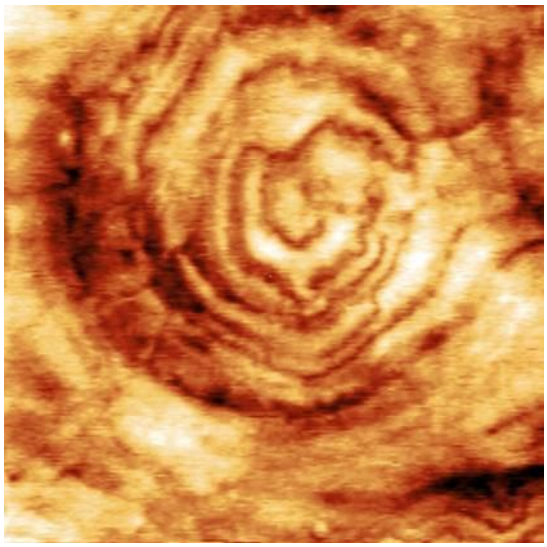

Figure 3.6: EFM (1.5 Vpp AC; 7 V DC) W-129 on ITO.

Finally, in the AFM (Atomic Force Microscopy) topography acquired without voltage, the texture looks very different:

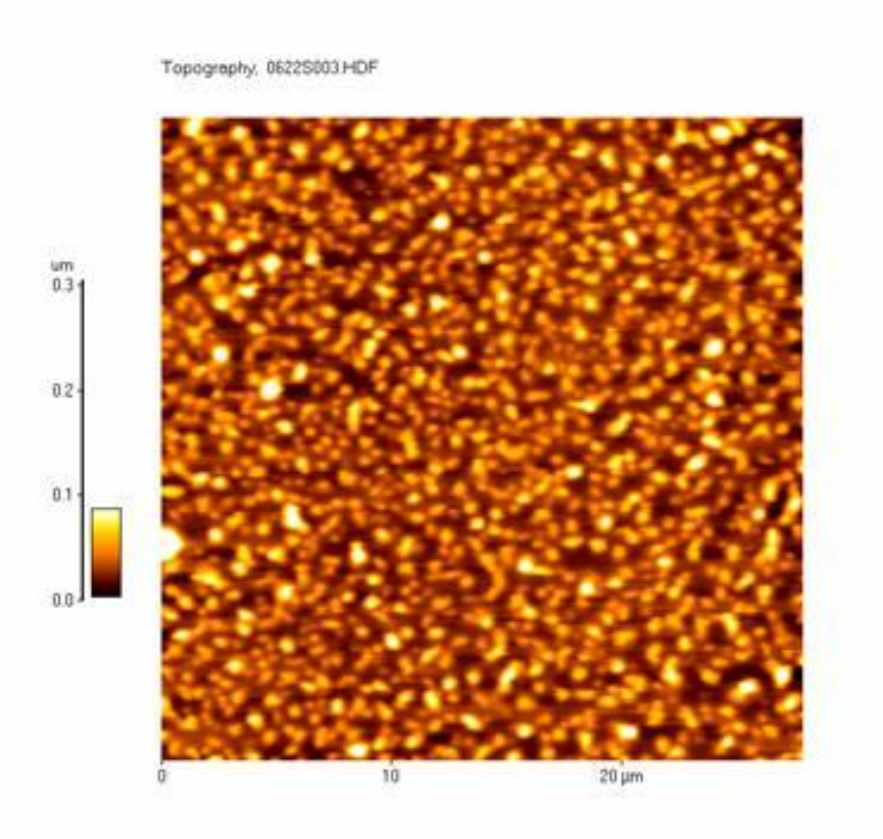

Figure 3.7: AFM topography (without applied voltage)[2].

Considering the possible presence of different SmC* subphases other techniques have been employed. A first step was made by considering DSC technique. In figure 3.8, the transition from SmCa* to SmC* weakly emerges in a range of temperature between 80°C and 90°C in heating condition. From 110°C the material began to melt. In cooling condition a transition between 90°C and 80°C appears and another weak signal is revealed between 45°C and 55°C degrees. In order to obtain the DSC thermograms the sample was held for one minute at 30°C then heated from 30°C to 150°C, finally the sample was cooled from 150°C to 30°C at a rate of 5°C/min.

[2] *AFM/EFM courtesy of Dr E. Bruno and Dr M. P. De Santo, Physics Department – University of Calabria.*

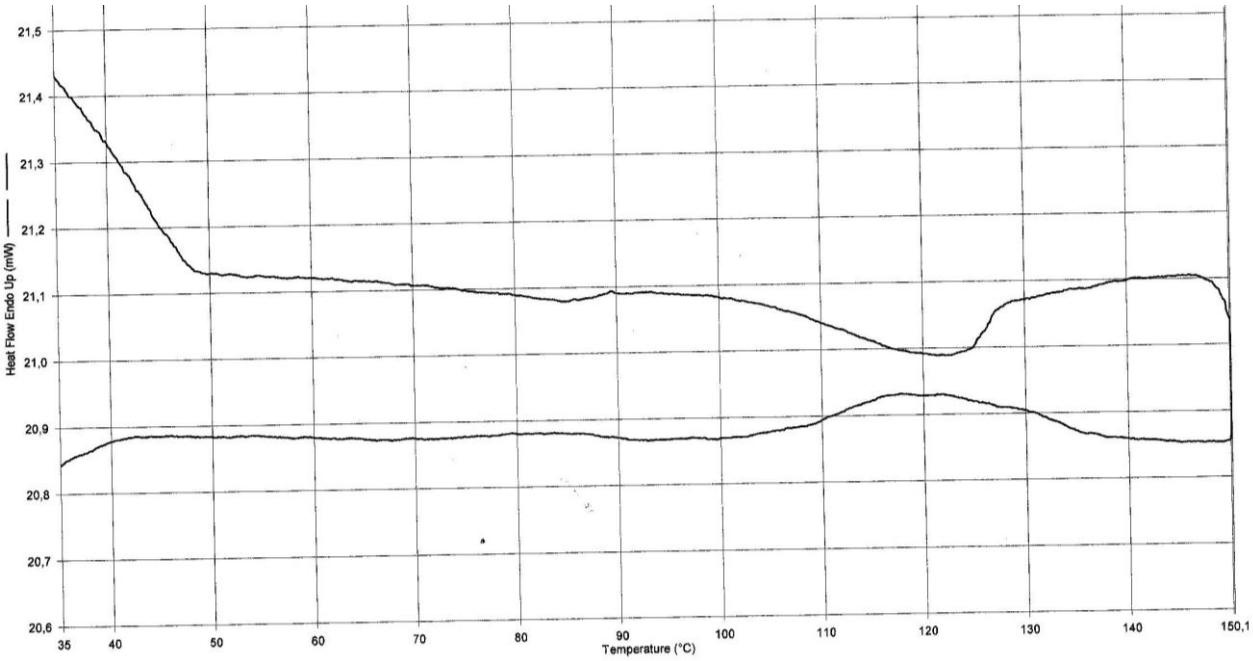

Figure 3.8: DSC thermograms on heating (lower curve) and on cooling (upper curve) of the W-129 mixture, obtained at 5°C/min scanning rate[3].

Typical "focal conic" textures were observed for smectic Ca* phase (Fig. 3.9) in polarizing microscope pictures acquired for the mixture between untreated glass slide. The stripes are associated with the pitch (less than 2 μm) of the helical suprastructure. From room temperature to 46°C there are not many changes. From polarizing microscope pictures emerges that the situation does not change abruptly as the temperature increases, even if a slight change seems to be between 45 and 50°C. At 57°C the liquid crystal mixture begins to transire and at 69°C the material is completely transit. At 72°C another subphase is detected and from 79°C the stripes are not more visible. During SmC* and SmA* phases, the typical chiral striped texture is not visible. The stripe texture is normally seen in materials with short pitch. If the pitch is equal to the wavelength of the visible light, then the texture has a color which is complementary to the color of the reflected light. Tilted phases with a long pitch, for instance SmC_γ*, SmC_α* and in some cases the SmC* phase and the SmA* phase, normally don't exhibit a striped texture [12]. At 110°C the material melts passing from smectic to isotropic phase.

[3] *DSC courtesy of Prof. D. Pucci, Chemistry Department – University of Calabria.*

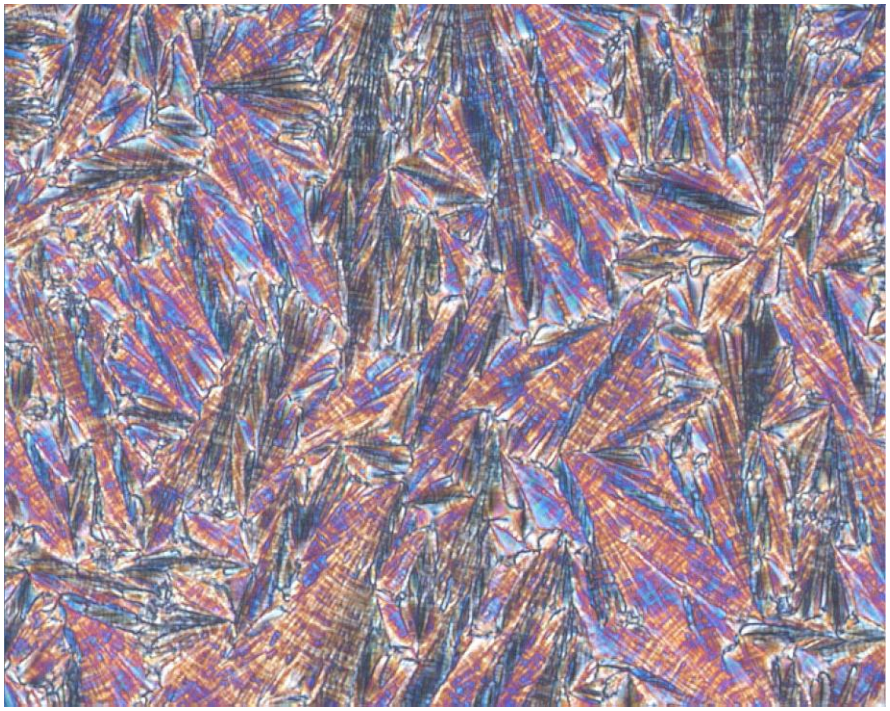

Figure 3.9: Polarizing microscope picture obtained at room temperature[4].

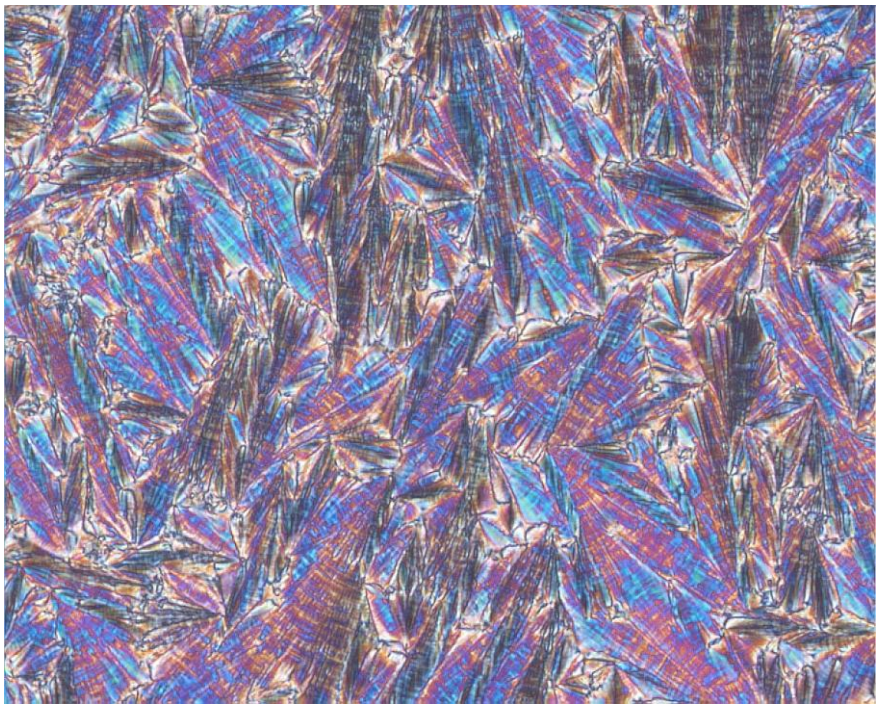

Figure 3.10: Polarizing microscope picture obtained at 46°C.

[4] Pictures were acquired using a 20x objective (*courtesy of Prof. D. Pucci, Chemistry Department – University of Calabria).*

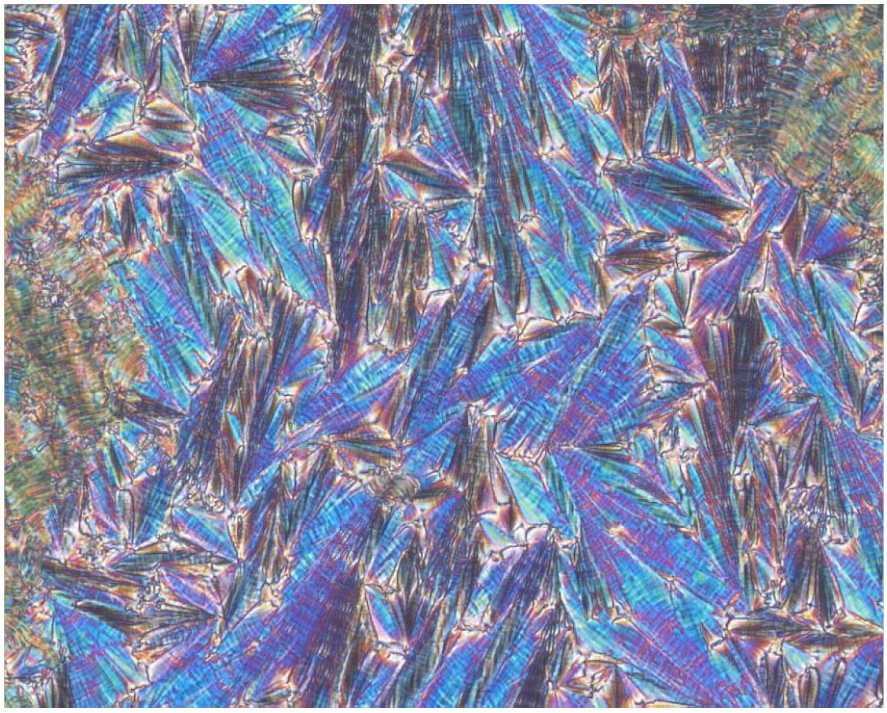

Figure 3.11: Polarizing microscope picture obtained at 57°C.

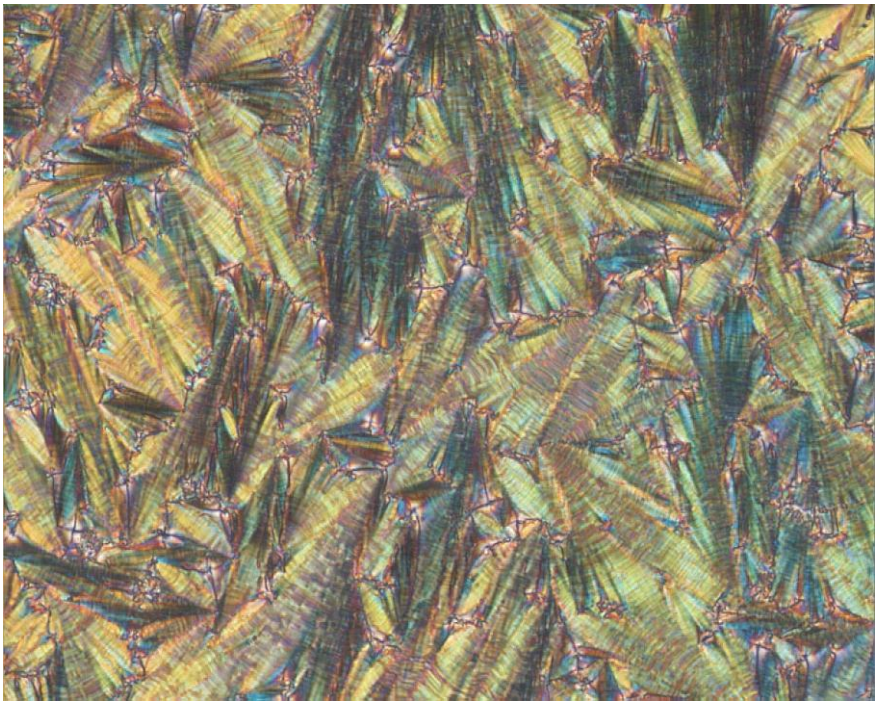

Figure 3.12: Polarizing microscope picture obtained at 69°C.

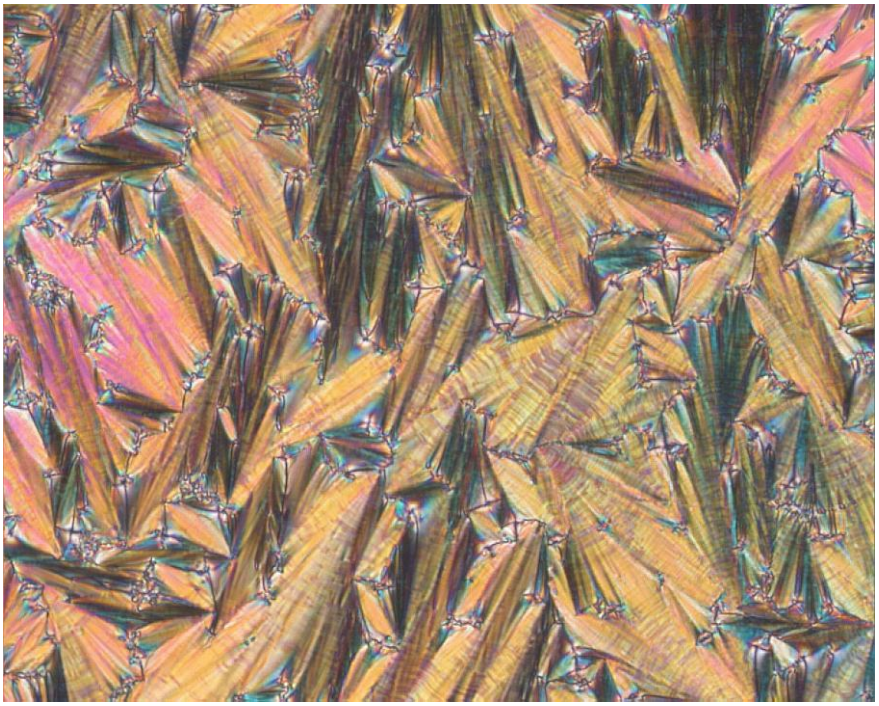

Figure 3.13: Polarizing microscope picture obtained at 72°C.

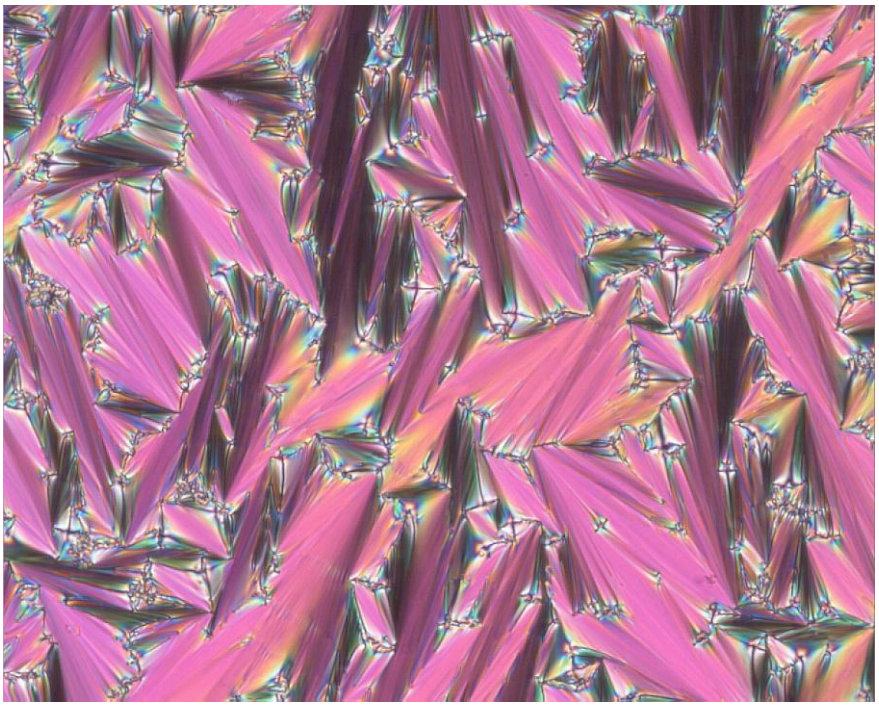

Figure 3.14: Polarizing microscope picture obtained at 79°C.

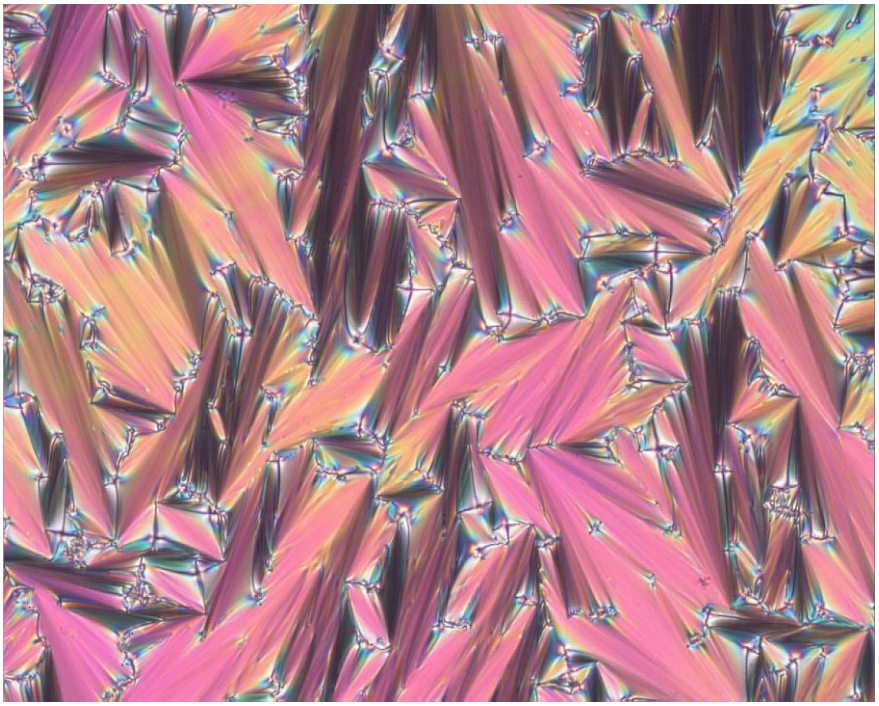

Figure 3.15: Polarizing microscope picture obtained at 98°C.

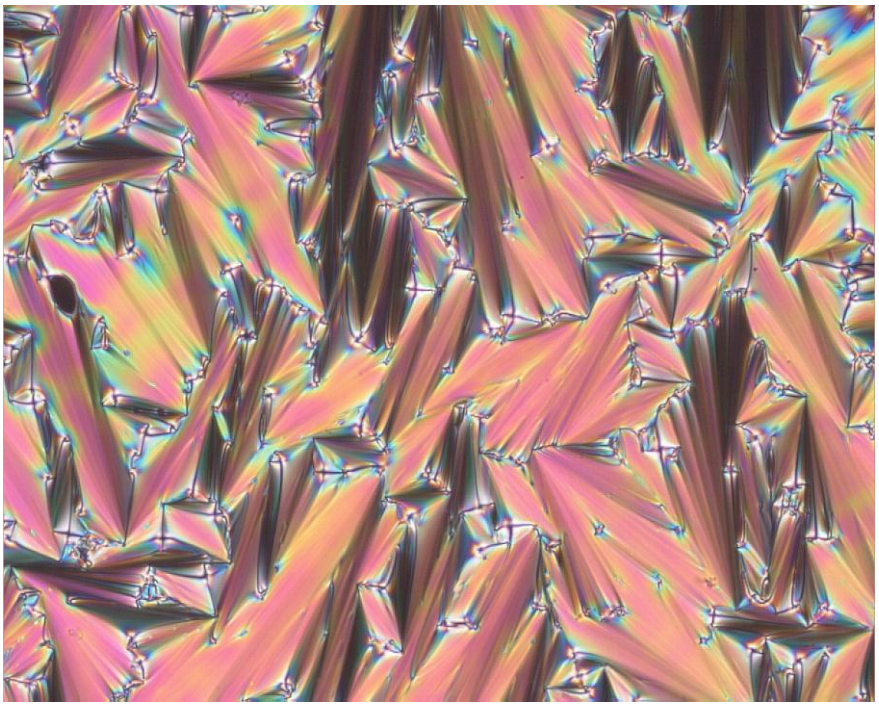

Figure 3.16: Polarizing microscope picture obtained at 101°C.

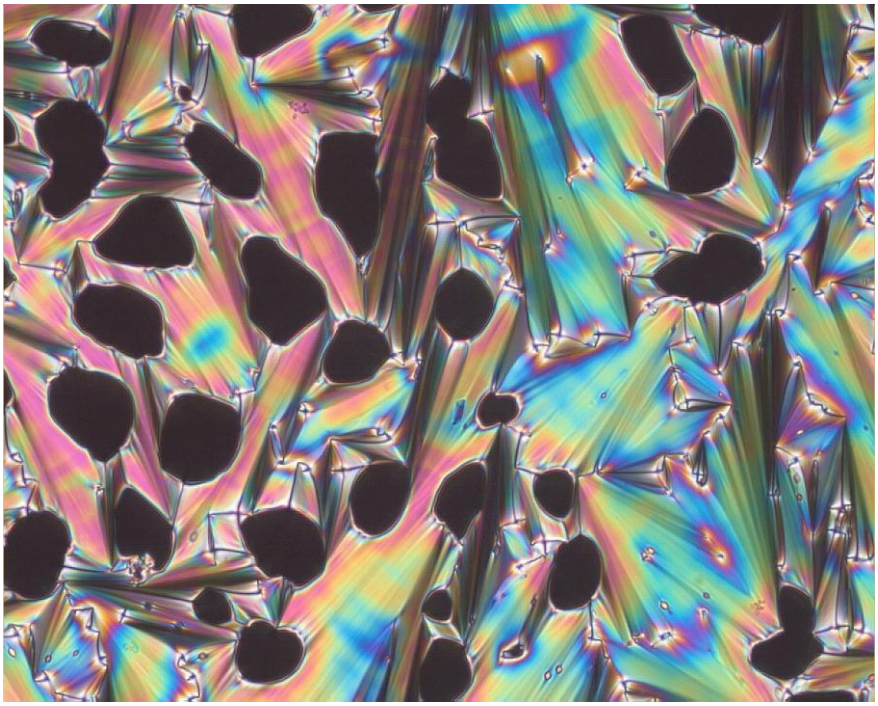

Figure 3.17: Polarizing microscope picture obtained at 104°C.

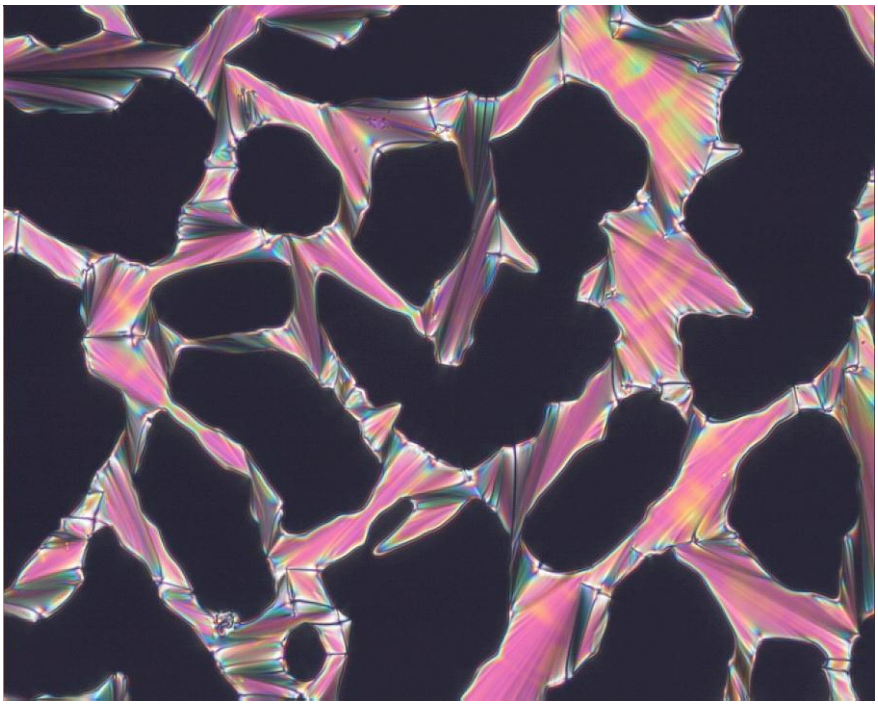

Figure 3.18: Polarizing microscope picture obtained at 110°C.

In cooling condition, microscope pictures look different from that obtained in heating condition. The transition from isotropic to smectic A* phase begins at 115°C (fig. 3.18). The typical focal conic texture is present without stripes from 105 to 80°C and finally, from 77°C striped texture makes its appearance. From 70 to 60°C another transition should be present and in Figure 3.24 we can see that the texture is similar to that obtained in heating condition at room temperature.

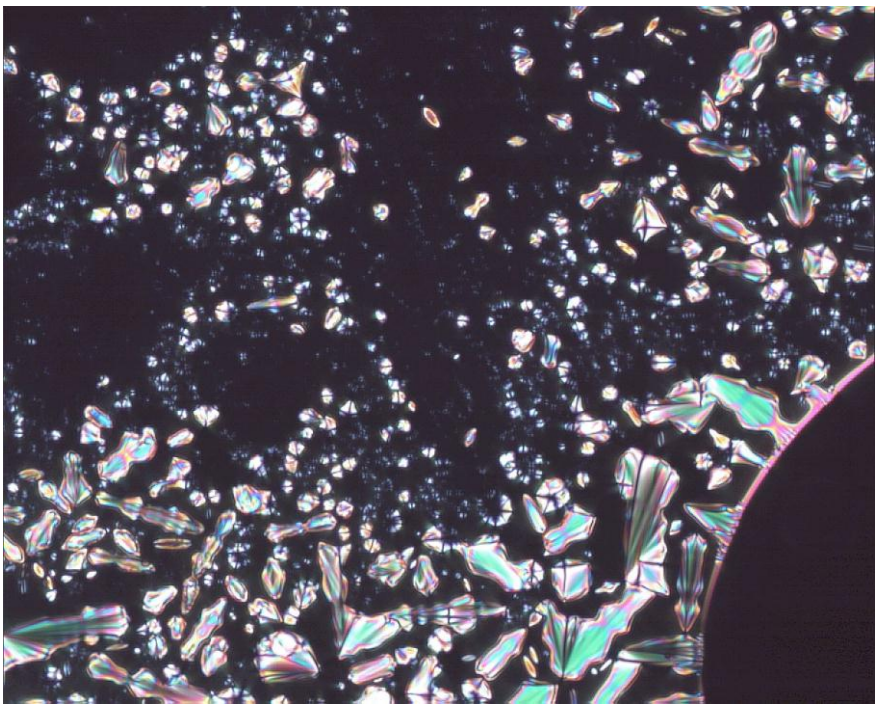

Figure 3.19: Polarizing microscope picture obtained at 115°C.

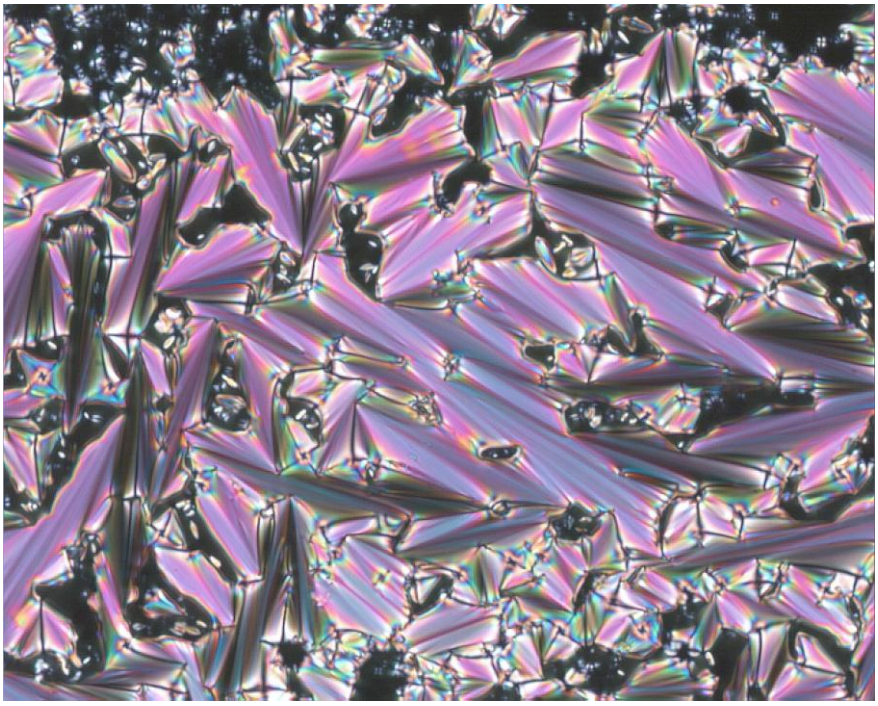

Figure 3.20: Polarizing microscope picture obtained at 105°C in cooling condition.

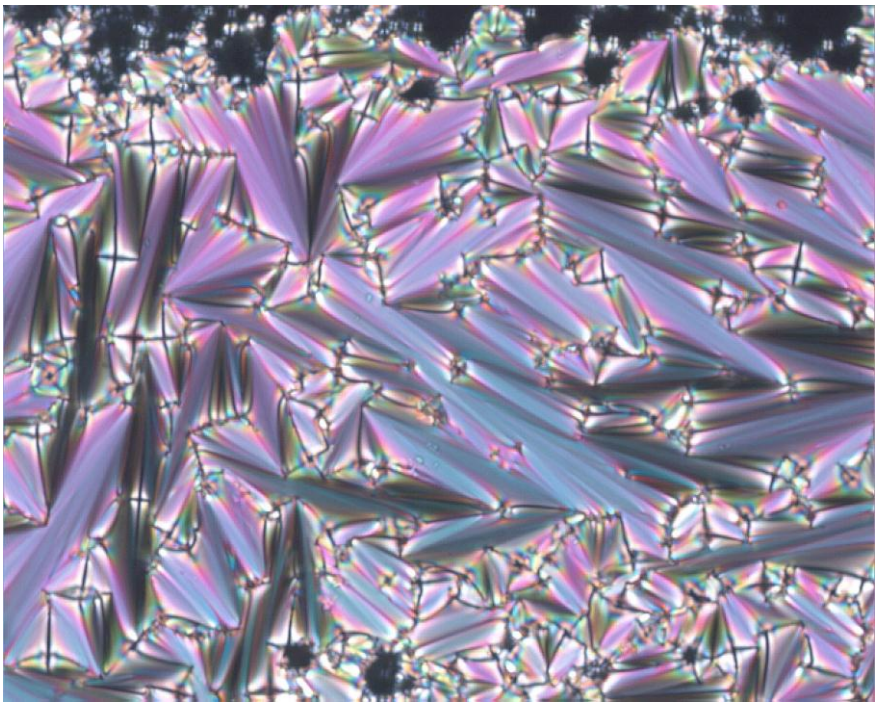

Figure 3.21: Polarizing microscope picture obtained at 90°C in cooling condition.

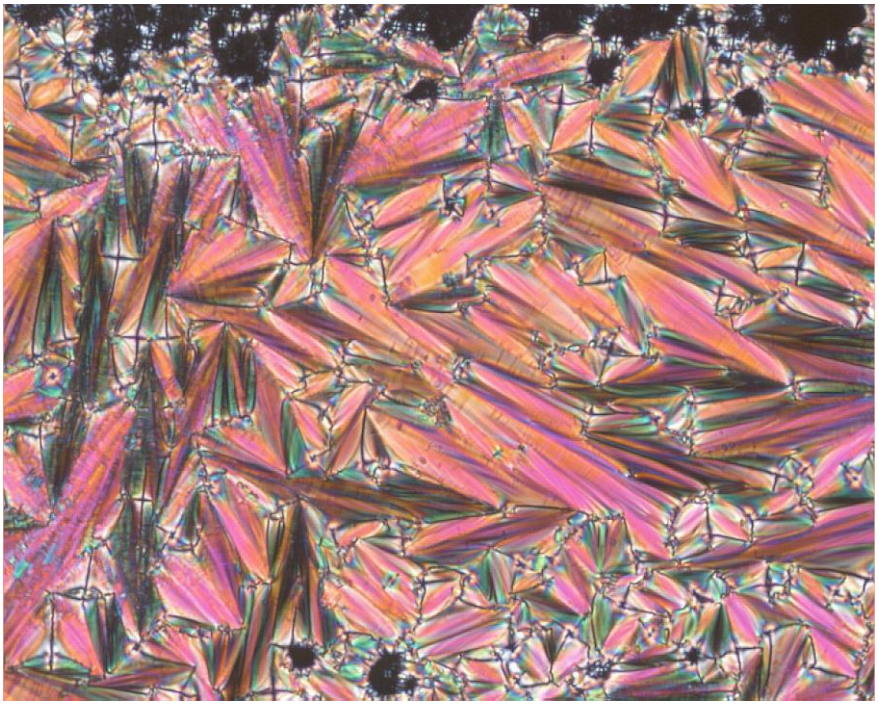

Figure 3.22: Polarizing microscope picture obtained at 77°C in cooling condition.

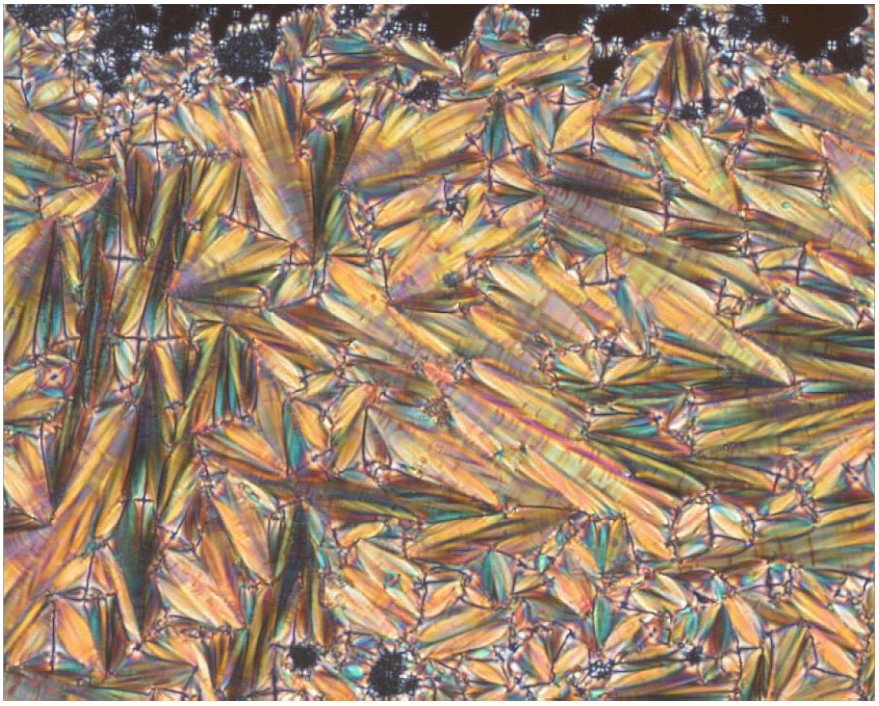

Figure 3.23: Polarizing microscope picture obtained at 70°C in cooling condition.

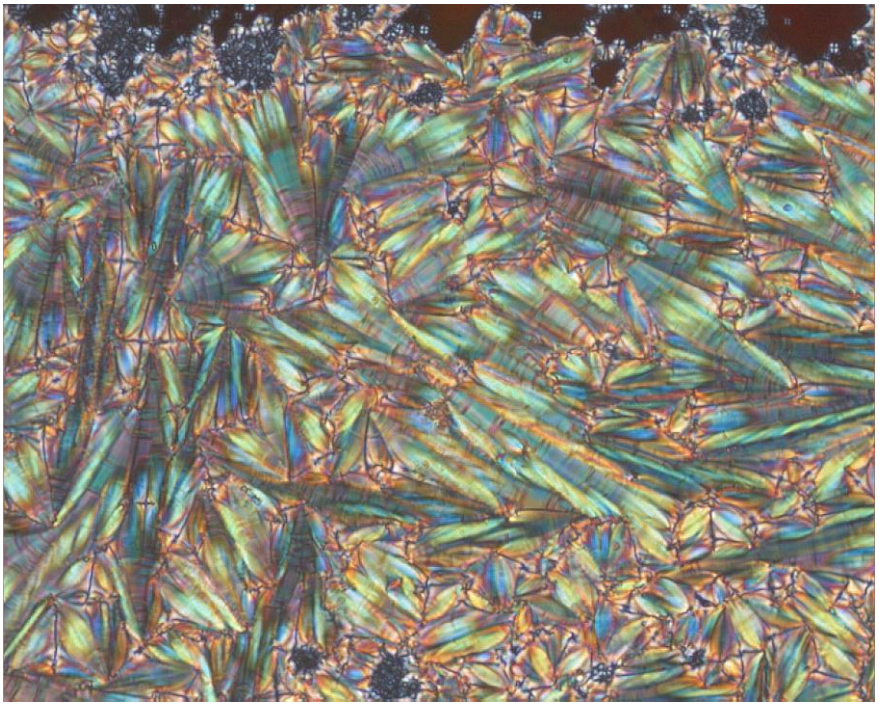

Figure 3.24: Polarizing microscope picture obtained at 63°C in cooling condition.

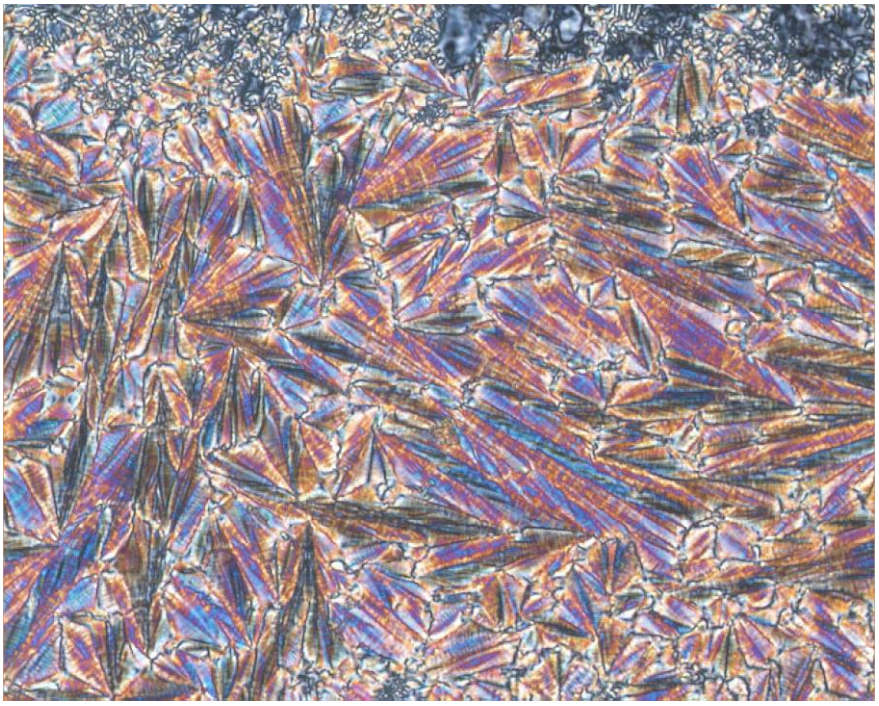

Figure 3.25: Polarizing microscope picture obtained at 30°C in cooling condition.

Other dielectric spectra were acquired at narrower intervals of temperature. In heating condition, from room temperature to 120°C and in cooling condition. A 3D Cole Cole plot in function of temperature shows the different behaviours present during SmCa* phase in a range from 30 to 80°C.

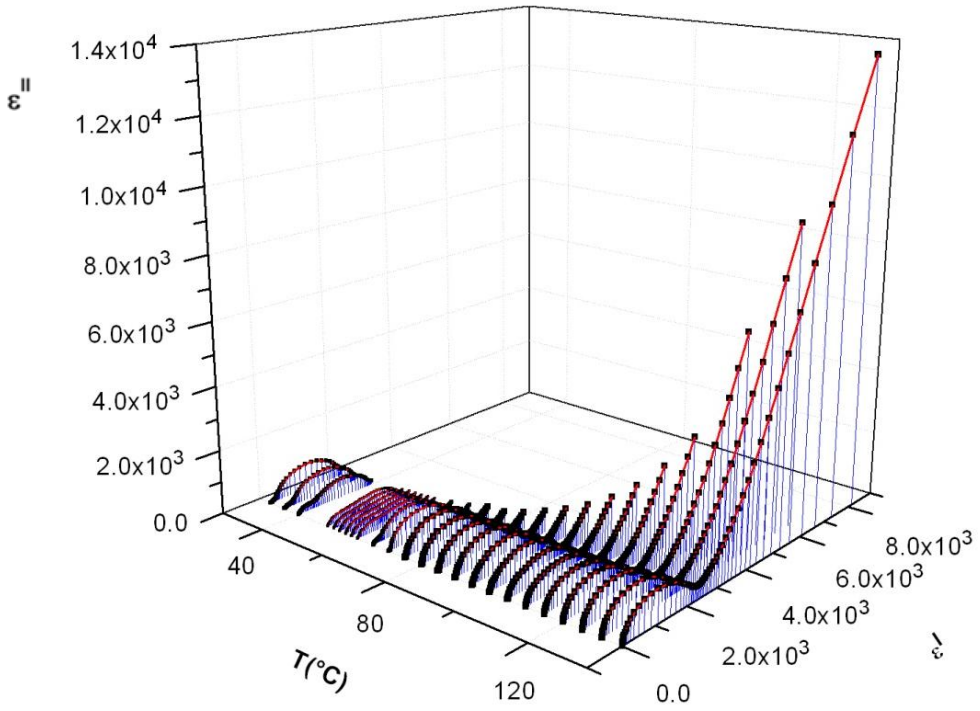

Figure 3.26: Cole Cole plots of W-129 in function of temperature.

Dielectric spectra acquired during heating condition show the presence of two subphases: one at 49.9°C (see Fig. 3.26) and another one at 57.7°C (see Fig.3.27). These transition temperatures confirm what we have just seen at the microscope. They could be identified with Sm*C*FI1* and Sm*C*FI2* phases. At ~ 80°C (Fig. 3.28) there is the transition to smectic C* phase with a well defined Goldstone mode (in the spectrum indicated with HN1) and at ~ 98°C (Fig. 3.29) the transition to SmA* begins. All experimental data have been fitted with Havriliak-Negami (HN) equation with the adjoint of conductivity contribution (due to ionic charges movement).

$$\varepsilon_{\perp}^{*}(f) = \varepsilon_{\infty} + \sum_{j} \frac{\Delta\varepsilon_{j}}{[1+(if\tau_{j})^{a_j}]^{b_j}} - \frac{i\sigma}{\varepsilon_0 (2\pi f)^{n}} \qquad (3.2)$$

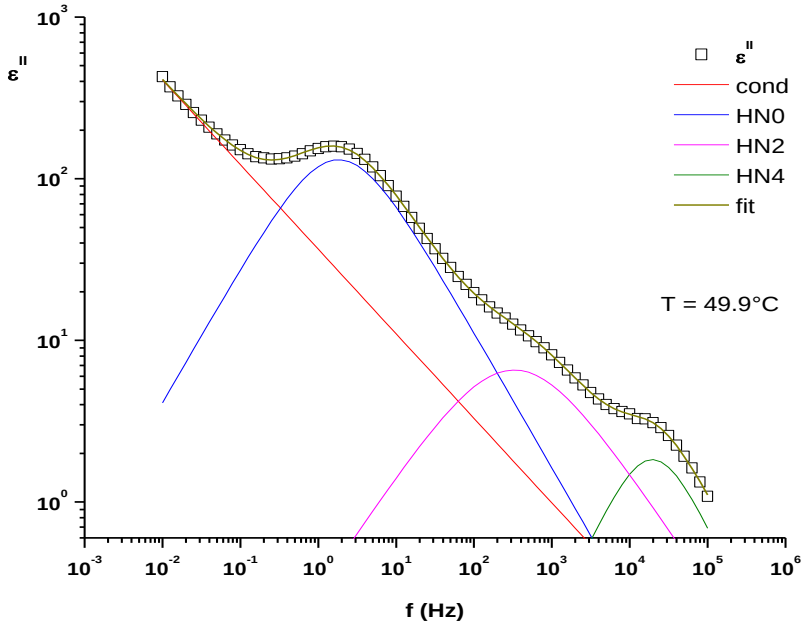

Figure 3.27: Loss curve acquired at 49.9°C.

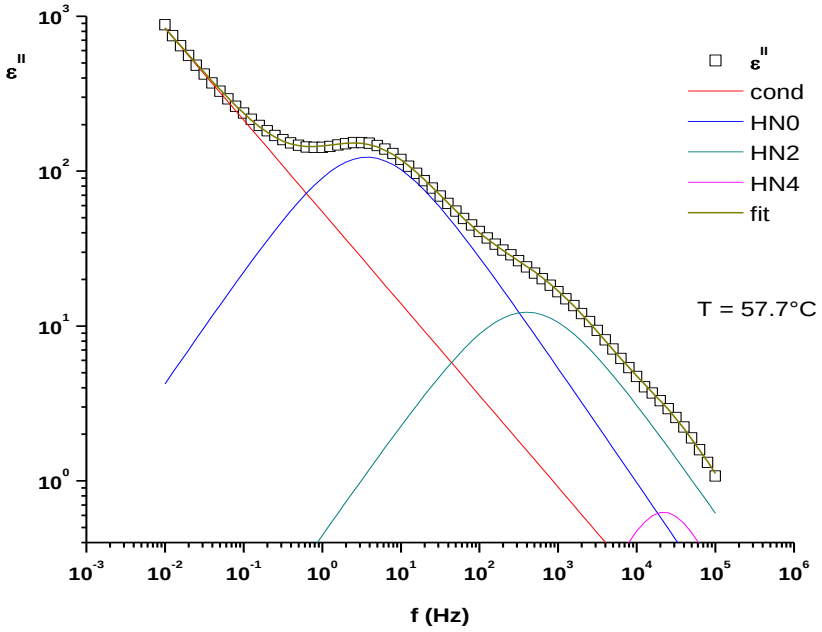

Figure 3.28: Loss curve acquired at 57.7°C.

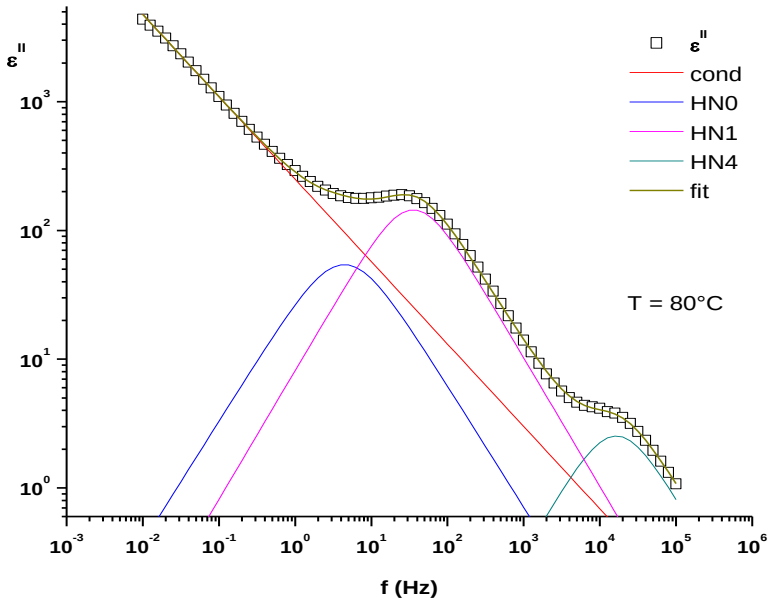

Figure 3.29: Loss curve acquired at 80°C.

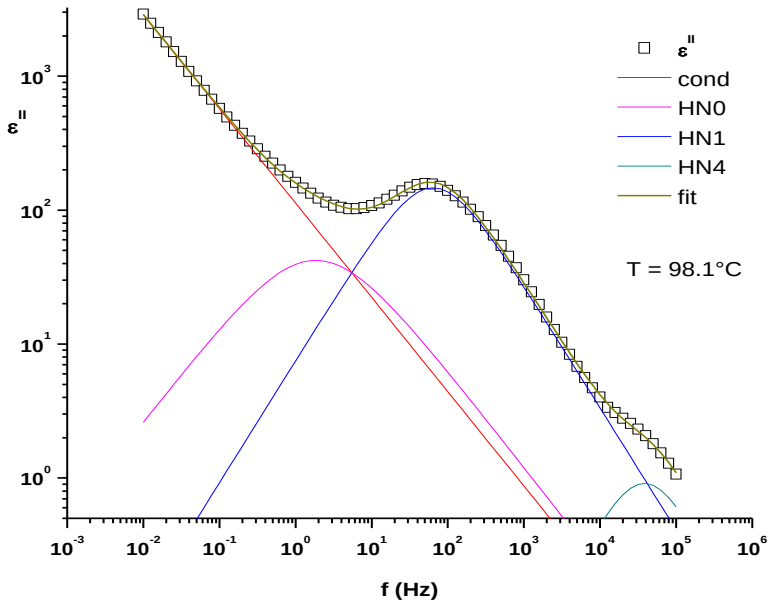

Figure 3.30: Loss curve acquired at 98.1°C.

Something different happens in cooling condition where different subphases make their appearance. This is a possible scheme of transition temperatures:

Iso 102.4°C SmA* 76.4°C SmC* 60.2°C SmC? 56°C SmC$_{FI2}$* 46.9 SmC$_{FI1}$* 37.3°C SmC? 25/20°C SmCa*

From results obtained with polarizing microscope, a transition should take place at 77°C and, from DSC, another one should be placed between 45°C and 55°C; this is in partial agreement with what has been obtained with dielectric spectroscopy. It is difficult to say anything definitive about the other two subphases; they could be do to other effects such as helix inversions or surface-induced effects (see paragraph 1.6.3). As regards the SmC_α* phase, it should not be present, but the memory effects of the W-129 make difficult an accurate evaluation.
The typical antiferroelectric phase with an in-phase (HN1) and an anti-phase mode (HN3) make its appearance at 25/20°C.

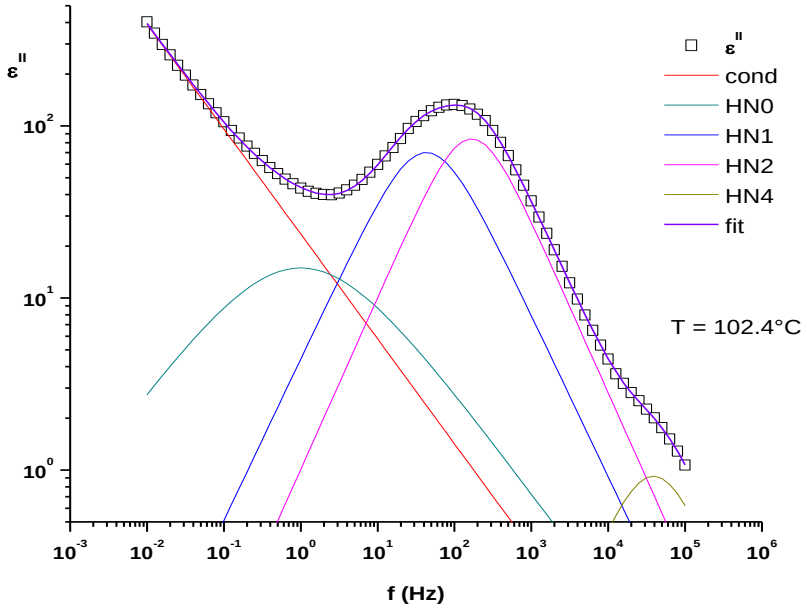

Figure 3.31: Loss curve acquired at 102.4°C in cooling condition.

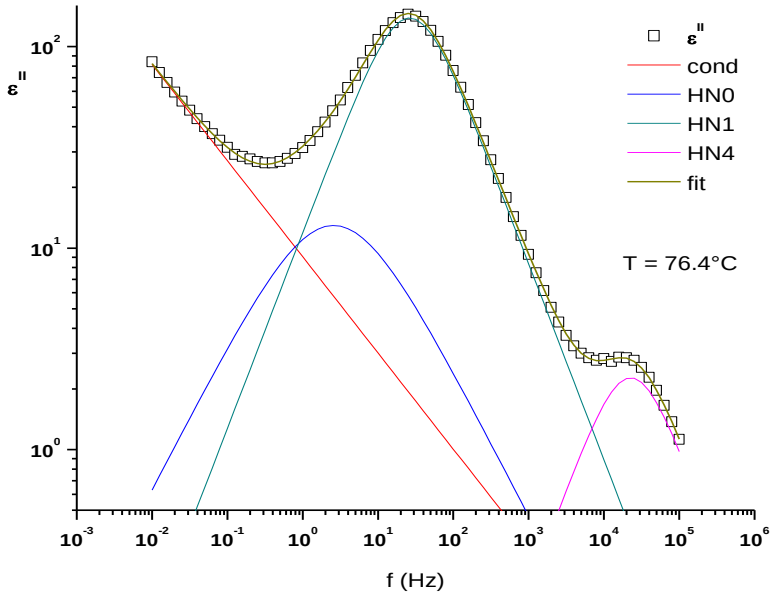

Figure 3.32: Loss curve acquired at 76.4°C in cooling condition.

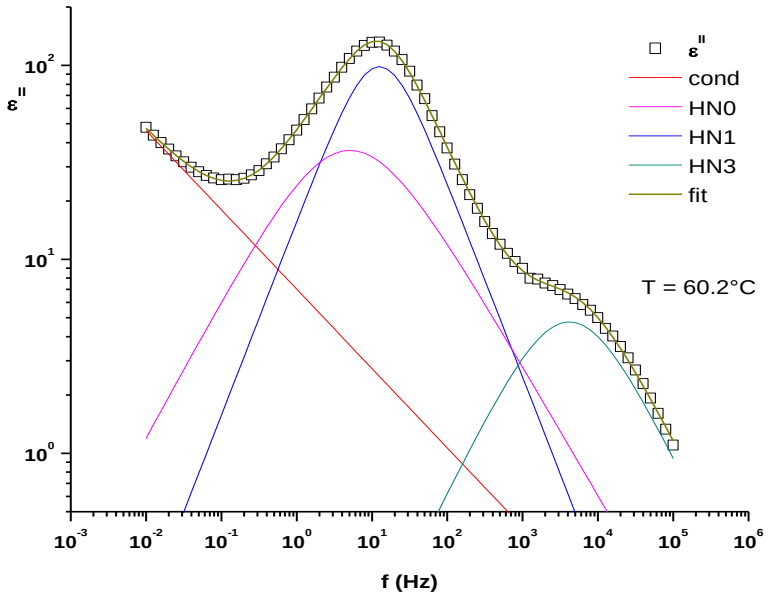

Figure 3.33: Loss curve acquired at 60.2°C in cooling condition.

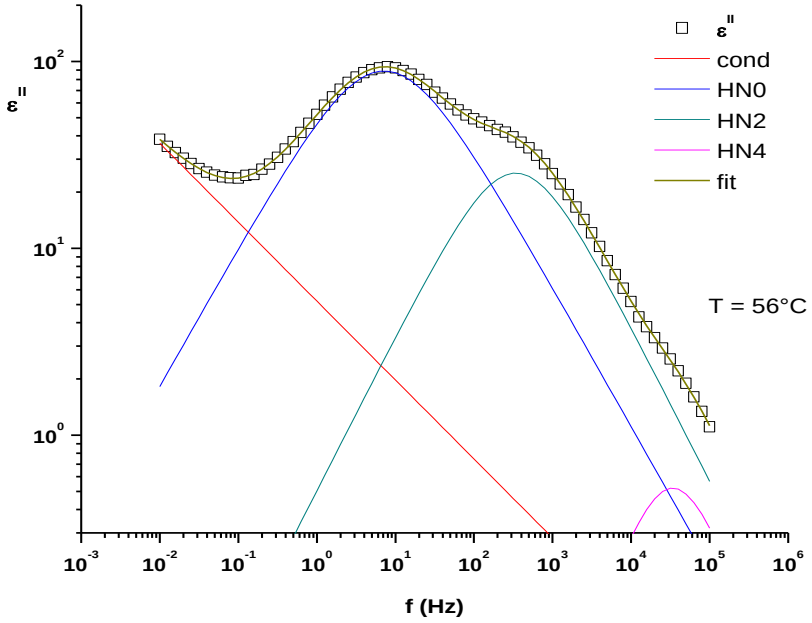

Figure 3.34: Loss curve acquired at 56°C in cooling condition.

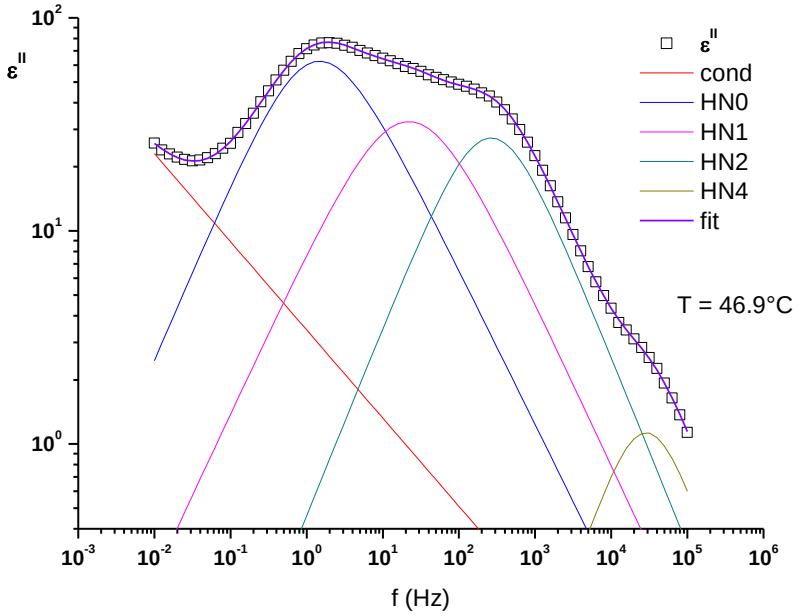

Figure 3.35: Loss curve acquired at 46.9°C in cooling condition.

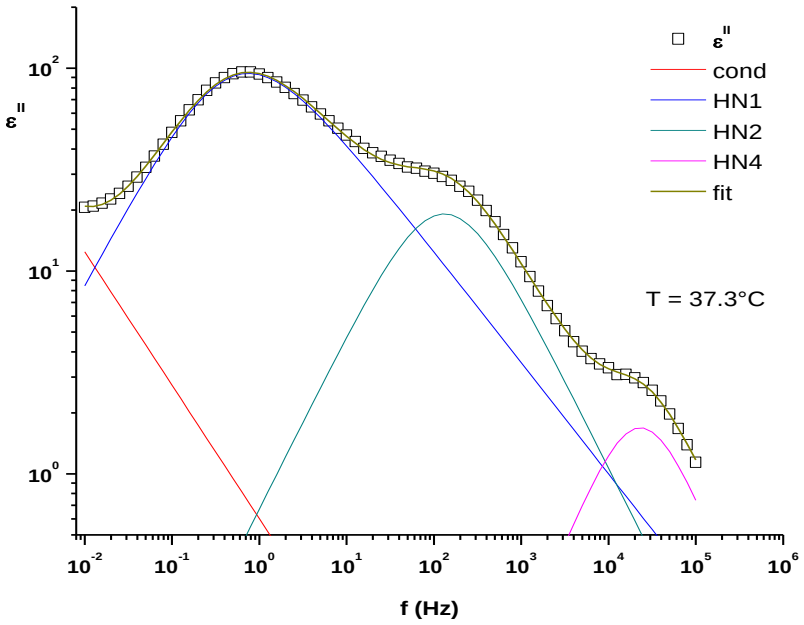

Figure 3.36: Loss curve acquired at 37.3°C in cooling condition.

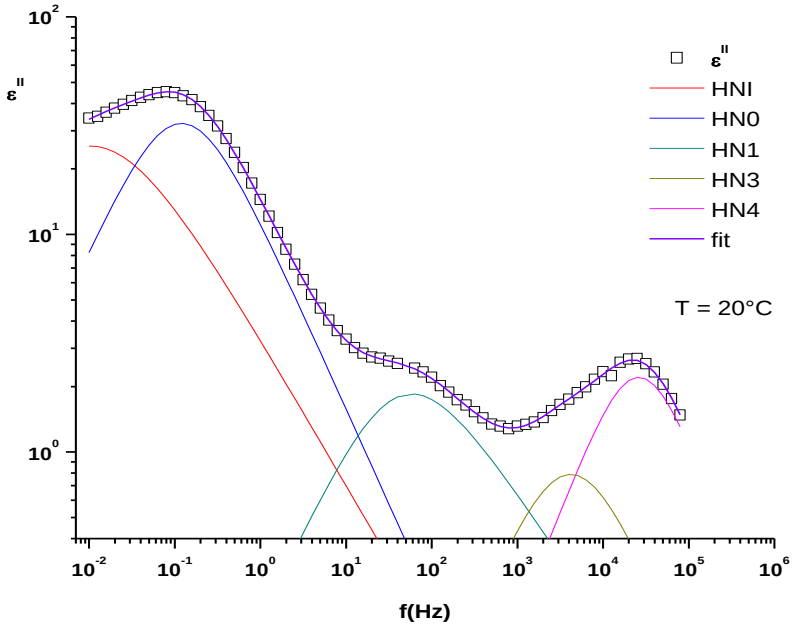

Figure 3.37: Loss curve acquired at 20°C in cooling condition.

Finally, in Figures 3.37 and 3.38, we see dielectric increments relative to Goldstone mode in function of temperature, acquired in heating and in cooling conditions.

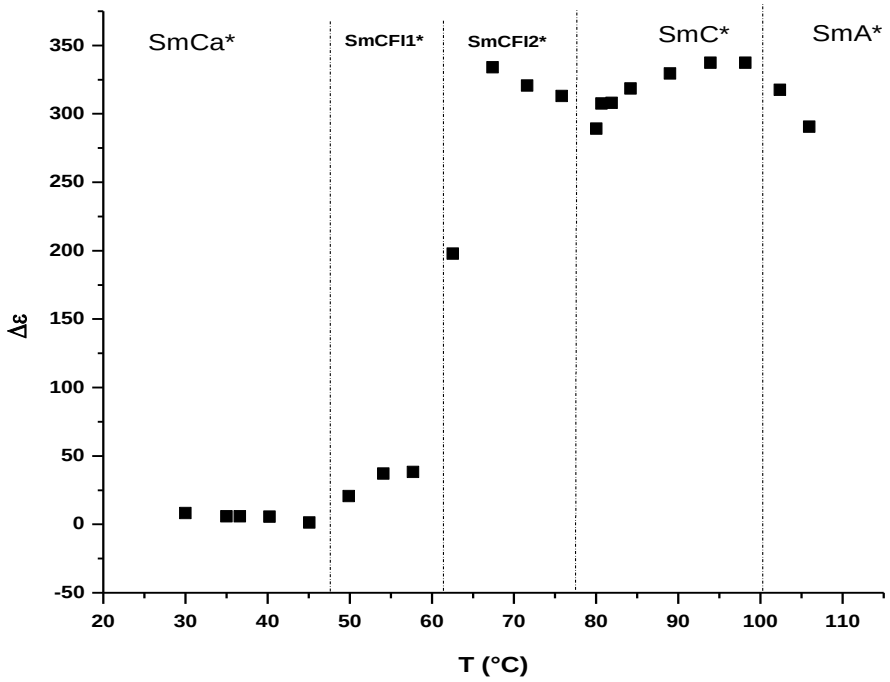

Figure 3.38: Dielectric increment acquired in heating condition in function of temperature. The dashed lines indicate the phase transitions.

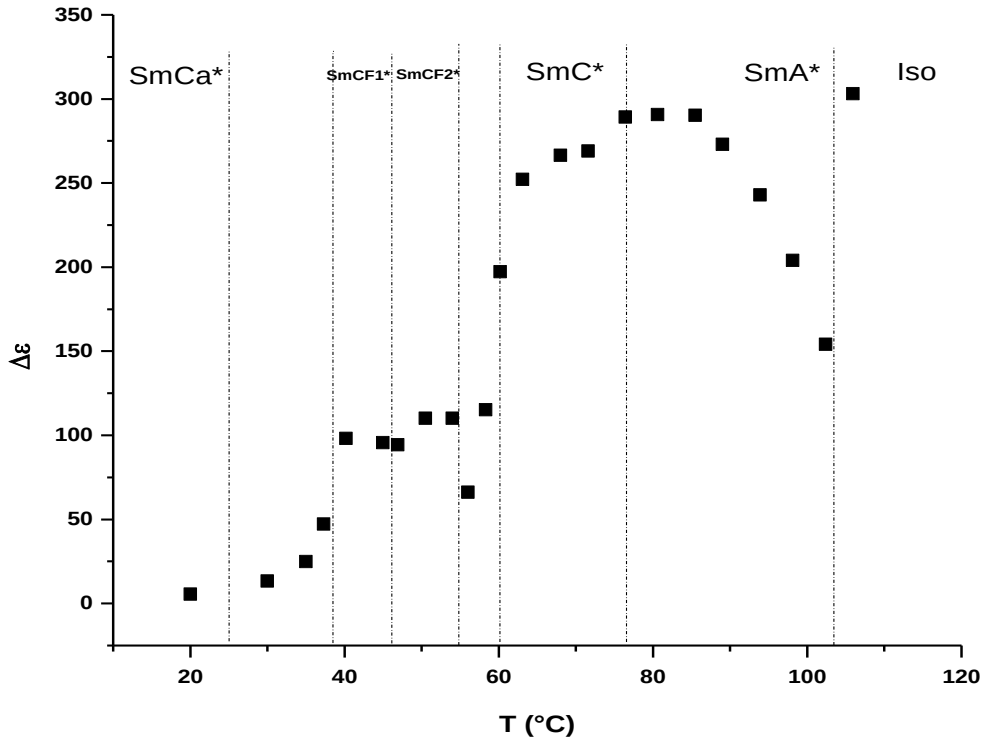

Figure 3.39: Dielectric increment acquired in cooling condition in function of temperature. The dashed lines indicate the phase transitions.

3.4 Determination of anti-phase viscosity using dielectric spectroscopy

Two of the collective modes of an AFLC are goldstone modes in which the motion of the directors around the smectic cone in adjacent layers are either in the same direction (the in-phase mode) or in opposite directions (the anti-phase mode) [13, 14]. These modes each have an associated time constant that can be measured either dielectrically or optically. It is well known that the anti-phase mode has a much smaller time constant than the in-phase mode [13].

The in-phase and anti-phase mode relaxations for W-129 occur at 63.47 Hz and 23.80 kHz, respectively at a temperature of 25°C (see Table 1). We therefore have the following time constants:

$$\tau_{in-phase} = 2.51 \cdot 10^{-3} s \tag{3.3}$$

$$\tau_{anti-phase} = 6.69 \cdot 10^{-6}\, s$$

Using the following relations we can evaluate the anti-phase viscosity [15]:

$$\eta_{anti-phase} = \tau_{anti-phase} \cdot 2(\Gamma + 4\Delta) \tag{3.4}$$

where Γ and Δ are coefficients of the interlayer coupling energy [15].
In modelling AFLCs, an interlayer interaction energy of the form:

$$F = \Gamma \cos^2 \varphi_b - \Delta \cos^2 2\varphi_b \tag{3.5}$$

is often assumed [16, 17]. The first term is a dipolar term that favours anticlinic ordering in preference to synclinic ordering (when Γ is positive). The second term is a quadrupolar term which favours both AF and F states equally (Δ is also positive). It is possible to measure values for the coefficients Γ and Δ using a variety of experimental techniques. For example, the strength of the anti-phase relaxation in the dielectric spectrum should be [16, 17]:

$$\Delta\varepsilon = \frac{P_s^2}{4\varepsilon_0(\Gamma + 4\Delta)} \tag{3.6}$$

which, knowing the spontaneous polarisation Ps, should give a value for the combination of parameters: $\Gamma + 4\Delta$. In the case of W-129, where:

$$P_s = 300\,\mathrm{nC/cm^2} \text{ (from Dabrowski [8])} \tag{3.7}$$

and $\Delta\varepsilon = 5.20$, we obtain:

$$\Gamma + 4\Delta = 4.89 \cdot 10^4 \frac{J}{m^3} \tag{3.8}$$

Finally, anti-phase viscosity is:

$$\eta_{antiphase} = \tau_{antiphase} \cdot 2(\Gamma + 4\Delta) \approx 0.7 Pa \cdot \sec \tag{3.9}$$

3.5 Summary

Some physical parameters like dielectric increments, dielectric relaxation times, characteristic frequencies of the various modes, have been determined for W-129. A great variety of relaxation responses that could indicate the presence of different SmC* subphases has been observed with the DS technique in partial agreement with other techniques like DSC and optical microscopy. An evaluation of the viscosity of the anti-phase motion has been done.

References

1. P. Maltese, Mol. Cryst. Liq. Cryst., 215, 57–72 (1992)

2. Koen D'havé, Application of Antiferroelectric Liquid Crystals with High Tilt, PhD Thesis, University of Gent: Belgium (2002)

3. P. Perkowski, D. Lada, K. Ogrodnik, J. Rutkowska, W. Piecek, Z.Raszewski, Opto-Electron. Rev., 16(3), 271–276 (2008)

4. C. Filipic, T. Carlsson, A. Levstik, B. Zeks, F. Gouda, S. T. Lagerwall, K. Skarp, Phys. Rev. E, 38, 5833–5839 (1988)

5. F. Gouda, K. Skarp, S. T. Lagerwall, Ferroelectrics, 113, 165–206 (1991)

6. S. Hiller, A. M. Biradar, S. Wrobel, W. Haase, Phys. Rev. E, 53, 641–649 (1998)

7. M. Rajiv, M. Abhishek Kumar, S. Abhishek Kumar, C. Purna Bahadur, J. P. Shukla, Soft Materials, 5(4), 207–218 (2007)

8. R. Dabrowski, Mol. Cryst. Liq. Cryst., 421, 1 (2004)

9. M. A. Perez Jubindo, A. Ezucer, J. Etxebarria, A. Remon, M. J. Tello, M. Marcos, J. L. Serrano, Mol. Cryst. Liq. Cryst., 159, 137 (1988)

10 K. S. Cole, R. H. Cole, J. Chem. Phys., 9, 341 (1941)

11. L. Marino, E. Bruno, M. P. De Santo, F. Ciuchi, S. Marino, N, Scaramuzza, Mol. Cryst. Liq. Cryst., 558(1),120 (2012)

12. A. Dahlgren, M. Buivydas, F. Gouda, L. Komitov, Liquid Crystals, 25 (5), 553, (1998)

13. M. Buivydas, F. Gouda, S. Lagerwall, B. Stebler, The molecular aspect of the double absorption peak in the dielectric spectrum of the antiferroelectric liquid crystal phase. Liq. Cryst., 18(6), 879–886 (1995)

14. Y. Panarin, O. Kalinovskaya, J. Vij, The investigation of the relaxation processes in antiferroelectric liquid crystals by broad band dielectric and electro-optic spectroscopy. Liq. Cryst., 25(2), 241–252 (1998)

15. Lesley A. Parry-Jones, Emmanouil E. Kriezis, Steve J. Elston, Determination of Material Constants of Antiferroelectric Liquid Crystal Mixture CS4001, Molecular Crystals and Liquid Crystals, 410:1, 129-140 (2004)

16. L. Parry-Jones, Field Driven Helix Distortion and Switching in Antiferroelectric Liquid Crystals. DPhil Thesis, Oxford University, United Kingdom (2001)

17. L. Parry-Jones, S. Elston, Theoretical prediction of the dielectric spectrum of an antiferroelectric liquid crystal. J. Appl. Phys., 92(1), 449–455 (2002)

Chapter 4

Dielectric Characterization of Gold Nanoparticles/Antiferrolectric Liquid Crystal Composites

4.1 Introduction

By its very nature, nanotechnology is of immense academic and industrial interest as it involves the creation and exploitation of materials with structural features in between those of atoms and bulk materials, with at least one dimension limited to between 1 and 100 nm. Most importantly, the properties of materials with nanometric dimensions are, in most instances, significantly different from those of atoms or bulk materials.

An important subset of nano-structured materials is represented by the so-called nano-composites which consist of nano-particles dispersed in a continuous three-dimensional matrix. In this context are of particular interest the nano-composites obtained by dispersing metallic nano-particles in liquid crystal materials. Liquid crystals by their very nature are suitable candidates for matrix-guided synthesis and self-assembly of nanoscale materials [1]. Since liquid crystals are anisotropic materials they provide an excellent support for self assembling of nano-particles into larger ordered superstructures. Moreover, as the liquid crystals responds to small external forces (electric, magnetic, mechanical stress), dispersed nano-particles can be forced to follow the molecular order of the hosting medium effectively controlling the order of the superstructure. Interesting results has been obtained by dispersing ferroelectric nano-particles [2] in nematic liquid crystals (NLCs). Low concentration of such nano-particles increase the orientational order of the hosting NLCs, the nematic-isotropic transition temperature and decrease the Frederiks transition threshold voltage.

We present our recent investigations on the electric properties of W-129, an orthoconic smectic liquid crystal mixture, and on the same liquid crystal mixture doped with gold nanoparticles (GNPs). W-129 presents both ferroelectric and antiferroelectric smectic C phases and an high spontaneous polarization (> 300 nC/cm^2 at room temperature) in virtue of its tilted chiral

structure. The gold nanoparticles are functionalized with a polymer which presents both hydrophilic and hydrophobic properties in dependence of temperature.

4.2 Materials and Techniques

The material used for this study is the liquid crystal mixture W-129, just seen in the previous chapter, which presents both ferroelectric and antiferroelectric smectic C phases, doped with gold nanoparticles suspended in water (50% W-129 + 50% AuNPs in ultrapure water).

The W-129 phase sequence (see Chapter 3), obtained from DSC measurements is:

Cr-13/15°C-SmCa*-84.5°C-SmC*-102.3°C-SmA*-117/125.2°C-Iso

The concentration of the nanoparticles suspended in water is 0.05 mg/ml. The diameter of the uncoated particles is 12 nm while the diameter of the coated particle is 25 nm (a SEM image of the gold nanoparticles is shown in Figure 4.1). The polymeric coating is (MEO2MA) 90-co-(OEGMA) 10 with a transition temperature from hydrophilic to hydrophobic equal to 40° C. In Fig. 4.2 we see a SEM (Scanning Electron Microscopy) image of W-129 doped with gold nanoparticles. We can appreciate that the nanoparticles are roughly randomly distributed.

A Japanese planar aligned commercial cell (EHC Ltd, Tokyo, Japan) with a thickness of (2.0 ± 0.2) μm and an ITO resistance of 100 Ω /□ has been used. The mixture with gold nanoparticles was introduced into the cells using capillary suction, after the cell was heated in order to make evaporate water.

The dielectric measurements have been carried out using an EG&G 273A galvanostat-potentiostat/impedentiometer controlled by the impedance software M398 in order to acquire the real and imaginary part of impedance in the frequency range 10 mHz – 100 kHz with a maximum applied voltage of 500 mV (RMS).

4.3 Results and discussion

Four spectra have been acquired at 25°C (below polymer capping transition temperature - 40°C -) and at 55°C (above transition temperature) for pure W-129 and for doped one respectively. The nanoparticles cause some changes in the spectra, in fact they emphasize the peak situated between 10 and 100 Hz

(see Fig. 4.3 and 4.4). This is a well-known result already seen in the past [3]. After transition temperature the situation changes; the peak at lower frequencies is not more emphasized but becomes expanded and a mode at higher frequencies appears (Fig. 4.5). The continuous red line represents fit of the real permittivity data and blue continuous line represents the fit of imaginary data. For this purpose we have used Havriliak-Negami equation with the adjoint of conductivity term (see Eq. 3.2).

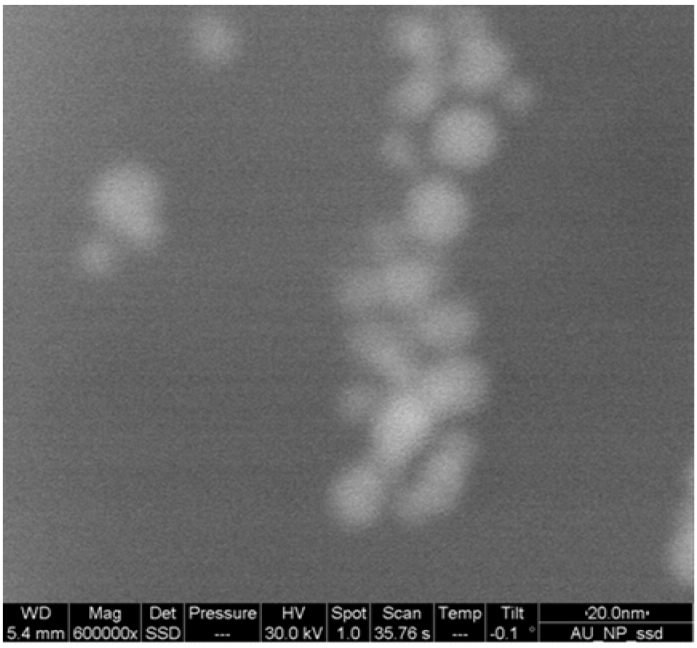

Figure 4.1: SEM image for AuNPs

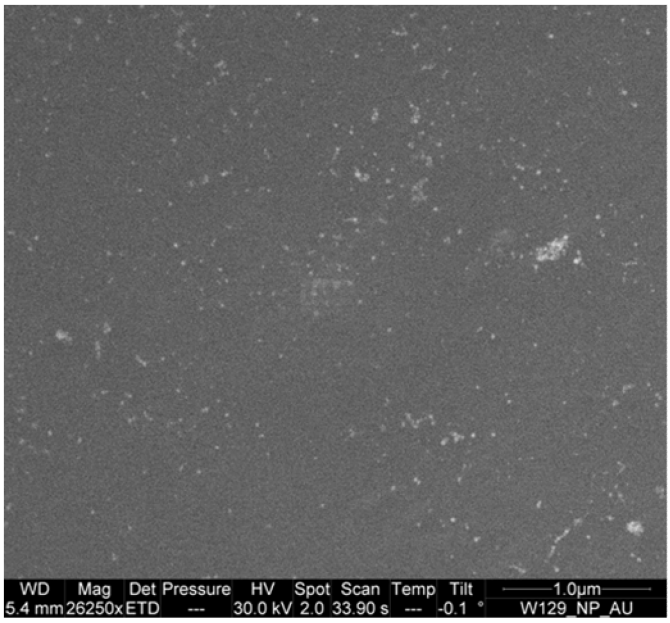

Figure 4.2: SEM image for W-129+AuNPs

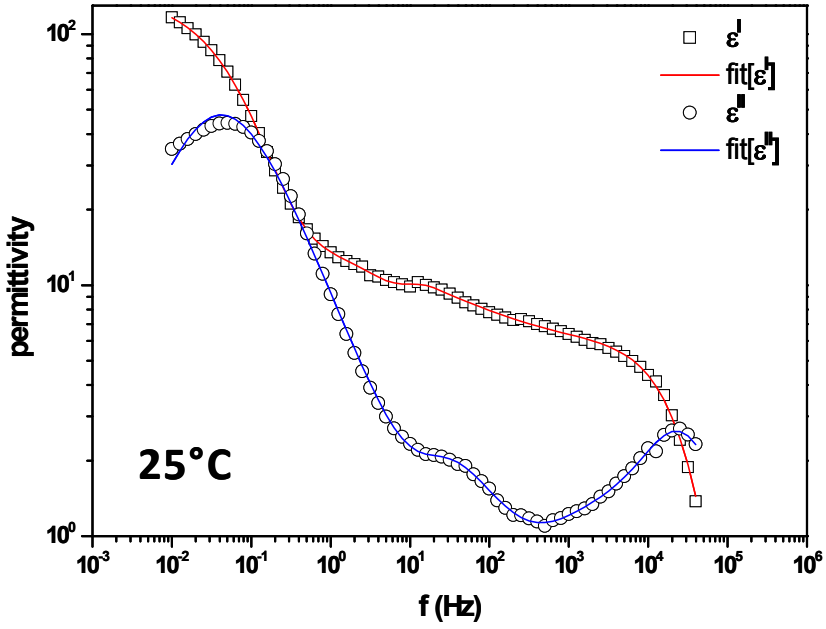

Figure 4.3: Real and imaginary part of permittivity of W-129 acquired at 25°C with an applied voltage of 500 mV.

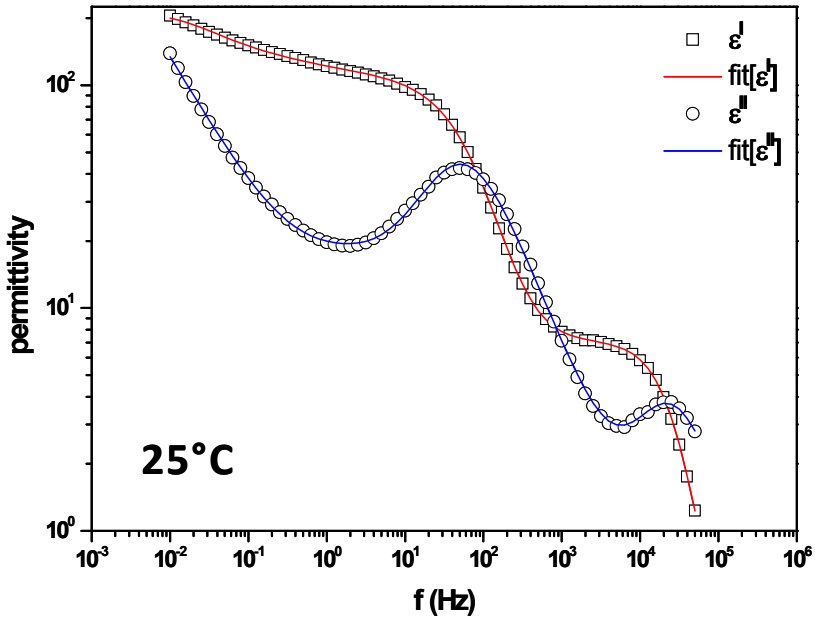

Figure 4.4: Real and imaginary part of permittivity of W-129 doped with gold nanoparticles acquired at 25°C with an applied voltage of 500 mV.

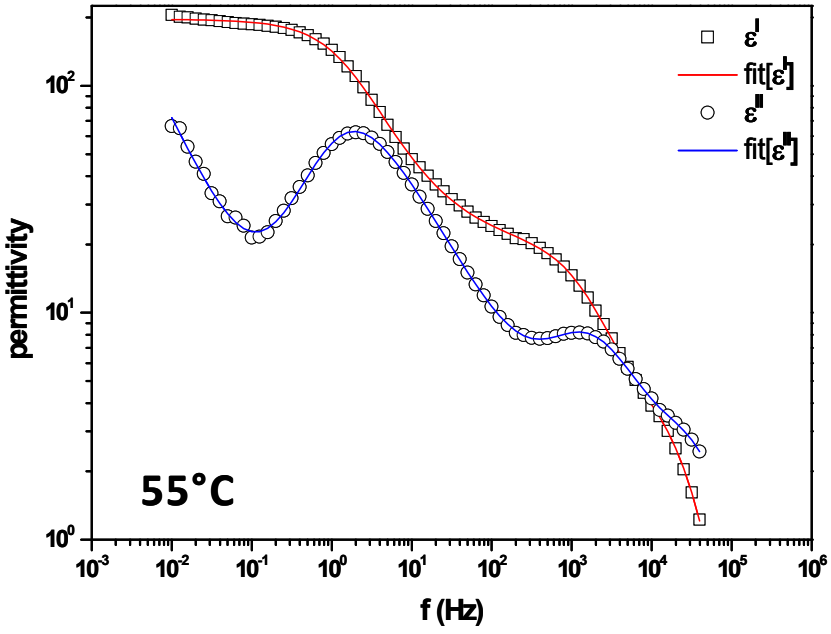

Figure 4.5: Real and imaginary part of permittivity of W-129 acquired at 55°C with an applied voltage of 500 mV.

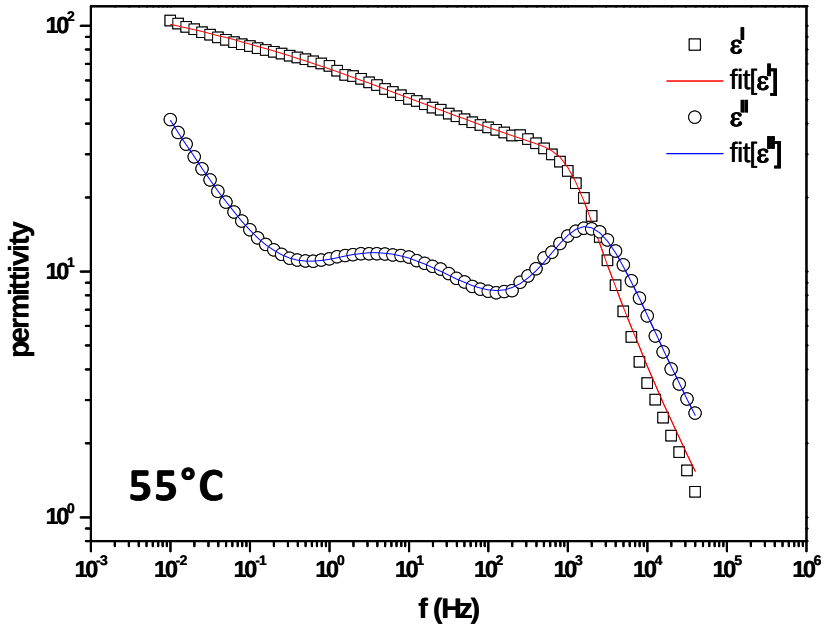

Figure 4.6: Real and imaginary part of permittivity of W-129 doped with gold nanoparticles acquired at 55°C with an applied voltage of 500 mV.

An important effect due to the presence of gold nanoparticles is the increasing of the dielectric strength. This increase can be understood on the basis of molecular interaction between the antiferroelectric liquid crystal mixture and the gold nanoparticles. It is assumed that after the addition of nanoparticles, the disorder in FLC is reduced unlike other cases where it increased considerably [4]. Results obtained from fitting of experimental data are synthesized in Tables 4.1 and 4.2.

Table 4.1. Fitting parameters for DC conductivity and relaxation processes of W-129 at two different temperatures in heating conditions.

T (°C)	σ [S/cm]	n	σ_err	n_err
55	2.64	0.72	0.01	0.02

T (°C)	HN1_f_r	HN1_$\Delta\varepsilon$	HN1_a	HN1_b	HN1_f_r_err	HN1_$\Delta\varepsilon$ _err	HN1_a_err	HN1_b_err
25	0.04	$1.30 \cdot 10^2$	0.80	1.00	1.03	1.45	0.01	0.00
55	1.39	$1.63 \cdot 10^2$	0.94	0.67	1.04	1.13	0.01	0.02

T (°C)	HN2_f_r	HN2_$\Delta\varepsilon$	HN2_a	HN2_b	HN2_f_r_err	HN2_$\Delta\varepsilon$ _err	HN2_a_err	HN2_b_err
25	$2.72 \cdot 10^1$	3.26	1.00	0.65	1.31	1.14	0.00	0.28

T (°C)	HN3_f_r	HN3_$\Delta\varepsilon$	HN3_a	HN3_b	HN3_f_r_err	HN3_$\Delta\varepsilon$ _err	HN3_a_err	HN3_b_err
25	$2.05\cdot10^3$	3.02	0.70	0.81	4.62	1.28	0.35	1.02
55	$1.58\cdot10^3$	$1.51\cdot10^1$	0.89	0.97	1.17	0.53	0.04	0.15

T (°C)	HN4_f_r	HN4_$\Delta\varepsilon$	HN4_a	HN4_b	HN4_f_r_err	HN4_$\Delta\varepsilon$ _err	HN4_a_err	HN4_b_err
25	$2.53\cdot10^4$	4.20	1.00	1.00	1.09	0.39	0.00	0.00
55	$2.75\cdot10^4$	2.86	1.00	1.00	1.05	0.37	0.00	0.00

Table 4.2. Fitting parameters for DC conductivity and relaxation processes of W-129 doped with AuNPs at two different temperatures in heating conditions.

T (°C)	σ [S/cm]	n	σ_err	n_err
25	8.82	0.59	0.07	0.02
55	3.74	0.52	0.04	0.01

T (°C)	HN1_f_r	HN1_$\Delta\varepsilon$	HN1_a	HN1_b	HN1_f_r_err	HN1_$\Delta\varepsilon$ _err	HN1_a_err	HN1_b_err
25	8.82	0.59	0.07	0.02	25	8.82	0.59	0.07
55	3.74	0.52	0.04	0.01	55	3.74	0.52	0.04

T (°C)	HN2_f_r	HN2_$\Delta\varepsilon$	HN2_a	HN2_b	HN2_f_r_err	HN2_$\Delta\varepsilon$ _err	HN2_a_err	HN2_b_err
25	$5.46\cdot10^1$	$9.23\cdot10^1$	0.92	1.00	1.03	4.42	0.01	0.00

T (°C)	HN3_f_r	HN3_$\Delta\varepsilon$	HN3_a	HN3_b	HN3_f_r_err	HN3_$\Delta\varepsilon$ _err	HN3_a_err	HN3_b_err
55	$1.71\cdot10^3$	$2.59\cdot10^1$	0.98	0.93	1.03	0.32	0.01	0.03

T (°C)	HN4_f_r	HN4_$\Delta\varepsilon$	HN4_a	HN4_b	HN4_f_r_err	HN4_$\Delta\varepsilon$ _err	HN4_a_err	HN4_b_err
25	$2.42\cdot10^4$	6.57	1.00	1.00	1.01	0.10	0.00	0.00

From DSC (see Fig. 4.6) two peaks clearly emerge; one situated at ~ 55°C and the other at ~ 72°C. In order to obtain the DSC thermograms the sample was held for ten minutes at 35°C then heated from 35°C to 80°C at 10°C/min, finally the sample was cooled from 80°C to 35°C at 10°C/min. Now, we have to recall that in chapter 3 we have just seen that W-129 has different subphases; by optical microscopy we have identified some possible phase transitions situated at ~ 57°C and at ~ 72°C respectively. The broadening of the sub-phase width and of the temperature range over which the transition occurs after the adjoint of gold nanoparticles are possible effects that have been found in recent works. It has been shown that by mixing chiral and achiral dopants or nanotubes with antiferroelectric liquid crystals it is possible to broaden the SmC* subphases significantly, in particular, the intermediate phases (ferrielectric) which typically have a very narrow temperature range [5, 6].

Mixtures of smectics with chiral or achiral dopants were studied to investigate phase stability in the SmC* sub-phases undoubtely linked to dopant concentration. These effects have been measured in the past via calorimetry (DSC), electro-optical measurements and optical microscopy even if it is not yet clear what role the addition of dopants will play. By the dielectric spectroscopy technique we have acquired spectra at different temperatures in order to see the possible phase transitions, in a frequency range of 1Hz-100 kHz (we are not interested to effect linked to ionic diffusion at lower frequencies) and with a maximum applied voltage of 20 mV (RMS) in order to avoid overload current in the cell (due to the presence of gold nanoparticles). From 30°C (see Fig. 4.8), we can see a first slight change at 43°C (Fig. 4.9). A transition is visible at 58.3°C (Fig. 4.10) and another slight change is detected at 62°C (Fig. 4.11) and then, another transition is showed at 68°C (Fig. 4.12). From 71.6°C (Fig. 4.13) to the isotropic phase there are no substantial changes. In the cooling condition, the first transition is detected at 68°C (Fig. 4.15), the next will be reported at 36.6°C (Fig. 4.16). These results are in partial agreement with DSC that reported a first transition at 55°C and another one at 72°C. Pictures captured by the optical microscope (Fig. 4.7) reveal no special changes.

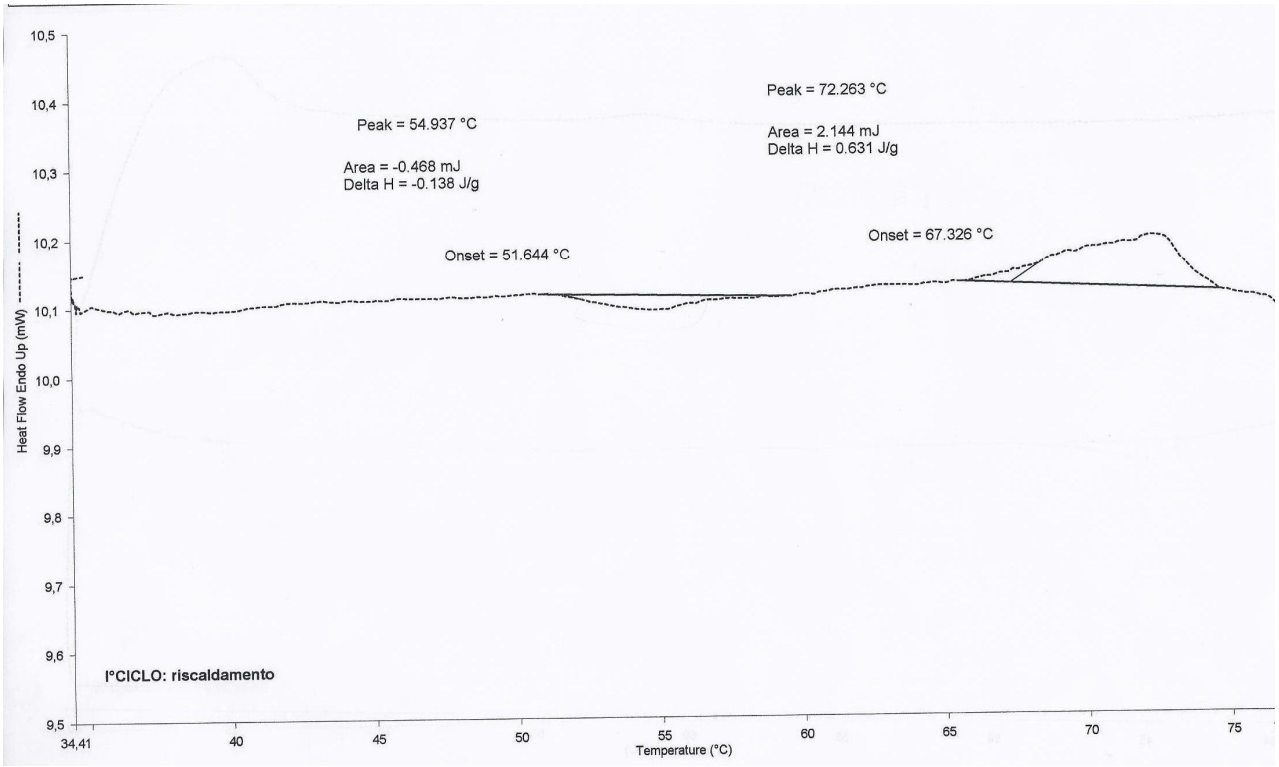

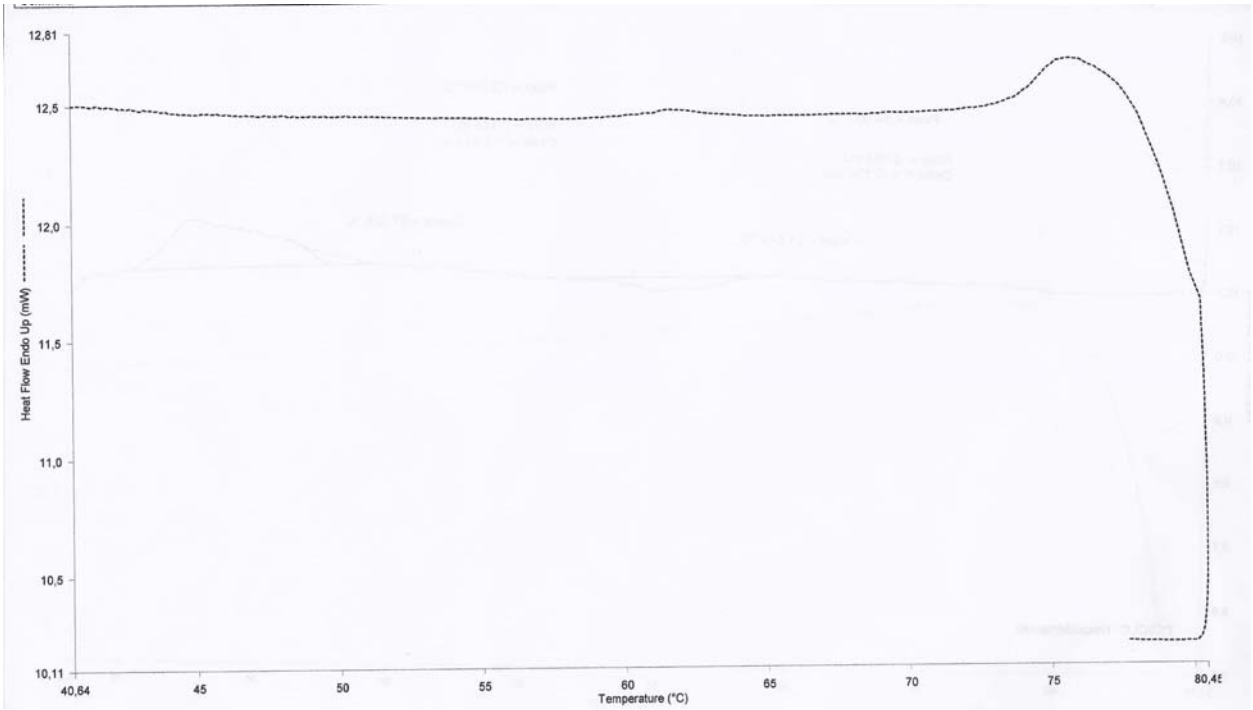

Figure 4.7: DSC thermograms on heating (upper curve) and on cooling (lower curve) of the W-129 mixture doped with gold nanoparticles, obtained at 10°C/min scanning rate[1].

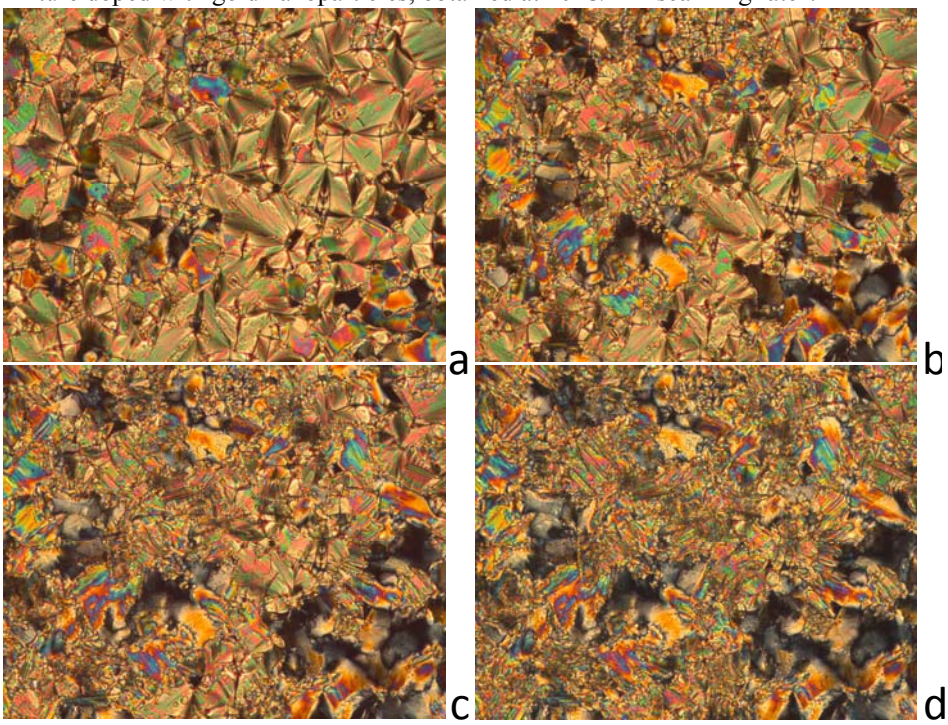

Figure 4.8: Polarizing microscope pictures acquired with a 20 x objective for W-129 mixture doped with gold nanoparticles at 85°C (a), 79°C (b), 73°C (c), 63°C (d).

[1] *DSC and microscope pictures courtesy of Prof. D. Pucci, Chemistry Department – University of Calabria.*

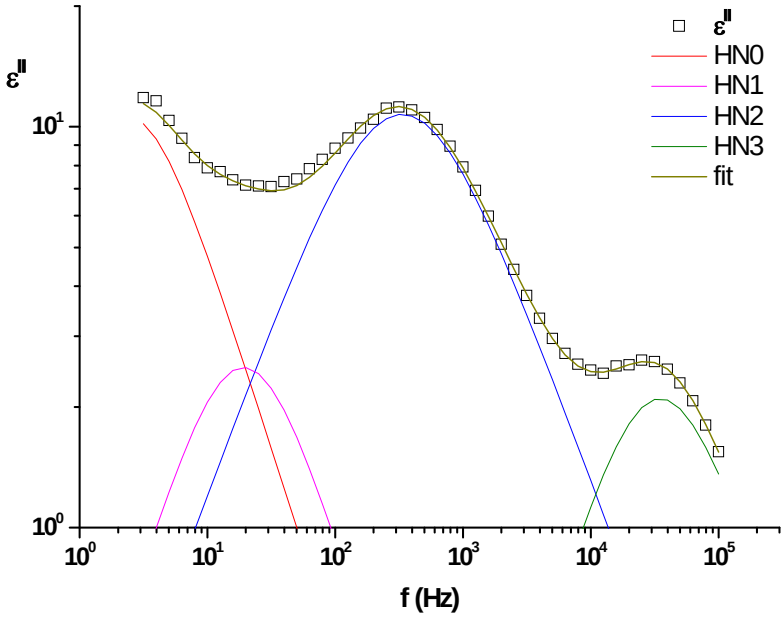

Figure 4.9: Imaginary part of permittivity of W-129 doped with gold nanoparticles acquired at 30°C with an applied voltage of 20 mV.

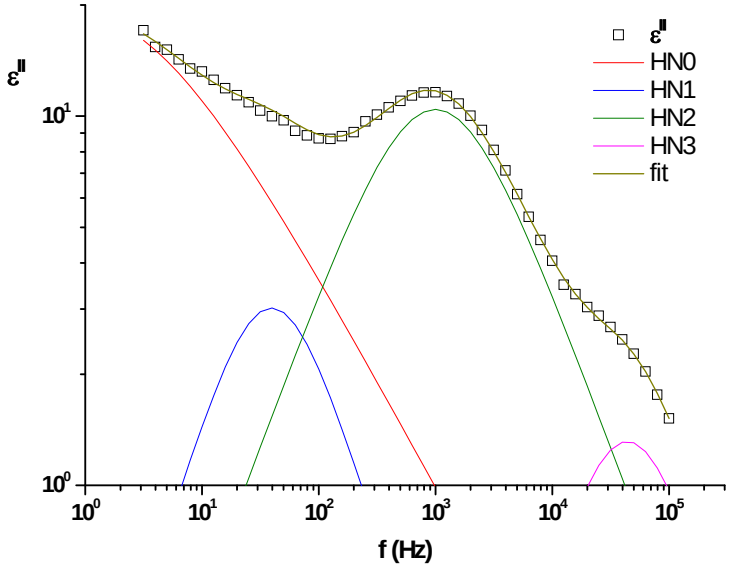

Figure 4.10: Imaginary part of permittivity of W-129 doped with gold nanoparticles acquired at 43°C with an applied voltage of 20 mV.

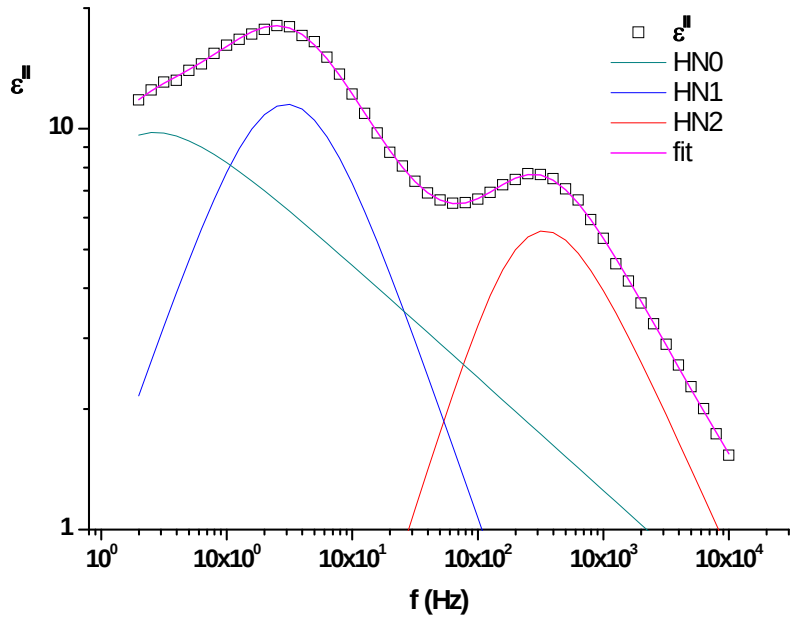

Figure 4.11: Imaginary part of permittivity of W-129 doped with gold nanoparticles acquired at 58.3°C with an applied voltage of 20 mV.

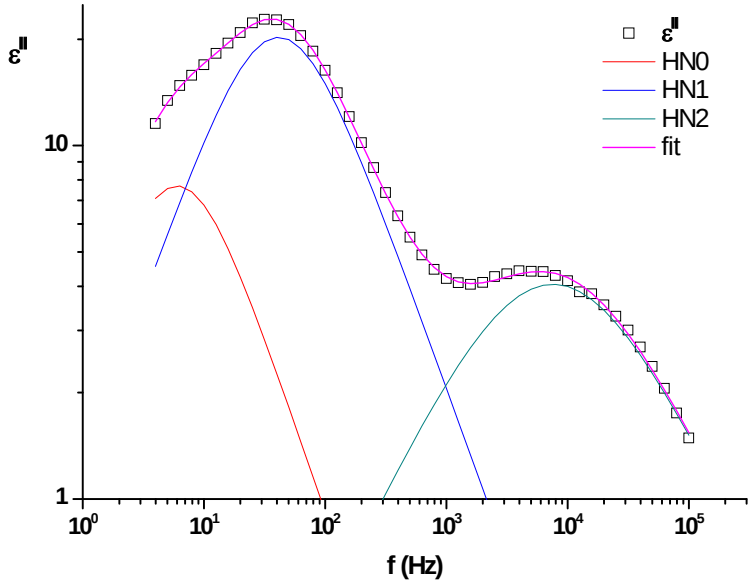

Figure 4.12: Imaginary part of permittivity of W-129 doped with gold nanoparticles acquired at 62°C with an applied voltage of 20 mV.

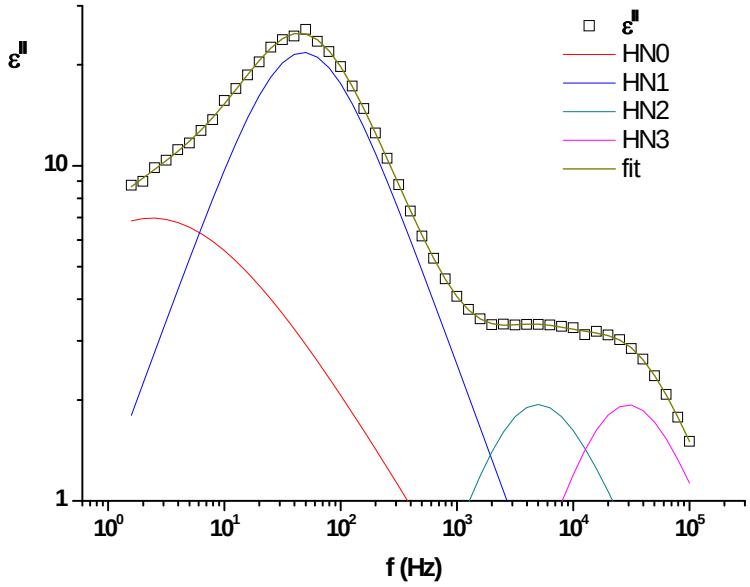

Figure 4.13: Imaginary part of permittivity of W-129 doped with gold nanoparticles acquired at 68°C with an applied voltage of 20 mV.

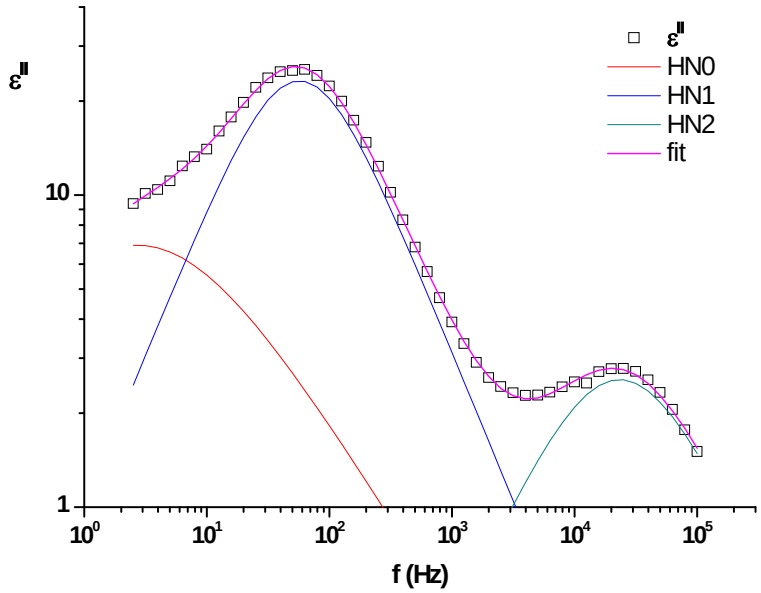

Figure 4.14: Imaginary part of permittivity of W-129 doped with gold nanoparticles acquired at 71.6°C with an applied voltage of 20 mV.

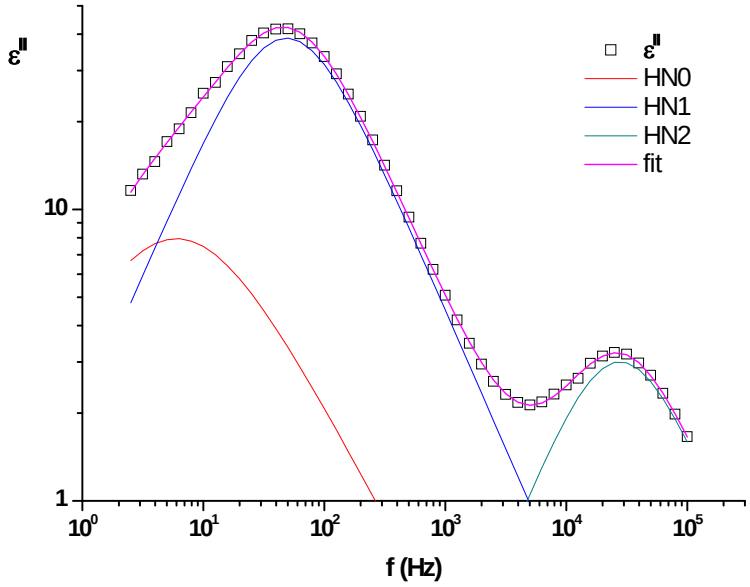

Figure 4.15: Imaginary part of permittivity of W-129 doped with gold nanoparticles acquired at 84.5°C during cooling condition with an applied voltage of 20 mV.

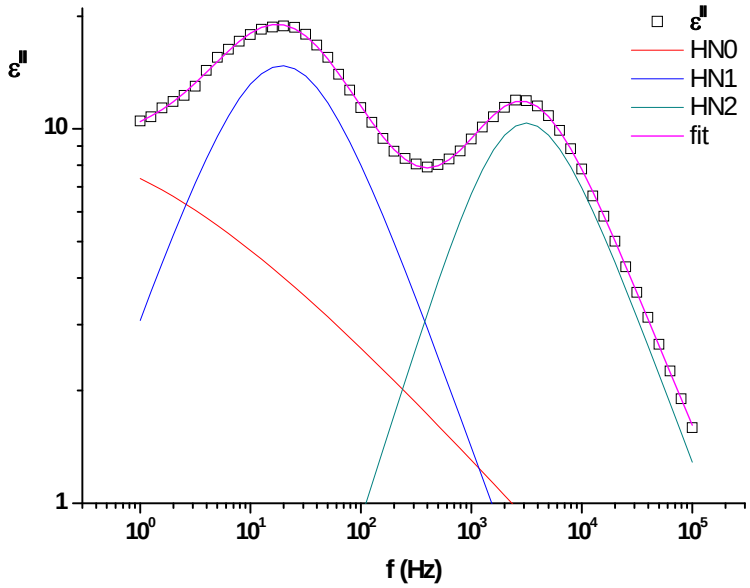

Figure 4.16: Imaginary part of permittivity of W-129 doped with gold nanoparticles acquired at 68°C during cooling condition with an applied voltage of 20 mV.

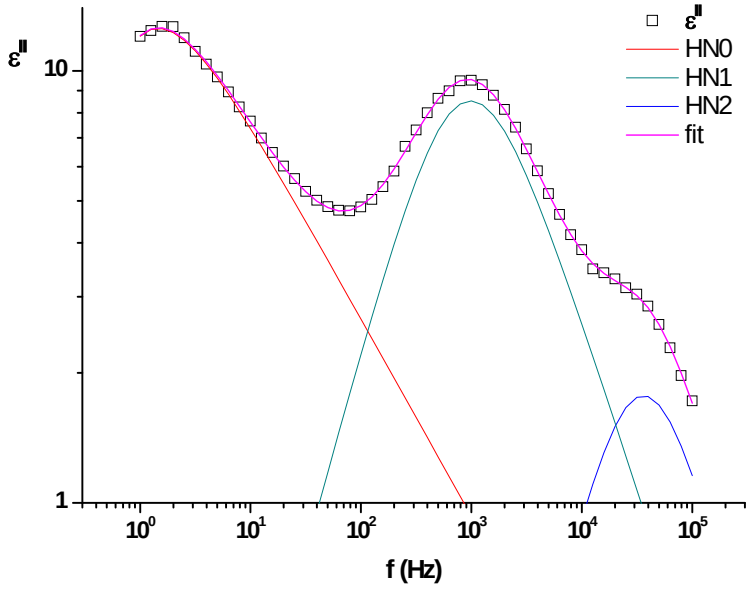

Figure 4.17: Imaginary part of permittivity of W-129 doped with gold nanoparticles acquired at 36.6°C during cooling condition with an applied voltage of 20 mV.

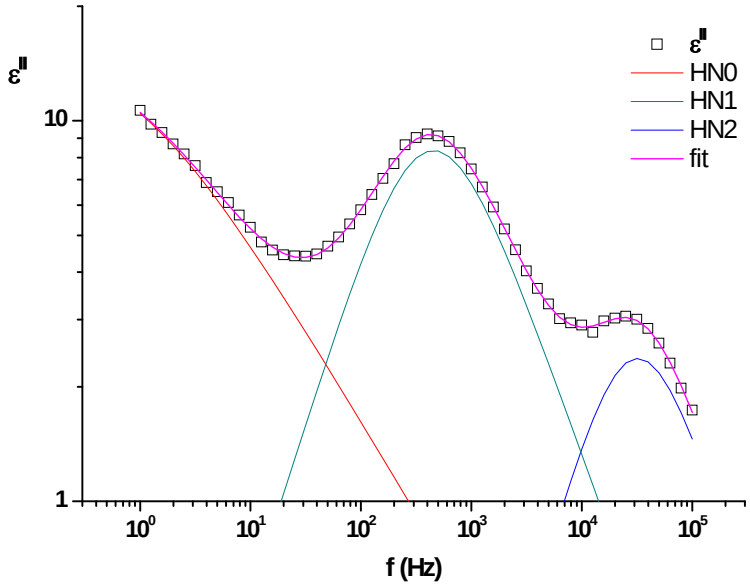

Figure 4.18: Imaginary part of permittivity of W-129 doped with gold nanoparticles acquired at 30°C during cooling condition with an applied voltage of 20 mV.

In this kind of doped mixture, nonvolatile memory effect has also been observed. In the past, similar phenomena were detected in filled nematics (nanoparticles or aerosils doped nematics) [7], in organic/metal nanoclusters/organic systems [8] and in a paticular way, the bistability or memory effect, was also been demonstrated in GNPs doped DHFLCs (deformed helix ferroelectric liquid crystal) [9]. In the last example, the long nonvolatile memory effect has been observed that it is probably due to the electric field induced charge transfer effect (from liquid crystal molecules to the GNPs), and to the stabilization of the helix deformation process. In our case the situation is different because W-129 already has memory effect. Figure 4.18 shows the dielectric permittivity (ε^{I}) as a function of frequency in pure and GNPs doped W-129 acquired at 85°C (during ferroelectric phase). As can be seen the change in bias voltage of measuring field from 0 to 4 V, and from 0 to 8 V makes the dielectric permittivity decrease to a minimum; this effect is due to the suppression of phason (Goldstone) mode which is linked to phase fluctuation of the molecules.

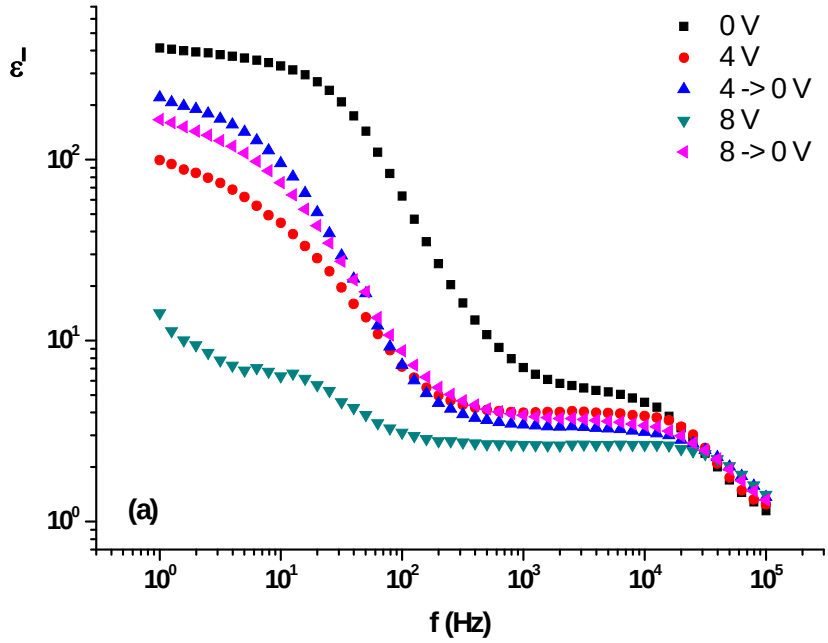

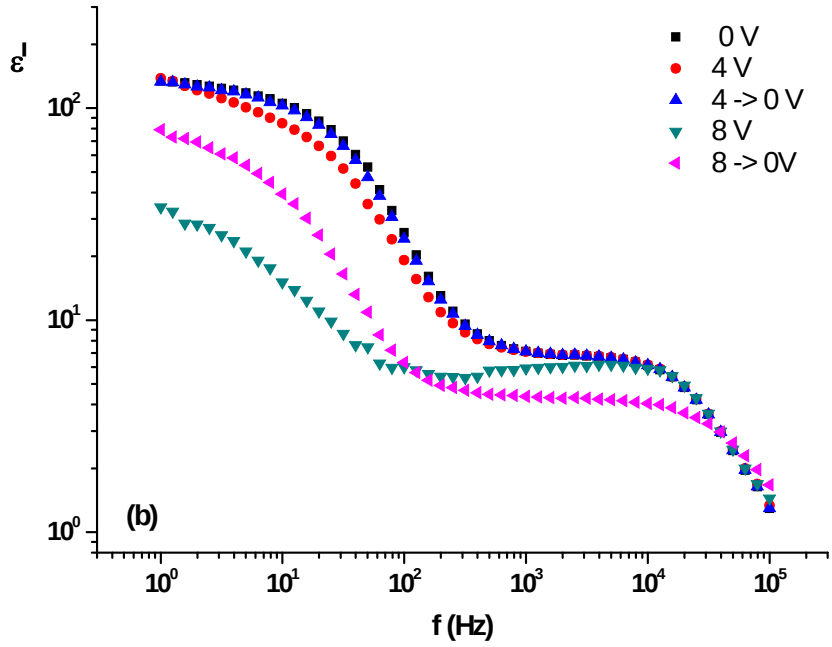

Figure 4.19: Dielectric permittivity as a function of frequency at 85°C at 0V, at 4V, again 0V (4 - > 0V), at 8V, and again 0V (8 - > 0V) of pure W-129 (a), and of GNPs doped W-129 (b).

Again on applying 0 V bias the dielectric permittivity doesn't appear same as it was before applying the bias. the cell remains in memory state up to some extent. With doped W-129 the effect is enhanced as it should be seen from magenta curve (8 -> 0 V) in Fig. 4.17 (b).

4.4 Summary

The basic physical parameters of an antiferroelectric liquid crystal mixture doped with gold nanoparticles have been determined. The gold nanoparticles influence the dielectric spectra; in fact the HN2 mode and the HN3 mode result shifted and changed in intensity. From DSC and dielectric spectroscopy comes the confirmation that nanoparticles also affect the persistence and the extension of smectic subphases. Finally we have seen that nanoparticles enhance nonvolatile memory effect already present in the pure antiferroelectric mixture.

References

1. T. Hegmann, H. Qi and V. M. Marx, Journal of Inorganic and Organometallic Polymers and Materials, 17, 3, 483-508 (2007)

2. L. M. Lopatina, J. V. Selinger, Physical review letters, 102 (19),197802 (2009)

3. Joshi, T. , Kumar, A. , Prakash, J. and Biradar, "Low frequency dielectric relaxations of gold nanoparticles/ferroelectric liquid crystal composites", Liquid Crystals, 37:11, 1433 – 1438 (2010)

4. A. Chaudhary, P. Malik, R. Mehra & K.K. Raina, "Electro-optic and dielectric studies of silica nanoparticle doped ferroelectric liquid crystal in SmC* phase", Phase Transitions: A Multinational Journal, 85:3, 244-254 (2012)

5. J. Kirchhoff and L. S. Hirst Investigation into liquid crystalline smectic-C* subphase stability using chiral and achiral dopants PHYSICAL REVIEW E 76, 051704 (2007)

6. Jan P.F. Lagerwall, Roman Dabrowski, Giusy Scalia, Antiferroelectric liquid crystals with induced intermediate polar phases and the effects of doping with carbon nanotubes, Journal of Non-Crystalline Solids 353 (2007) 4411–4417

7. S. Kaur, S. P. Singh, A. M. Biradar, A. Choudhary, and K. Sreenivas, Appl. Phys. Lett. 91, 023120 (2007).

8. L. P. Ma, J. Liu, and Y. Yang, Appl. Phys. Lett. 80, 2997 (2002)

9. J. Prakash, A. Choudhary, A. Kumar, D. S. Mehta, and A. M. Biradar, Appl. Phys. Lett. 93, 112904 (2008)

Chapter 5

Dielectric Investigations on a New Bent-core Liquid Crystal

5.1 Introduction

The discovery of the mesogenic properties of bent-core molecules has opened another exciting dimension in the field of thermotropic liquid crystals (LCs). Different aspects, for instance the observation of ferroelectricity due to a spontaneous chiral symmetry breaking in smectic phases composed of non-chiral molecules, [1] make this kind of liquid crystals very interesting and useful for a great number of applications. Up today most of the research effort has focused on bent-core smectics, because liquid phases exhibiting mainly orientational order (nematic phases) are less common. However there has been a sudden increase in the theoretical studies [2–7] predicting bent-core nematic and isotropic structures with interesting properties, such as biaxiality and spontaneous chirality. In this context the experimental evidence of a ferroelectric response to a switching electric field in a low molar mass nematic bent-core liquid crystal can be placed. [8]

This kind of response could be explained by considering the effect of the molecules' kinked shape; while rod-shaped molecules can translate during shear flow, bent-shaped molecules experience a steric barrier caused by neighboring molecules and this may promote the formation of temporary clusters even in isotropic phase. For the same reason the bent-core nematic (BCN) structure is much less common than the nematic (N) phase of the calamitics. This is mainly because of the kinked shape that is not really compatible with the translational freedom of the calamitic nematics. For this reason BCNs exhibit some unusual physical properties compared to calamitic ones. These include giant flexoelectricity, [9] unprecedented scenarios in electroconvection, [10–12] as well as an unusual behavior found by light scattering [13] and ^{2}H NMR measurements [8] indicating the presence of clusters with higher ordering.

Dielectric spectroscopy (DS) is a widespread tool for studying liquid crystals which is based on determining the frequency (f) dependent complex permittivity of the substance. It provides not only important material parameters like the static dielectric permittivity and dc electrical conductivity but it also

provides information on the molecular dynamics. The number of relaxation modes is characteristic of the phase and can be associated with certain molecular rotations; the characteristic frequencies reflect how those motions are hindered.

In this chapter the DS technique is used to investigate the smectic, nematic and isotropic phases of a bent-shaped liquid crystal ODA-9, and in order to find the parameters of observed phenomenon (relaxation time, conductivity, dielectric increment etc.) it is necessary to fit the data with generalized relaxation functions. Nowadays the phenomenological Havriliak-Negami (HN) equation is the most frequently used to determine the frequency and temperature dependence of the dielectric parameters.

A low frequency relaxation response seen even in the nematic and isotropic phase, probably could be explained by the formation of SmC-type cybotactic clusters, regarded as strongly fragmented SmC phases. Such clustering effect has been suggested by several studies [10-18] though the exact size, shape, and temporal behavior of the clusters are not known.

5.2 Materials and techniques

The material used for this study is ODA-9 (manufacturers: S.Torgova, Lebedev Physical Institute, Russian Academy of Sciences). The phase sequence of this sample is:

$$\mathrm{Cr} \underset{68.0\ ^\circ\mathrm{C}}{\overset{73.6\ ^\circ\mathrm{C}}{\rightleftharpoons}} \mathrm{SmC} \underset{98.2\ ^\circ\mathrm{C}}{\overset{98.0\ ^\circ\mathrm{C}}{\rightleftharpoons}} \mathrm{N} \underset{109.5\ ^\circ\mathrm{C}}{\overset{110.3\ ^\circ\mathrm{C}}{\rightleftharpoons}} \mathrm{I}$$

obtained from DSC measurements.

A Japanese planar aligned commercial cell (EHC Ltd, Tokyo, Japan) with a thickness of (2.0 ± 0.2) μm and an ITO resistance of 100 Ω /□ has been used. The material was introduced into the cells using capillary suction in its isotropic state. The dielectric measurements have been carried out using an EG&G 273A galvanostat-potentiostat/impedentiometer controlled by the impedance software M398 in order to acquire the real and imaginary part of impedance in the frequency range 10 mHz – 100 kHz with a maximum applied voltage of 1.0 V (RMS) below the Freedericksz threshold. No bias field was applied. In order to perform dielectric measurements as a function of temperature the sample has been placed in a CaLCTec FB150 programmable temperature hot stage. The measurements have been done at different constant temperatures starting from

the smectic to isotropic phase and then slowly cooled from isotropic to crystalline phase.

5.3 Results and discussion

In the specified conditions, real and imaginary parts of the perpendicular component of the complex dielectric permittivity has been measured in function of frequency at fixed temperatures.

The director relaxation can be described in terms of the complex dielectric permittivity, which is given by

$$\varepsilon_{\perp}^{*}(f) = \varepsilon^{I}(f) - i\varepsilon^{II}(f) \tag{5.1}$$

where ε^{I} gives the real part of dielectric permittivity and its spectrum is called the dispersion curve, ε^{II} gives the imaginary part of the complex permittivity and its spectrum is called the absorption or dielectric loss curve, f being the frequency of the applied electric field. In order to understand the temperature dependence of measured dielectric relaxation, $\varepsilon_{\perp}^{*}(f)$ can be described by the Havriliak-Negami function [19] (already seen in Chapter 3) with the addition of a conductivity contribution (term 3) present at lower frequencies

$$\varepsilon_{\perp}^{*}(f) = \varepsilon_{\infty} + \sum_{j} \frac{\Delta\varepsilon_{j}}{[1+(if\tau_{j})^{a_j}]^{b_j}} - \frac{i\sigma}{\varepsilon_0 (2\pi f)^{n}} \tag{5.2}$$

where $\Delta\varepsilon_j$ is the dielectric strength, ε_∞ is the high-frequency limit of permittivity, $\tau_j = 1/f_{r_j}$ is the relaxation time and f_{r_j} is the corresponding relaxation frequency, a_j and b_j are shape parameters describing the asymmetry and broadness of the dielectric dispersion curve, ranging between 0 and 1, and j is the number of the relaxation processes. In the last term σ is related to the conductivity, n is a fitting parameter responsible for the slope of the conductivity. In the case of pure Ohmic conductivity n = 1 while the decrease of n, n < 1, could be observed if, in addition to the contribution to ε^{II} from conductivity, there is an influence of electrode polarization. The Havriliak-Negami (HN) response reduces to Cole-Davidson [20] response when $a = 1$, and to Cole-Cole response [21] when $b = 1$.

It has to be noticed that the real part $\varepsilon^{I}(f)$ of the complex dielectric permittivity is proportional to the imaginary part $\sigma^{II}(f)$ of the complex ac-conductivity $\sigma^{*}(f)$, $\varepsilon^{I}(f) \propto -\sigma^{II}(f)/f$, and the dielectric losses $\varepsilon^{II}(f)$ are proportional to the real part $\sigma^{I}(f)$ of the ac-conductivity, $\varepsilon^{II}(f) \propto \sigma^{I}(f)/f$ [22].

Dielectric spectra for smectic C (see Fig. 5.1 and 5.2), nematic (see Fig. 5.3 and 5.4) and isotropic phase (see Fig. 5.5) are reported in function of frequency and collected at the augmenting of temperature. At the temperature of 86.1°C there are composite dispersions consisting of different molecular processes with their characteristic frequencies not so distant to each other; a sum of two different overlapping modes results from the fit, the first and the second related respectively to the ions diffusion and to the interfacial polarization relaxation at the liquid crystal-electrode interface. In fact the processes are too slow (10^{-2} -1 Hz) to predict the presence of other physical phenomena. [22, 23] In the other spectra, from 93.9 to 154.8 °C, another loss peak is present (10 – 20 Hz). It is not so improbable that this low frequency peak represents a collective process connected with the formation of antiferroelectric order as just be seen in smectic bent-core phases. [24-26] In this perspective the large relative permittivity is perhaps justified from the formation of (anti)ferroelectric clusters.

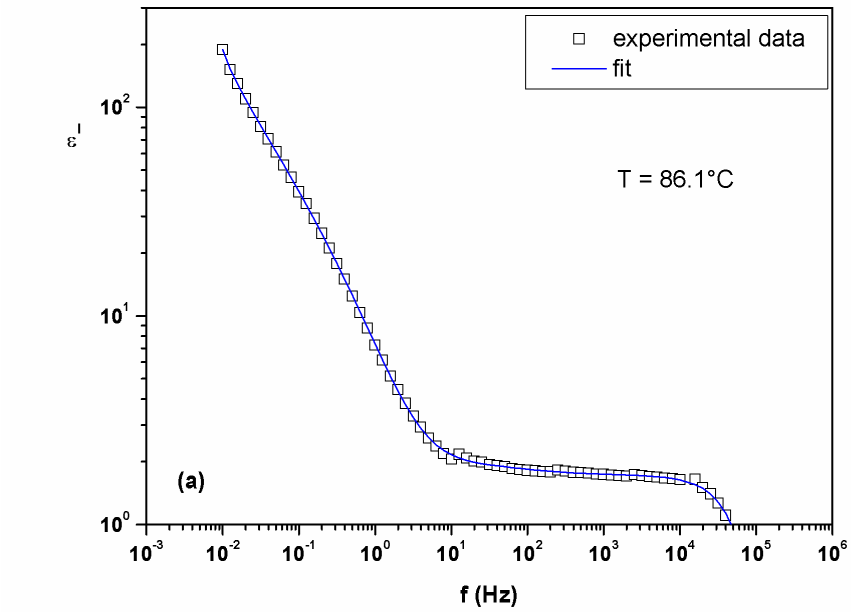
experimental data
fit
T = 86.1°C
(a)
ε'
f (Hz)

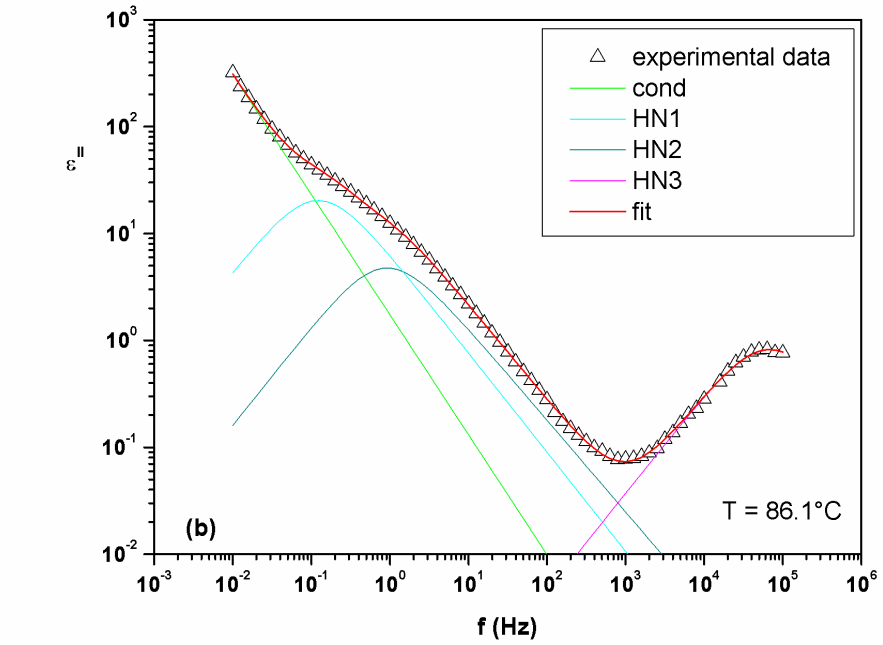
experimental data
cond
HN1
HN2
HN3
fit
T = 86.1°C
(b)
ε''
f (Hz)

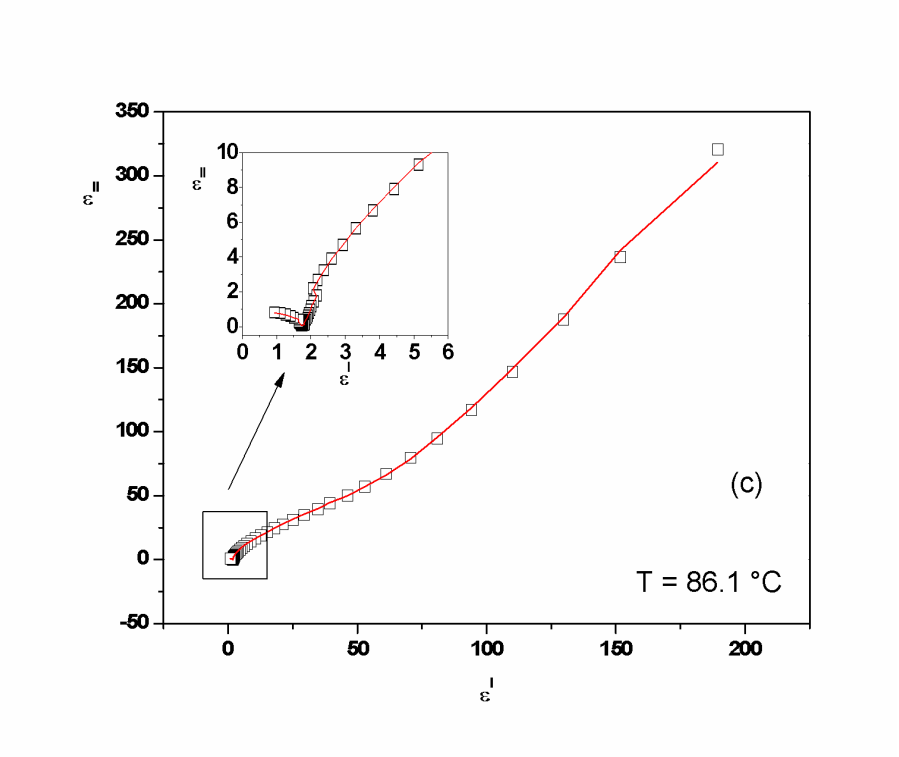

Figure 5.1: Dielectric spectrum of ODA-9 acquired at T = 86.1 °C in heating conditions: (a) Real part, (b) imaginary part. (c) Cole-Cole plot. In the inset is shown a magnification of the selected region. Symbols: experiment; solid lines: fitting[1].

The resulting distribution parameters a and b, derived from fitting the experimental points (see Table 5.2) are more or less equal to one for all phases, reducing the H-N equation to a Cole-Cole or a Debye equation. Only the second process at 86.1°C exhibits an asymmetrical relaxation peak broadening (a $\approx$0.93, b $\approx$0.92) and the first at 154.8 °C that is of Cole-Davidson kind (a $\approx$1.0, b $\approx$ 0.85).

Data analysis shows that the strong frequency dependence of ε^{II} for f < 0.1 Hz is due to Ohmic conductivity at 86.1 °C (see table 5.1) and at increasing temperature (from 93.9 to 154.8 °C) there is a small contribution from the electrode polarization that becomes increasingly important during the cooling process (from 137.9 to 86.1 °C).

[1] L. Marino et al., Journal of Applied Physics, DOI: 10.1063/1.4767915

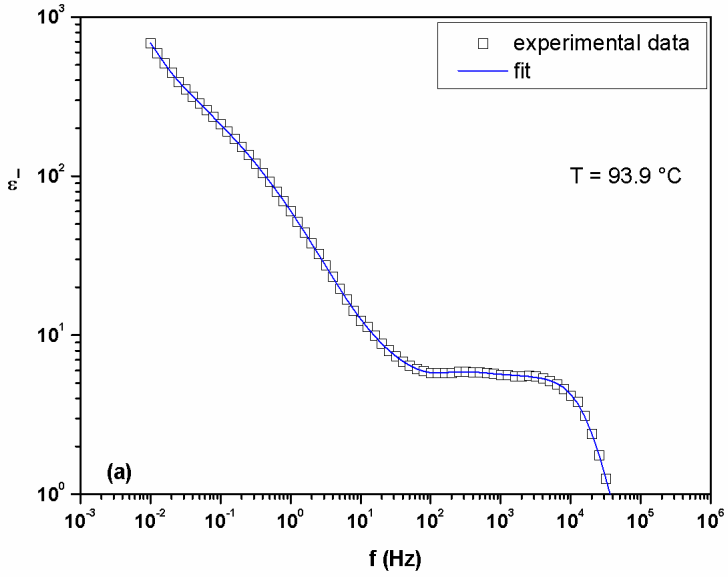
experimental data
fit
T = 93.9 °C
(a)
ε'
f (Hz)

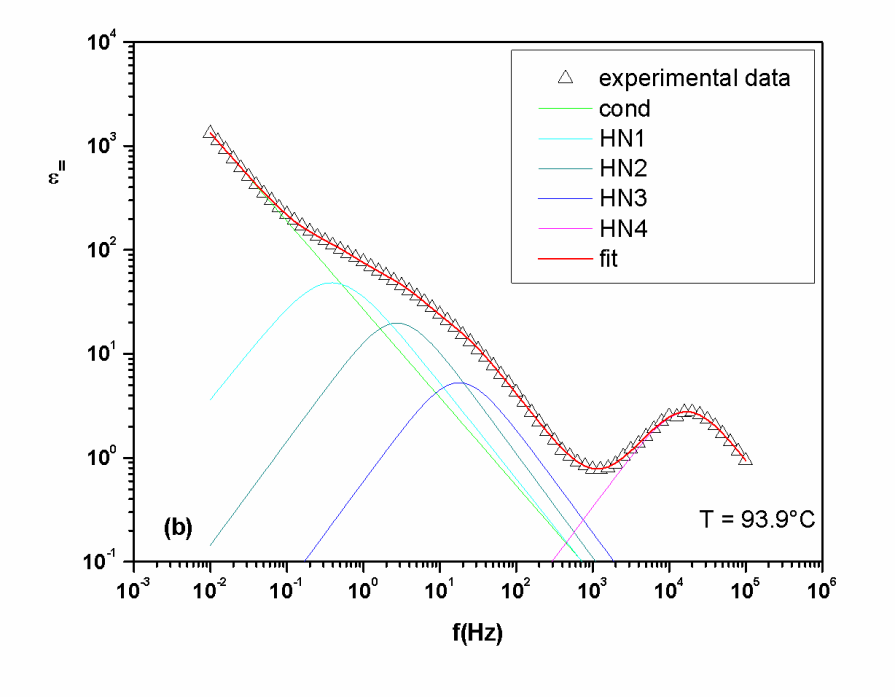
experimental data
cond
HN1
HN2
HN3
HN4
fit
T = 93.9°C
(b)
ε''
f(Hz)

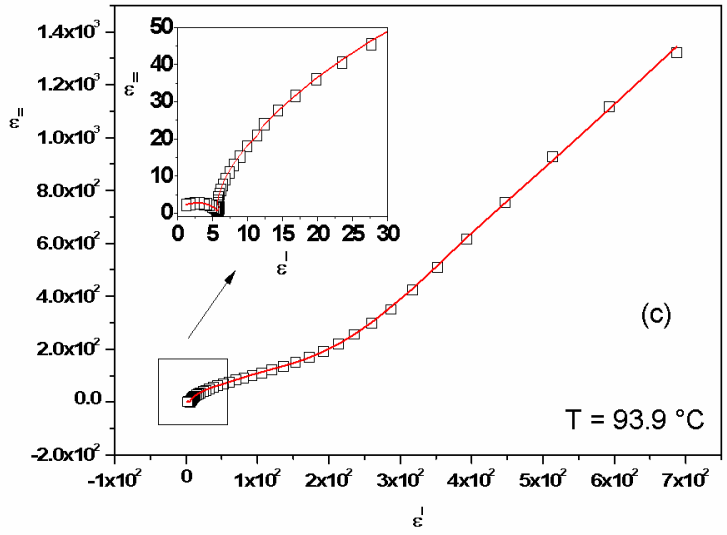

Figure 5.2: Dielectric spectrum of ODA-9 acquired at T = 93.9 °C in heating conditions: (a) Real part, (b) imaginary part. (c) Cole-Cole plot. In the inset is shown a magnification of the selected region. Symbols: experiment; solid lines: fitting.

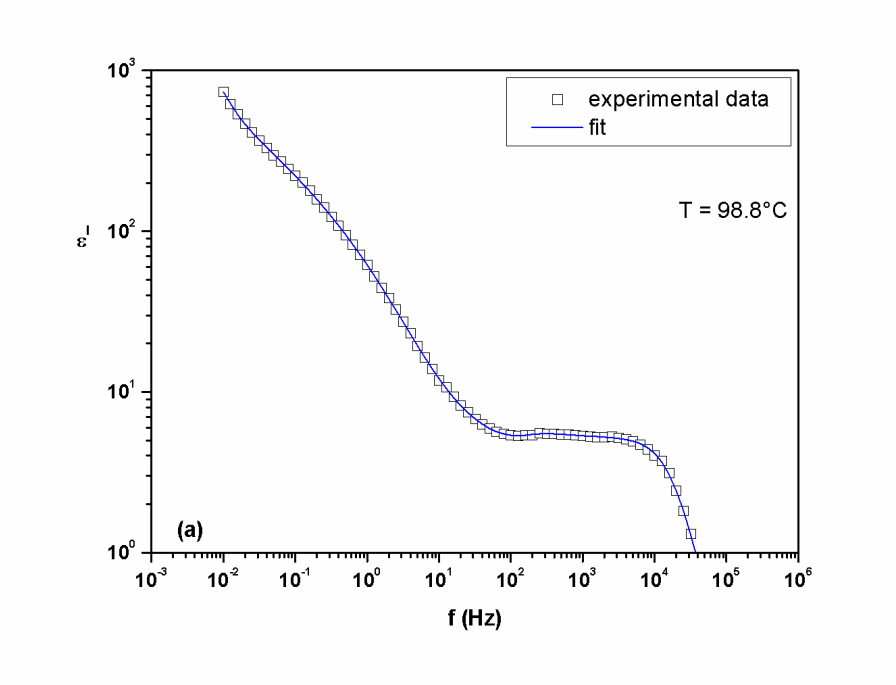

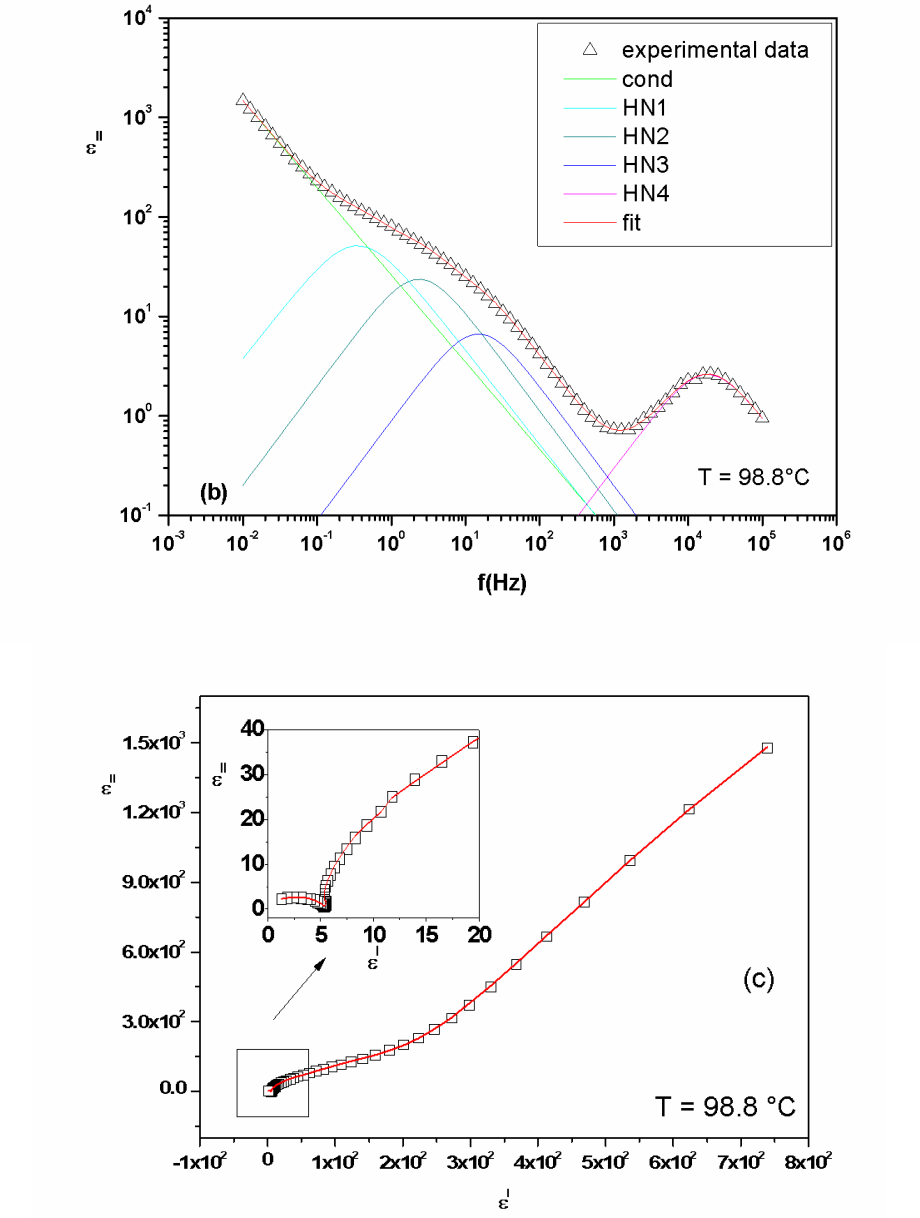

Figure 5.3 Dielectric spectrum of ODA-9 acquired at T = 98.8 °C in heating conditions: (a) Real part, (b) imaginary part. (c) Cole-Cole plot. In the inset is shown a magnification of the selected region. Symbols: experiment; solid lines: fitting.

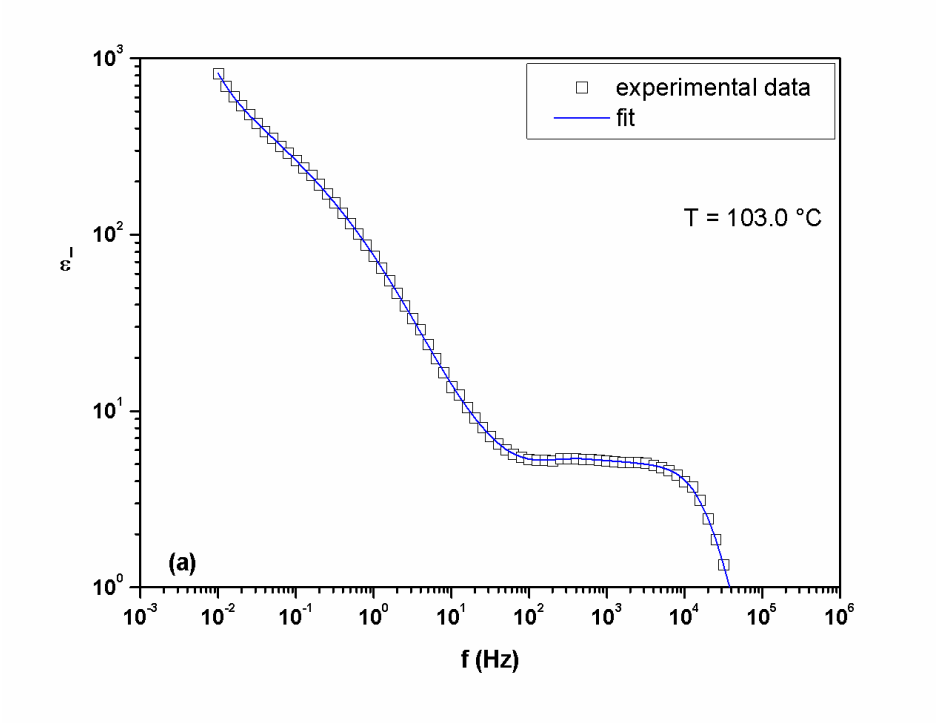
experimental data
fit
T = 103.0 °C
(a)
ε'
f (Hz)

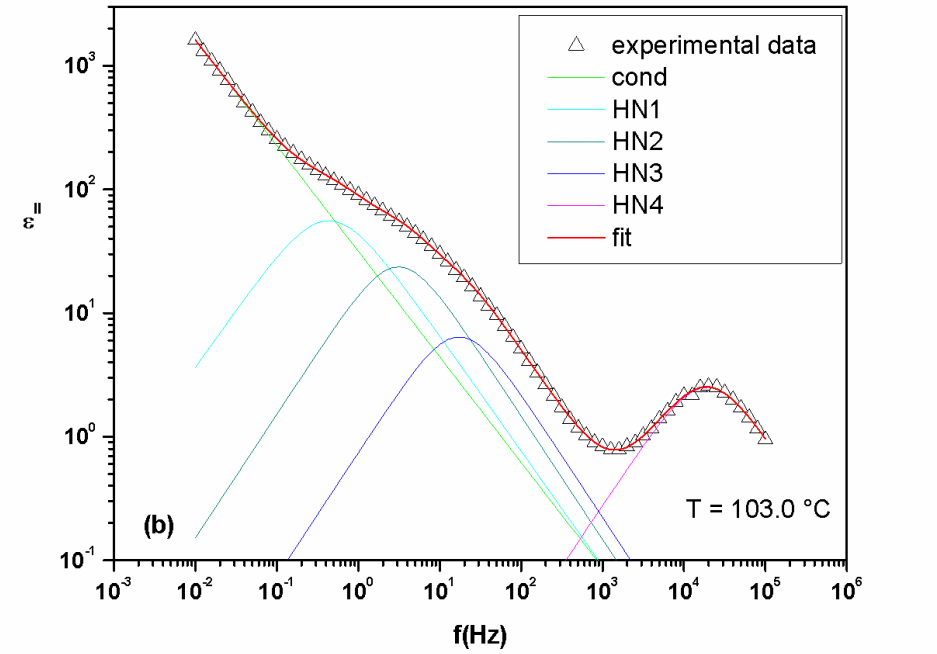
experimental data
cond
HN1
HN2
HN3
HN4
fit
T = 103.0 °C
(b)
ε''
f(Hz)

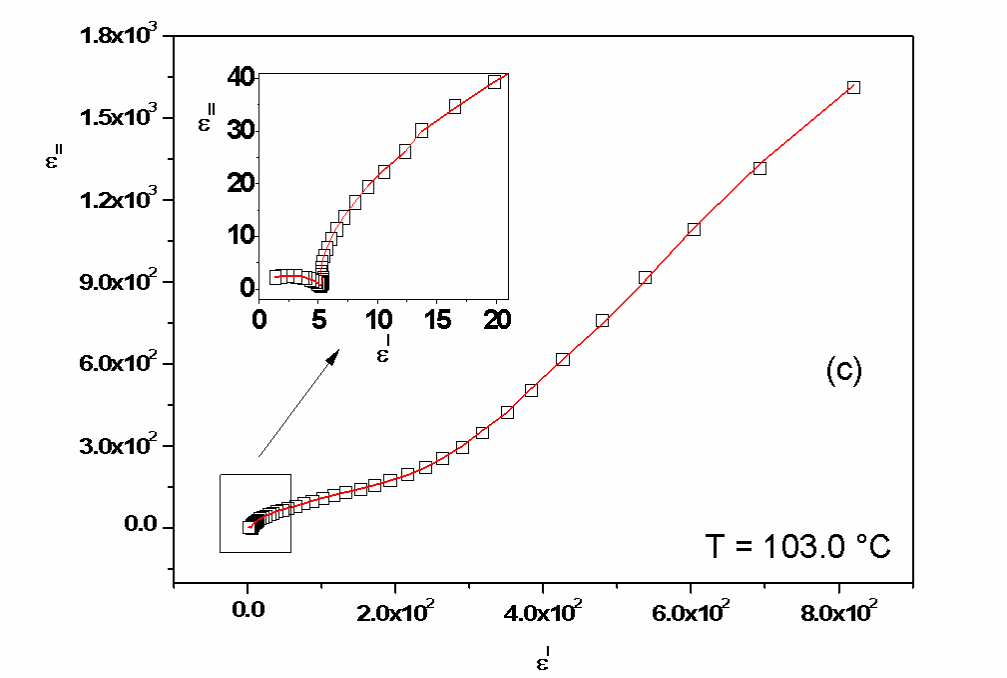

Figure 5.4: Dielectric spectrum of ODA-9 acquired at T = 103.0 °C in heating conditions: (a) Real part, (b) imaginary part. (c) Cole-Cole plot. In the inset is shown a magnification of the selected region. Symbols: experiment; solid lines: fitting.

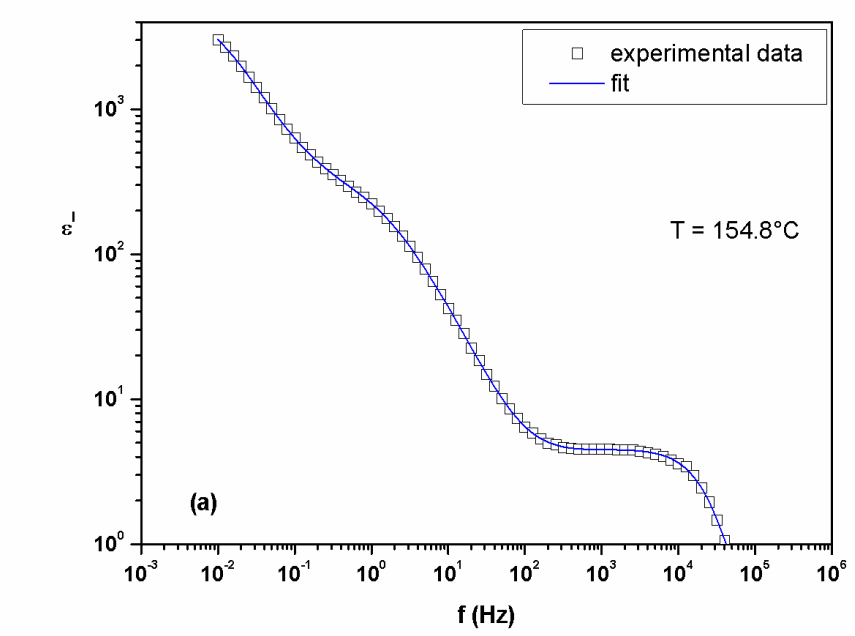

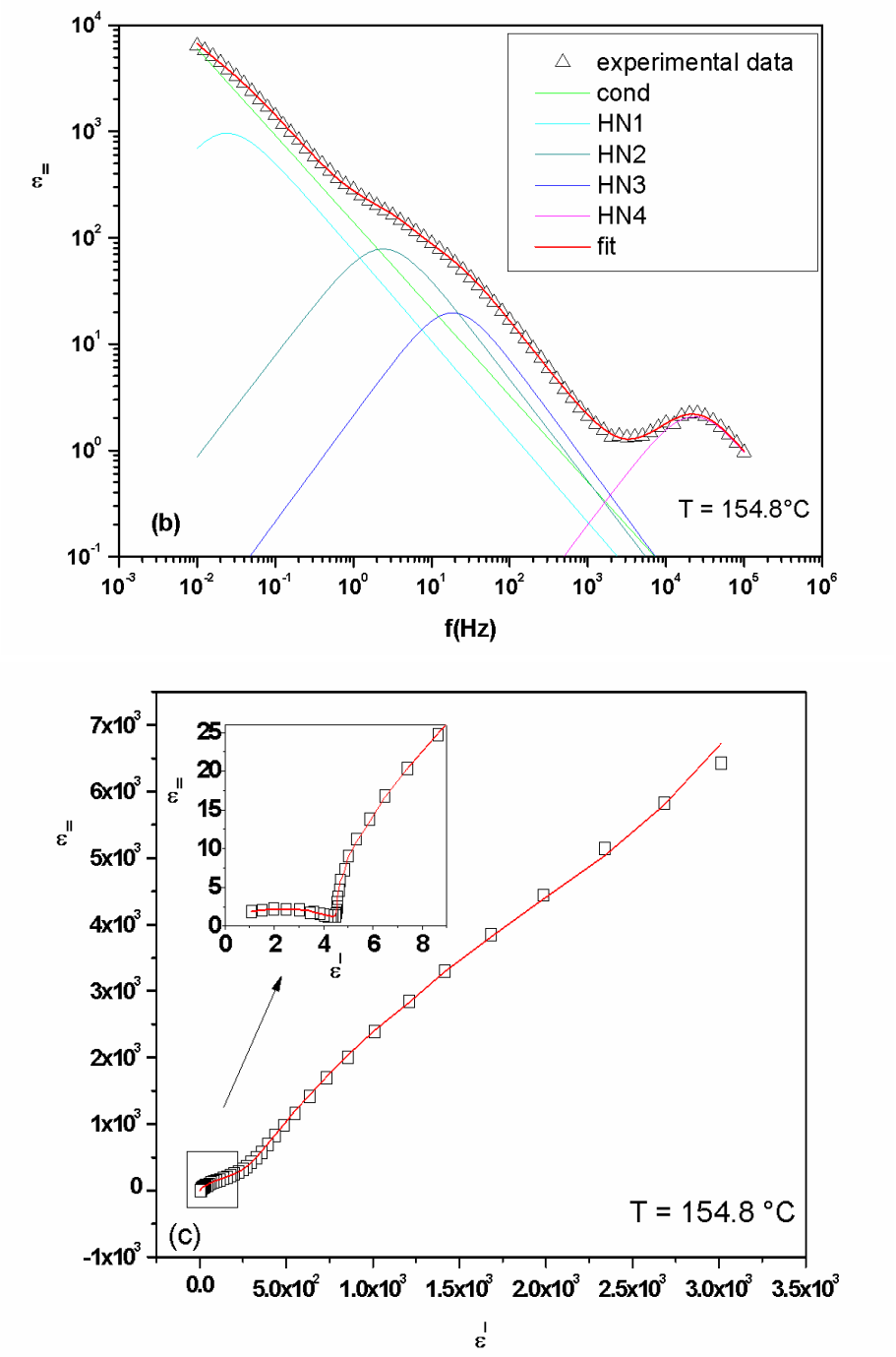

Figure 5.5: Dielectric spectrum of ODA-9 acquired at T = 154.8 °C in heating conditions: (a) Real part, (b) imaginary part. (c) Cole-Cole plot. In the inset is shown a magnification of the selected region. Symbols: experiment; solid lines: fitting.

The results obtained in the cooling down conditions appear very different from those obtained at heating up. The third mode (HN3) disappears decreasing the temperature and from 103.0 °C to 86.1 °C is not more visible. In figures 7-9 it is shown that the Cole-Cole plots obtained in cooling conditions appear very different from those obtained in heating conditions. The last peak at higher frequencies (10^4 Hz) is a very clear process measured for all phases which is visible without detailed analysis. It suggests a reorientation around the molecular long axis probably shifted to lower frequencies for the high viscosity of the sample. [27] The nematic phase of ODA-9 has been compared with the nematic phase of E7, a typical rod-like liquid crystal. Real and imaginary part of E7 are plotted in figure 5.10 with Cole-Cole plot. Even in this case the dielectric response at low frequencies is due to a combination of ions diffusion and interfacial polarization at the liquid crystal-electrode interface. The peak at higher frequencies is instead due to a reorientation around the molecular long axis. The corresponding fitting parameters are synthesised in Table 5.6 [28].

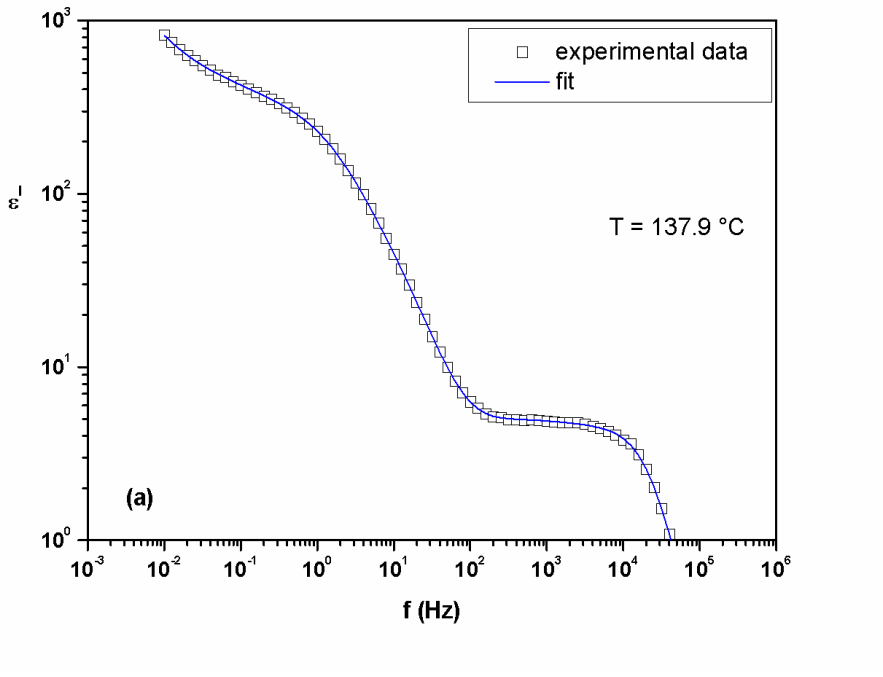

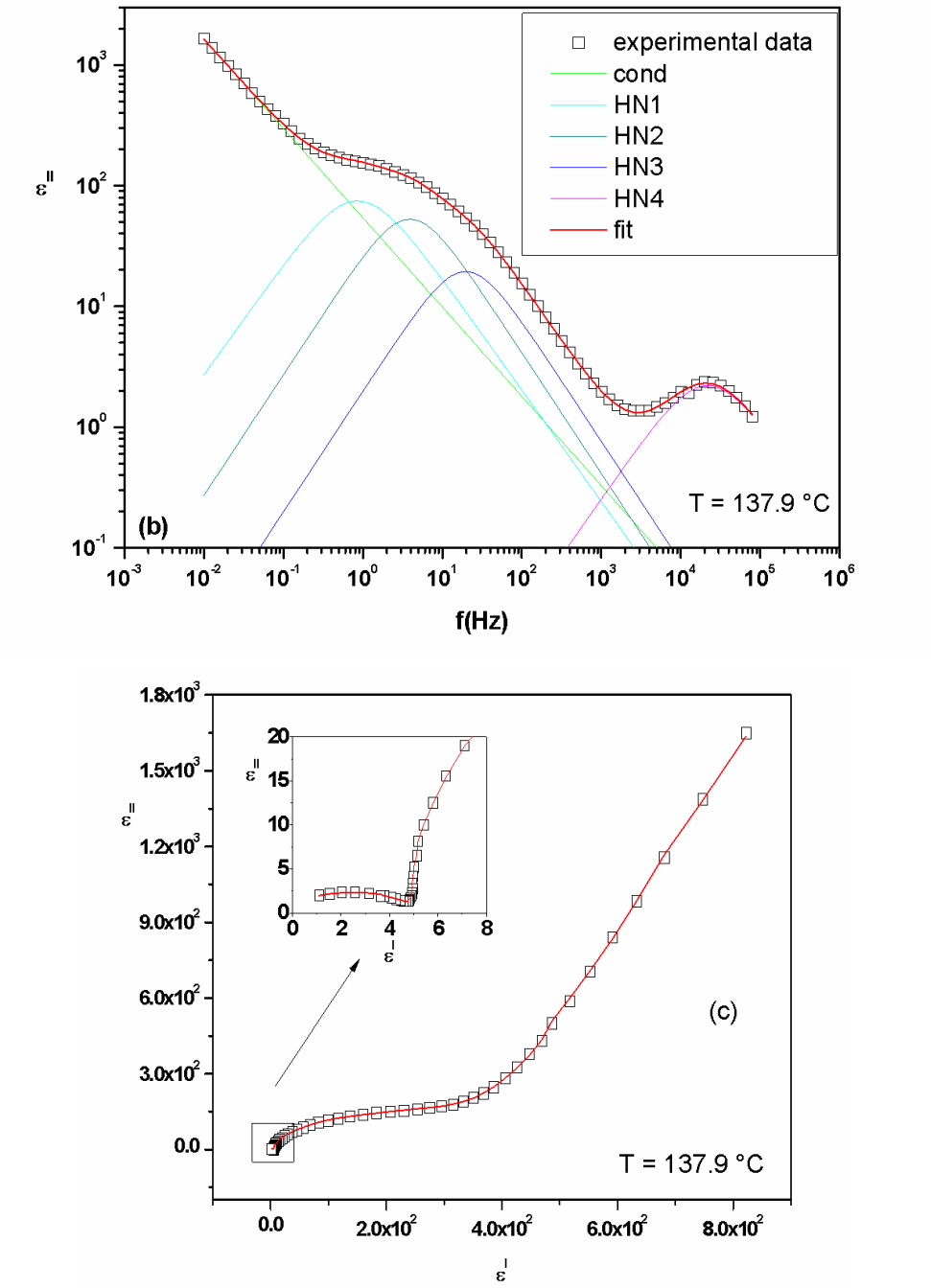

Figure 5.6: Dielectric spectrum of ODA-9 acquired at T = 137.9 °C in cooling conditions: (a) Real part, (b) imaginary part. (c) Cole-Cole plot. In the inset is shown a magnification of the selected region. Symbols: experiment; solid lines: fitting.

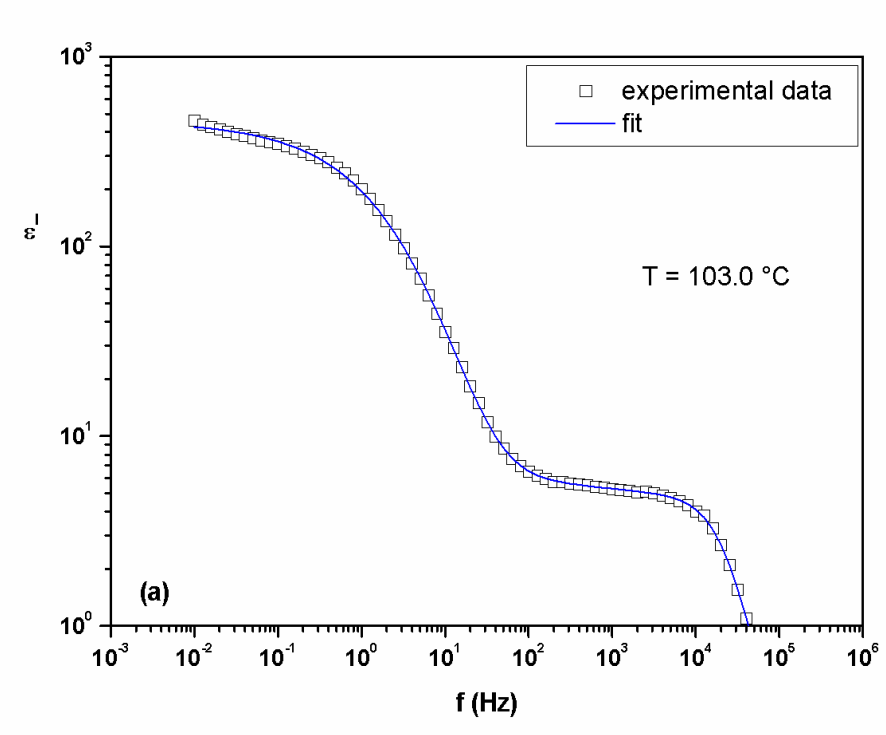
experimental data
fit
T = 103.0 °C
(a)
ε'
f (Hz)

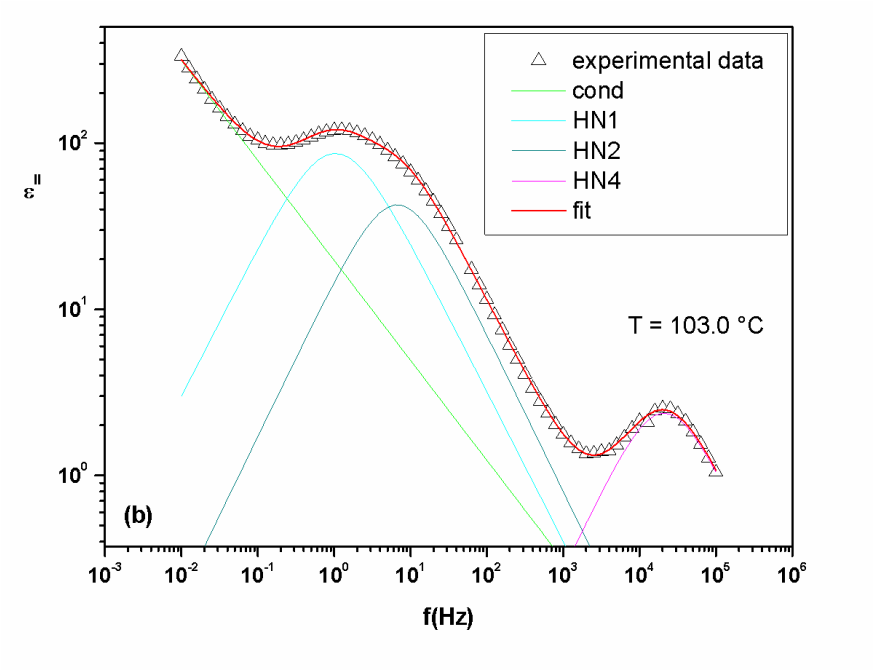
experimental data
cond
HN1
HN2
HN4
fit
T = 103.0 °C
(b)
ε''
f(Hz)

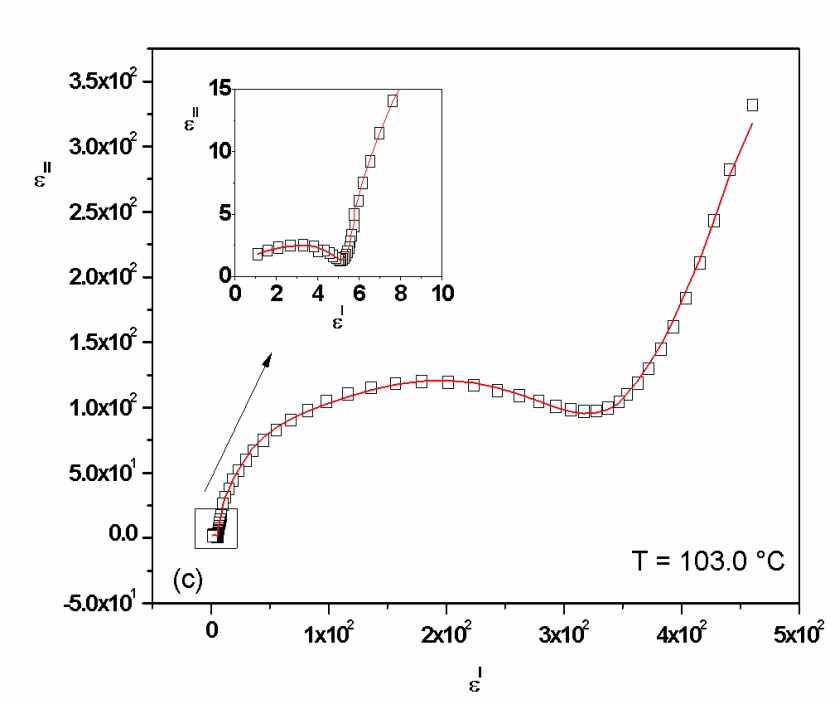

Figure 5.7: Dielectric spectrum of ODA-9 acquired at T = 103.0 °C in cooling conditions: (a) Real part, (b) imaginary part. (c) Cole-Cole plot. In the inset is shown a magnification of the selected region. Symbols: experiment; solid lines: fitting.

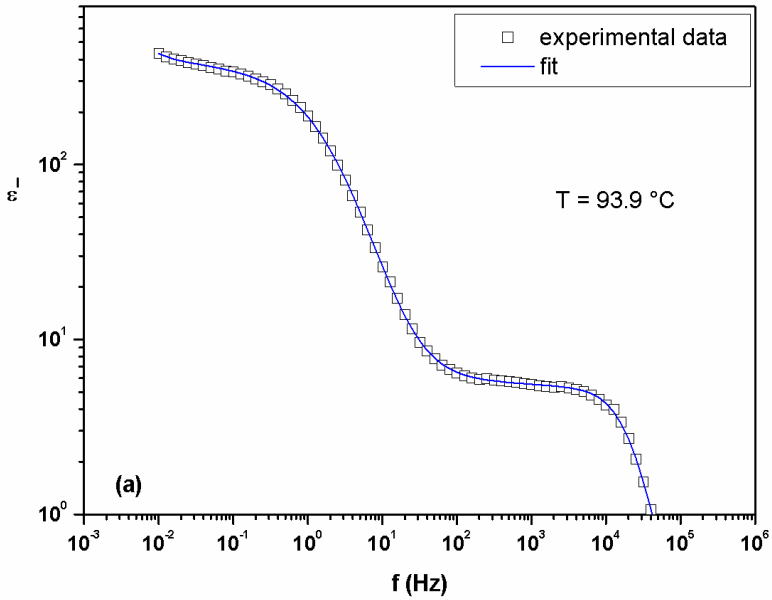

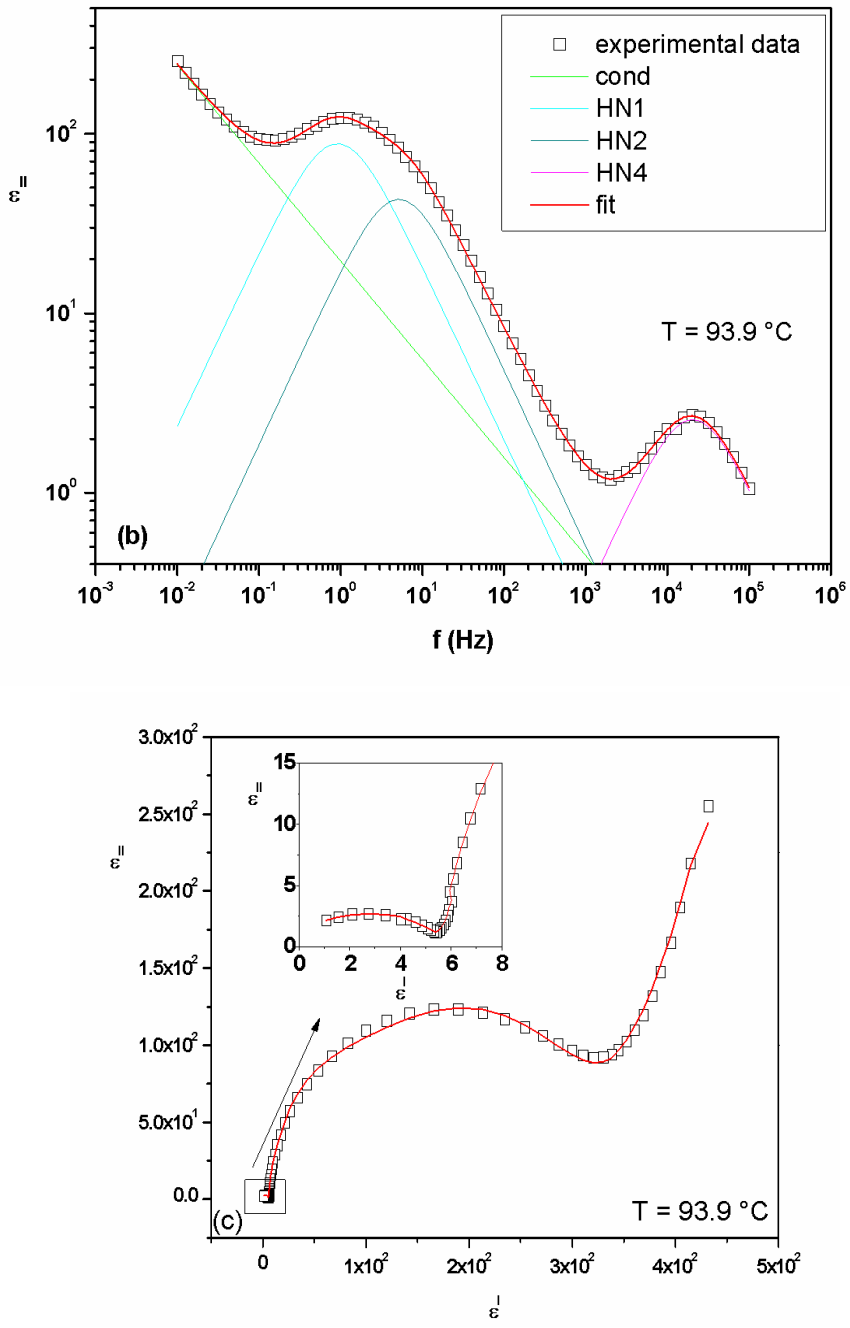

Figure 5.8: Dielectric spectrum of ODA-9 acquired at T = 93.9 °C in cooling conditions: (a) Real part, (b) imaginary part. (c) Cole-Cole plot. In the inset is shown a magnification of the selected region. Symbols: experiment; solid lines: fitting.

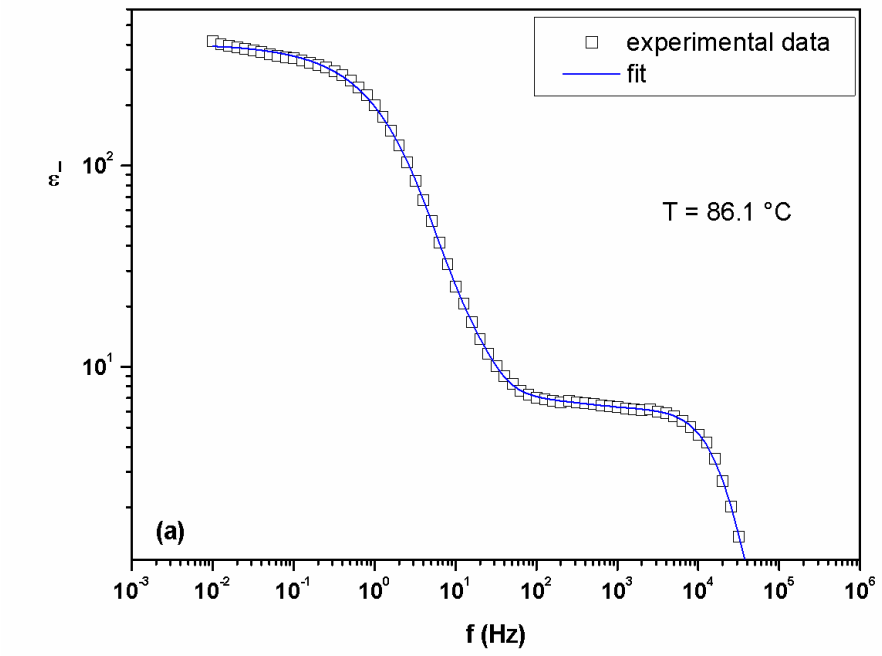
experimental data
fit
T = 86.1 °C
(a)
ε_
f (Hz)

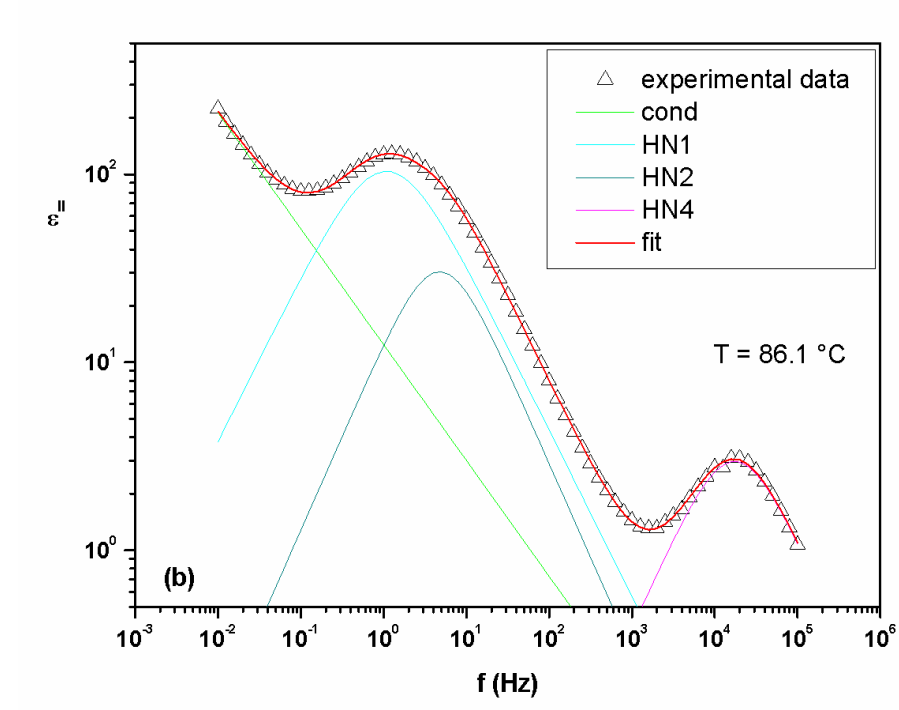
experimental data
cond
HN1
HN2
HN4
fit
T = 86.1 °C
(b)
ε=
f (Hz)

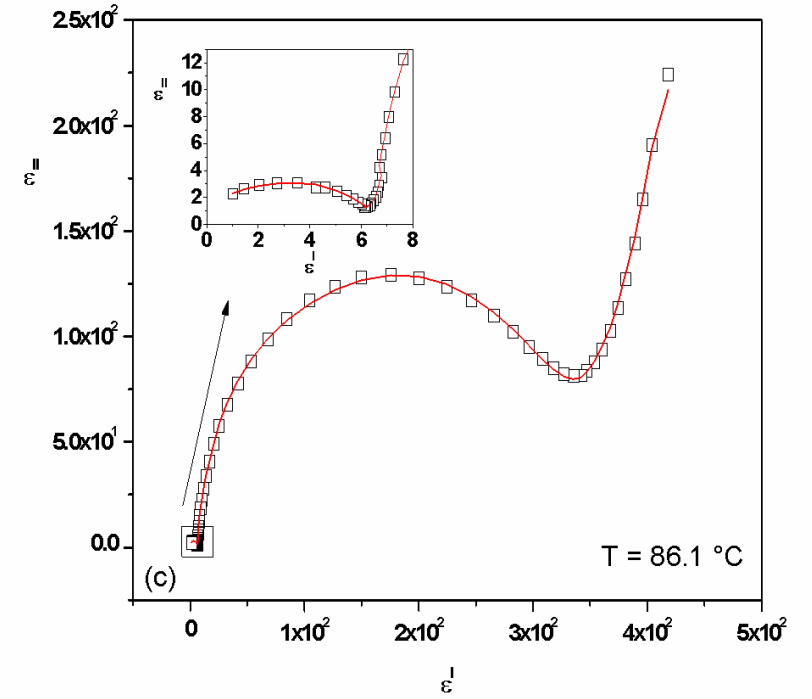

Figure 5.9: Dielectric spectrum of ODA-9 acquired at T = 86.1 °C in cooling conditions: (a) Real part, (b) imaginary part. (c) Cole-Cole plot. In the inset is shown a magnification of the selected region. Symbols: experiment; solid lines: fitting.

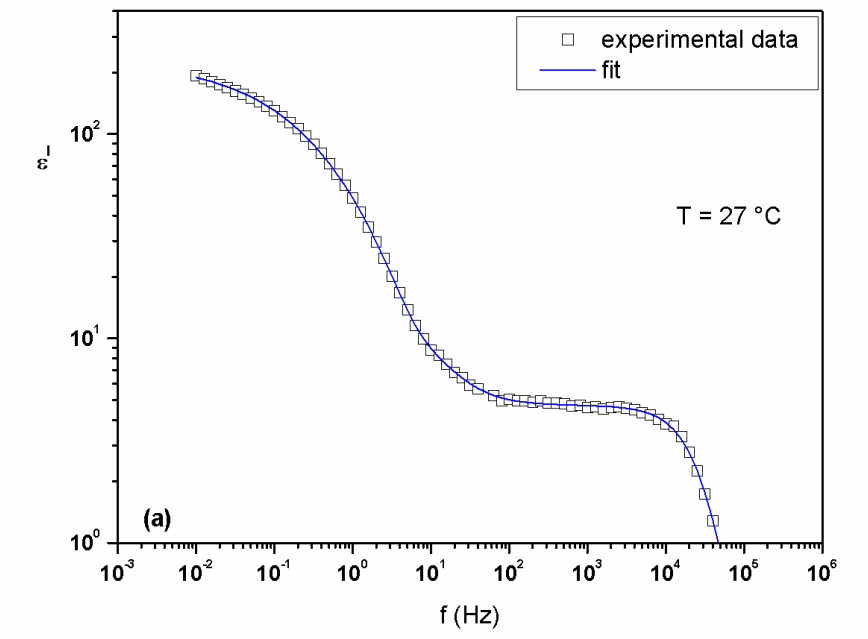

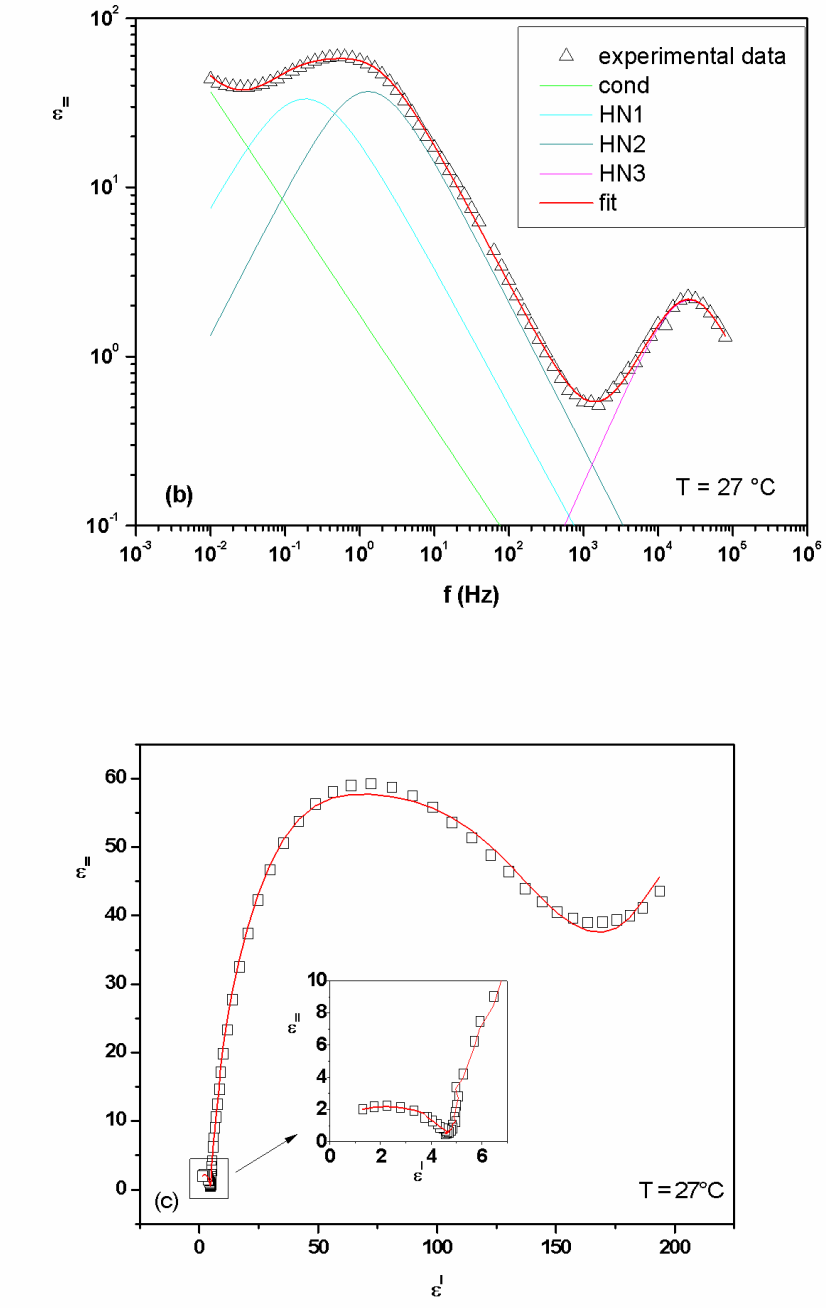

Figure 5.10: Dielectric spectrum of E7 acquired at T = 27 °C: (a) Real part, (b) imaginary part. (c) Cole-Cole plot. In the inset is shown a magnification of the selected region. Symbols: experiment; solid lines: fitting.

Finally in figures 5.11 and 5.12 3D graphs are represented in order to visualize the variation of the imaginary part of permittivity in function of frequency and

temperature. The differences between heating and cooling conditions are evident. The results are displayed in a smaller range of frequencies in order to better appreciate the contribution of the third dielectric mode. The formation of temporary clusters could be an explanation for the presence of the low frequency relaxation process even in nematic and isotropic phase. In order to verify the presence of ferroelectricity or antiferroelectricity, measurements of the polarization reversal current should be done. All the parameters resulting from fitting are synthesised in Tables 5.2 – 5.6.

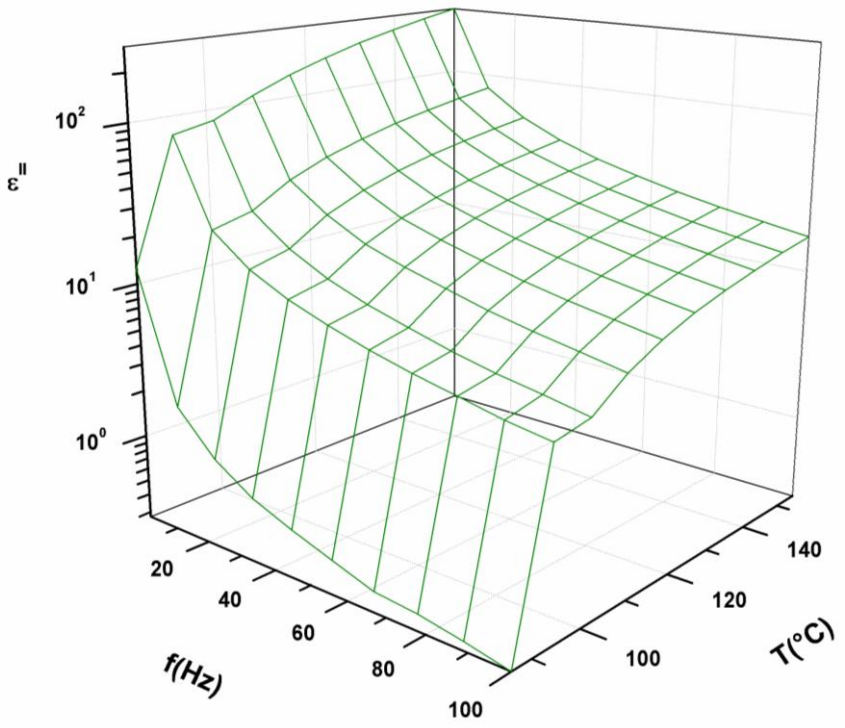

Figure 5.11: Imaginary part of complex permittivity in function of frequency and temperature in heating conditions.

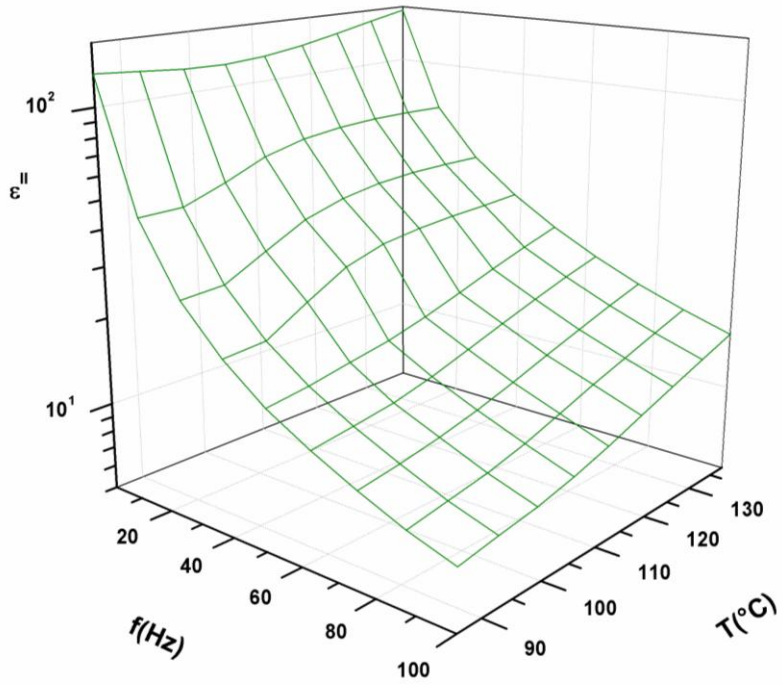

Figure 5.12: Imaginary part of complex permittivity in function of frequency and temperature in cooling conditions.

Table 5.1. Fitting parameters for DC conductivity of ODA-9 at different temperatures in heating and cooling conditions.

T (°C)	σ (S/cm)	n	σ_err	n_err
86.1	1.739	1.12	1.27	0.09
93.9	26.97	0.85	1.03	0.02
98.8	26.10	0.88	1.04	0.02
103.0	31.65	0.85	1.03	0.01
154.8	140.7	0.82	1.47	0.11
103.0	19.71	0.60	1.04	0.02
93.9	19.50	0.55	1.03	0.01
86.1	12.44	0.62	1.03	0.02

Table 5.2. Fitting parameters for the first relaxation process (HN1) of ODA-9 at different temperatures in heating and cooling conditions.

T (°C)	f_r (Hz)	$\Delta\varepsilon$	a	b	f_r_err	$\Delta\varepsilon$ _err	a_err	b_err
86.1	0.12	$0.46\cdot10^{2}$	0.93	1.00	1.22	$0.30\cdot10^{2}$	0.22	0.00
93.9	0.39	$0.11\cdot10^{3}$	0.93	1.00	1.09	$0.14\cdot10^{2}$	0.04	0.00
98.8	0.35	$0.11\cdot10^{3}$	0.95	1.00	1.09	$0.16\cdot10^{2}$	0.05	0.00
103.0	0.43	$0.12\cdot10^{3}$	0.93	1.00	1.08	$0.14\cdot10^{2}$	0.04	0.00
154.8	0.02	$0.21\cdot10^{4}$	1.00	0.85	1.49	$0.14\cdot10^{4}$	0.00	0.19
137.9	0.85	$0.17\cdot10^{3}$	0.93	1.00	1.11	$0.23\cdot10^{2}$	0.05	0.00
103.0	1.04	$0.20\cdot10^{3}$	0.90	1.00	1.08	$0.20\cdot10^{2}$	0.04	0.00
93.9	0.91	$0.19\cdot10^{3}$	0.97	1.00	1.08	$0.17\cdot10^{2}$	0.03	0.00
86.1	1.09	$0.25\cdot10^{3}$	0.89	1.00	1.03	$0.58\cdot10^{1}$	0.01	0.00

Table 5.3. Fitting parameters for the second relaxation process (HN2) of ODA-9 at different temperatures in heating and cooling conditions.

T (°C)	f_r (Hz)	$\Delta\varepsilon$	a	b	f_r_err	$\Delta\varepsilon$ _err	a_err	b_err
86.1	0.86	$0.11\cdot10^{2}$	0.93	0.93	1.84	$0.15\cdot10^{2}$	0.20	0.18
93.9	2.76	$0.40\cdot10^{2}$	1.00	1.00	1.09	$0.46\cdot10^{1}$	0.00	0.00
98.8	2.36	$0.47\cdot10^{2}$	1.00	1.00	1.09	$0.56\cdot10^{1}$	0.00	0.00
103.0	3.11	$0.47\cdot10^{2}$	1.00	1.00	1.09	$0.47\cdot10^{1}$	0.00	0.00
154.8	2.41	$0.17\cdot10^{3}$	0.96	1.00	1.12	$0.44\cdot10^{2}$	0.09	0.00
137.9	3.90	$0.11\cdot10^{3}$	1.00	1.00	1.12	$0.15\cdot10^{2}$	0.00	0.00
103.0	6.68	$0.92\cdot10^{2}$	0.95	1.00	1.10	$0.16\cdot10^{2}$	0.01	0.00
93.9	5.15	$0.89\cdot10^{2}$	0.98	1.00	1.11	$0.15\cdot10^{2}$	0.02	0.00
86.1	4.76	$0.61\cdot10^{2}$	1.00	1.00	1.06	$0.50\cdot10^{1}$	0.00	0.00

Table 5.4. Fitting parameters for the third relaxation process (HN3) of ODA-9 at different temperatures in heating and cooling conditions.

T (°C)	f_r (Hz)	$\Delta\varepsilon$	a	b	f_r_err	$\Delta\varepsilon$ _err	a_err	b_err
93.9	17.95	10.62	1.00	1.00	1.07	0.96	0.00	0.00
98.8	14.89	13.35	1.00	1.00	1.06	1.20	0.00	0.00
103.0	17.27	12.85	1.00	1.00	1.08	1.42	0.00	0.00
154.8	18.51	39.49	1.00	1.00	1.11	9.51	0.00	0.00
137.9	19.57	38.87	1.00	1.00	1.08	4.54	0.00	0.00

Table 5.5. Fitting parameters for the fourth relaxation process (HN4) of ODA-9 at different temperatures in heating and cooling conditions.

T (°C)	f_r (Hz)	$\Delta\varepsilon$	a	b	f_r_err	$\Delta\varepsilon$ _err	a_err	b_err
86.1	$6.75\cdot10^4$	1.85	0.92	1.00	1.04	0.04	0.01	0.00
93.9	$1.68\cdot10^4$	5.61	0.99	0.99	1.04	0.03	0.01	0.04
98.8	$1.82\cdot10^4$	5.30	0.99	1.00	1.01	0.03	0.01	0.00
103.0	$1.91\cdot10^4$	5.12	0.99	1.00	1.01	0.03	0.01	0.00
154.8	$2.28\cdot10^4$	4.30	0.98	1.00	1.02	0.08	0.01	0.00
137.9	$2.18\cdot10^4$	4.79	0.95	1.00	1.01	0.05	0.01	0.00
103.0	$2.09\cdot10^4$	5.05	0.96	1.00	1.01	0.06	0.01	0.00
93.9	$2.03\cdot10^4$	5.22	0.99	1.00	1.01	0.07	0.01	0.00
86.1	$1.73\cdot10^4$	6.22	0.97	1.00	1.01	0.04	0.01	0.00

Table 5.6. Fitting parameters for DC conductivity of E7 at T = 27 °C.

σ (S/cm)	n	σ_err	n_err
1.75	0.66	0.53	0.38

HN_mode	f_r (Hz)	$\Delta\varepsilon$	a	b	f_r_err	$\Delta\varepsilon$ _err	a_err	b_err
1	0.19	$0.90 \cdot 10^2$	0.81	1.00	1.62	$0.90 \cdot 10^2$	0.26	0.00
2	1.30	$0.92 \cdot 10^2$	0.86	1.00	1.38	$0.58 \cdot 10^2$	0.05	0.00
3	$2.61 \cdot 10^4$	$0.44 \cdot 10^1$	0.98	1.00	1.02	0.07	0.01	0.00

5.4 Summary

The relaxation behaviour of dielectric permittivity has been determined with some basic physical parameters in the frequency range from 10 mHz to 100 kHz and during the different phases of a new bent-core liquid crystalline material. From dielectric spectra emerges the presence of four distinct modes during heating conditions that are unusual for this kind of liquid crystals and the third mode (HN3), a Debye type response, could indicate the formation of temporary polarized clusters even in fluid phases. The large permittivity at low frequencies is also unusual for this kind of liquid crystals and could be seen as another proof of the presence of cybotactic clusters.

References

1. T. Niori, T. Sekine, J. Watanabe, T. Furukawa, H. Takezoe, J. Mater. Chem. 6(7), 1231-1233 (1996)

2. T. Sekine, T. Niori, M. Sone, J. Watanabe, S.W. Choi, Y. Takanishi, H.Takezoe, Jpn. J. Appl. Phys., 36, 6455 (1997)

3. D.R. Link, G. Natale, R. Shao, J.E. Maclennan, N.A. Clark, E. Körblova, D.M. Walba, Science 278, 1924-1927 (1997)

4. H.R. Brand, P.E. Cladis, H. Pleiner Eur. Phys. J. B, 6, 347-352 (1998)

5. T.C. Lubensky, L. Radzihovsky Phys. Rev. E, 66, 031704-1-27 (2002)

6. L. Radzihovsky and T. C. Lubensky Europhys. Lett., 54, 206-212 (2001)

7. H. R. Brand, H. Pleiner, and P. E. Cladis Eur. Phys. J. E, 7, 163-166 (2002)

8. O. Francescangeli, V. Stanic, S. I. Torgova, A. Strigazzi, N. Scaramuzza, C. Ferrero, I.P. Dolbnya, T. M. Weiss, R. Berardi, L. Muccioli, S. Orlandi, and C. Zannoni, Adv. Funct. Mater., 19, 2592-2600 (2009)

9. J. Harden, B. Mbanga, N. Éber, K. Fodor-Csorba, S. Sprunt, J.T. Gleeson, and A. Jákli, Phys. Rev. Lett. 97, 157802 (2006)

10. D. B. Wiant, J. T. Gleeson, N. Éber, K. Fodor-Csorba, A. Jákli, and T. Tóth-Katona, Phys. Rev. E 72, 041712 (2005)

11. S. Tanaka, H. Takezoe, N. Éber, K. Fodor-Csorba, A. Vajda, and Á. Buka, Phys. Rev. E 80, 021702 (2009).

12. P. Tadapatri, U. S. Hiremath, C. V. Yelamaggad, and K. S. Krishnamurthy, J. Phys. Chem. B 114, 10 (2010)

13. M. Majumdar, K. Neupane, J. T. Gleeson, A. Jakli, S. Sprunt, Flexoelectric effect in a bent-core liquid crystal measured by Dynamic Light Scattering, Abstract: W8.00006, APS March meeting, New Orleans, 2008 (unpublished).

14. D. Wiant, S. Stojadinovic, K. Neupane, S. Sharma, K. Fodor-Csorba, A. Jákli, J. T. Gleeson, S. Sprunt, Phys. Rev. E 73, 030703 (R) (2006)

15. J. Harden, B. Mbanga, N. Éber, K. Fodor-Csorba, S. Sprunt, J.T. Gleeson, A. Jákli, Physical Review Letters, 97, 157802 (2006)

16. A. Jákli, M. Chambers, J. Harden, M. Majumbar, R. Teeling, J. Kim, Q. Li, G.G. Nair , N. Éber, K. Fodor-Csorba, J.T. Gleeson, S. Sprunt, Proc. SPIE 6911 (2008)

17. V. Domenici, C.A. Veracini, and B. Zalar, Soft Matt., 1, 408 (2005)

18. G. Cinacchi, and V. Domenici, Phys. Rev. E, 74, 030701 (2006)

19. S. Havriliak, and S. Negami, Polymer 8, 101 (1967)

20. D.W. Davidson, and R.H. Cole, J. Chem. Phys. 19, 1484-1490 (1951)

21. K.S. Cole, and R.H. Cole, J. Chem. Phys 9, 341-351 (1941)

22. Y. Feldman, A. Puzenko and Y. Ryabov, Fractals, Diffusion, and Relaxation in Disordered Complex Systems: A Special Volume of Advances in Chemical Physics (John Wiley & Sons, Inc, Hoboken, 2006) Volume 133, Part A.

23. F. Kremer and A. Schonhals, Broadband Dielectric Spectroscopy (Springer-Verlag, Berlin, 2003)

24. G.P. Sinha, and F.M. Aliev, Phys. Rev. E, 58, 2001 (1998)

25. T. Salfetnikova, G. Zhuchkova, C. Dantlgraber, C. Tschierske and H. Kresse Liq. Cryst., 29, 155-158 (2002)

26. H. Schlacken, P. Schiller, and H. Kresse, Liq. Cryst., 28, 1235 (2001)

27. F. Kremer, S. U. Vallerien, and R. Zentel, Adv. Mater., 2, 145 (1990)

28. L. Marino, A. Th. Ionescu, S. Marino, N. Scaramuzza, Dielectric investigations on a bent-core liquid crystal. In print on Journal of Applied Physics, DOI: 10.1063/1.4767915

Conclusions

The family of chiral smectic C* liquid crystal phases constitutes a fascinating set of structural variations in fluids. The combination of chirality and a layered structure in which the director tilts with respect to the layer normal makes all these phases locally polar, in the sense that every smectic layer carries a nonzero spontaneous polarization in the layer plane. In Chapter 3 some physical parameters like dielectric increments, dielectric relaxation times, characteristic frequencies of the various modes, have been determined for W-129. Contributions to permittivity arise principally from the Goldstone mode and, in particular, dielectric increment is very large (∼ 287). A very high relaxation peak, probably due to the ionization diffusion in the limit of zero mobility of slow ions, is also present at low temperatures (20/25°C) and at low frequencies (∼ 0.1 Hz). A great variety of relaxation responses that could indicate the presence of different SmC* subphases has been observed with the DS technique in partial agreement with other techniques like DSC and optical microscopy. The study of SmC* subphases is still open and collects a lot of interest in academic environments. It is important to know that for a better comprehension of the structure of these subphases other characterization techniques like resonant x-ray scattering should be employed. An evaluation of the viscosity of the anti-phase motion has also been done.

In a second step the basic physical parameters of an antiferroelectric liquid crystal mixture doped with gold nanoparticles have been determined. The gold nanoparticles influence the dielectric spectra; in fact the HN2 mode and the HN3 mode result shifted and changed in intensity. The nano-composite material obtained by the dispersion of the gold nanoparticles presents interesting characteristics, such as an enhancement of dielectric increments (or strengths) probably due to the molecular interactions between the ferroelectric liquid crystal and the gold nanoparticles, which translates into an increase of the order of the liquid crystal host. From DSC and dielectric spectroscopy comes the confirmation that nanoparticles also affect the persistence and the extension of smectic subphases; This result may have interesting implications for the realization of commercial switchable devices. Finally we have seen that nanoparticles enhance nonvolatile memory effect, promising for digital nonvolatile memory devices, already present in the pure antiferroelectric mixture.

In the last part of this work the relaxation behaviour of dielectric permittivity has been determined with some basic physical parameters in the frequency range from 10 mHz to 100 kHz and during the different phases of a new bent-core liquid crystalline material. From dielectric spectra emerges the presence of four distinct modes during heating conditions that are unusual for this kind of liquid crystals and the third mode (HN3), a Debye type response, that could indicate the formation of temporary polarized clusters even in fluid phases. The large permittivity at low frequencies is also unusual for this kind of liquid crystals and could be seen as another proof of the presence of cybotactic clusters. Other measurements, like reversal current method or XRD could be carried out to verify the presence of polar clusters with ferroelectric or antiferroelectric properties.

PUBLISHED PAPERS (1 – 2)

Molecular Crystals and Liquid Crystals
Publication details, including instructions for authors and subscription information:
http://www.tandfonline.com/loi/gmcl20

Dielectric Characterisation of an Orthoconic Antiferroelectric Liquid Crystal Mixture

L. Marino [a], E. Bruno [a], M. P. De Santo [a b], F. Ciuchi [b], S. Marino [a b] & N. Scaramuzza [a b]

[a] Dept. of Physics, University of Calabria, Ponte P. Bucci, Cubo 33B, Rende (CS), 87036, Italy

[b] CNR-IPCF, UOS Cosenza, and Excellence Centre CEMIF.CAL, Ponte P. Bucci, Rende (CS), 87036, Italy

Available online: 18 Apr 2012

To cite this article: L. Marino, E. Bruno, M. P. De Santo, F. Ciuchi, S. Marino & N. Scaramuzza (2012): Dielectric Characterisation of an Orthoconic Antiferroelectric Liquid Crystal Mixture, Molecular Crystals and Liquid Crystals, 558:1, 120-126

To link to this article: http://dx.doi.org/10.1080/15421406.2011.653717

Mol. Cryst. Liq. Cryst., Vol. 558: pp. 120–126, 2012

ISSN: 1542-1406 print/1563-5287 online
DOI: 10.1080/15421406.2011.653717

Taylor & Francis
Taylor & Francis Group

Dielectric Characterisation of an Orthoconic Antiferroelectric Liquid Crystal Mixture

L. MARINO,[1,*] E. BRUNO,[1] M. P. DE SANTO,[1,2] F. CIUCHI,[2] S. MARINO,[1,2] AND N. SCARAMUZZA[1,2]

[1]Dept. of Physics, University of Calabria, Ponte P. Bucci, Cubo 33B, Rende (CS), 87036, ITALY
[2]CNR-IPCF, UOS Cosenza, and Excellence Centre CEMIF.CAL, Ponte P. Bucci, Rende (CS), 87036, ITALY

Dielectric properties of the orthoconic smectic liquid crystalline mixture W-129, which presents both antiferroelectric and ferroelectric smectic C phases, have been studied in the frequency range from 10 mHz to 100 kHz in planar aligned cells. Some important relaxation modes were detected in SmCa and SmC* phases. Dielectric increments, distribution parameters and relaxation frequencies of these modes have been evaluated at different temperatures. From the study of dielectric spectra a great variety of relaxation responses emerges that could indicate the presence of different SmCa* subphases.*

Keywords Dielectric spectroscopy; orthoconic antiferroelectric mixtures; relaxation modes

Introduction

It is well known that tilted chiral structures in smectic liquid crystal phases exhibit spontaneous polarization and if the structure is synclinic the liquid crystal is called ferroelectric liquid crystal (FLC) while if the structure is anticlinic (the director is tilted in opposite direction in alternate layers) the liquid crystal is an antiferroelectric liquid crystals (AFLC).

The study of FLCs and AFLCs is important for different aspects: the interesting physical properties and their application in electro-optical devices. Moreover, due to their fast response time, they can be employed in visual display applications [1,2].

Dielectric spectroscopy is a useful tool for characterizing liquid crystals phases which allows a temperature dependent analysis of their physical properties.

The electro-optical response of a liquid crystal cell is related to dielectric modes observed in liquid crystals phases. In fact if the dielectric relaxation mode is fast, the electrooptical switching related to this mode can be fast as well [3].

If a smectic C* (SmC*) phase is present in the Liquid Crystal (LC) phase diagram, the dielectric response would be a result of two relaxation modes [4–7]. The first, Goldstone mode, due to the phase fluctuation in the azimuthal orientation of the director, is usually observed in the low frequency range. The second is the soft mode that corresponds to

*Address correspondence to L. Marino, Dept. of Physics, University of Calabria, Ponte P. Bucci, Cubo 33B, Rende (CS), 87036, ITALY. E-mail: lucia.marino@fis.unical.it

fluctuations in the tilt-angle of the director and appears in the SmC* and in the SmA* phases becoming more evident near SmC* to SmA* phase transition.

In this work, dielectric spectroscopy is used to investigate the high-tilted chiral smectic phases of the antiferroelectric liquid crystal W-129. This material exhibits an high spontaneous polarization at room temperature (300 nC/cm^2) in virtue of its tilted chiral structure (the tilt angle is 45° at room temperature). The Cole-Cole function has been used to determine the dependence of distribution parameter, dielectric increment (also called dielectric strength) and relaxation frequency as a function of temperature.

Experimental

W-129 has been synthesized from R. Dabrowski group at the Military University of Technology, in Warsav, Poland, it is a smectic liquid crystalline mixture which presents both ferroelectric and antiferroelectric smectic C phases. The phase sequence of this material is the following: Cr - 13/15°C - SmCa* - 84.5°C - SmC* - 102.3°C - SmA* - 117/125.2°C Iso, obtained from DSC measurements. The study of electro-optical properties of W-129 has been already done in the past as detailed in Ref. [8].

A Japanese commercial cell (EHC Ltd, Tokyo, Japan) with a thickness of (2.0 ± 0.2) μm and a ITO resistance of 100 Ω/□ has been used. The cell was filled by capillary method in the isotropic phase [9].

The dielectric measurements have been carried out using an EG&G 263A galvanostat-potentiostat in the frequency range 10 mHz–100 kHz with a maximum applied voltage of 0.5 V (RMS) and no bias field was applied. In order to perform dielectric measurements as a function of temperature the sample has been placed in a CaLCTec FB150 programmable temperature hot stage, it has been slowly heated to a temperature of 110°C and then slowly cooled in order to achieve the best conditions for dielectric measurements.

Results and Discussion

The real part of the dielectric permittivity (ε^I) is almost constant in the SmA* phase and for frequencies from 0.1 to 10 Hz (see Fig. 1). For these frequencies, ε^I is also almost constant in the SmC* phase. For the other frequencies the real part of the permittivity decreases gradually with decreasing temperature until the SmA*-SmC* transition temperature is reached, then it increases slowly for frequencies equal to 100 Hz and 10 kHz and increases rapidly for frequency equal to 1 kHz. In this last region the soft ferroelectric mode contributes to the increase of the dielectric constant.

Further cooling the sample, below the SmC*- SmCa* transition, the dielectric constant decreases slowly till the temperature of 70°C is reached, then decreases very rapidly. The measurements performed at 10 kHz show an opposite behaviour.

The frequency dependence of the real and imaginary parts of the dielectric constant, respectively called, dispersion and absorption or dielectric loss curve, shows different relaxation responses (see Fig. 2(a),(b)). The dielectric loss curve (Fig. 2(b)) shows a very high relaxation peak, probably due to the ionization diffusion in the limit of zero mobility of slow ions at room temperature (20/25°C) and at very low frequencies (∼0.1 Hz). The Goldstone mode results more evident in the region from 10 to 10^2 Hz and for temperatures from 85°C to 110°C.

For a complete overiew of experimental data, dispersion/absorption spectra are shown together with the Cole-Cole plots obtained for every fixed temperature. All parameters

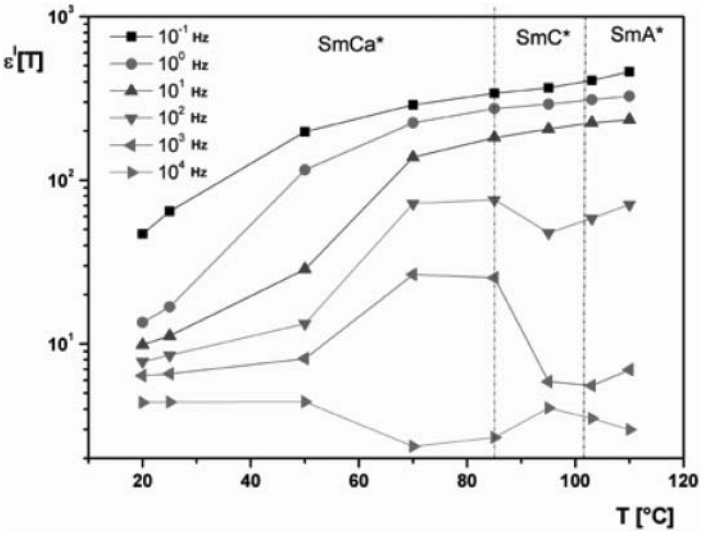

Figure 1. Temperature dependence of the real part of the dielectric constant at different fixed frequencies.

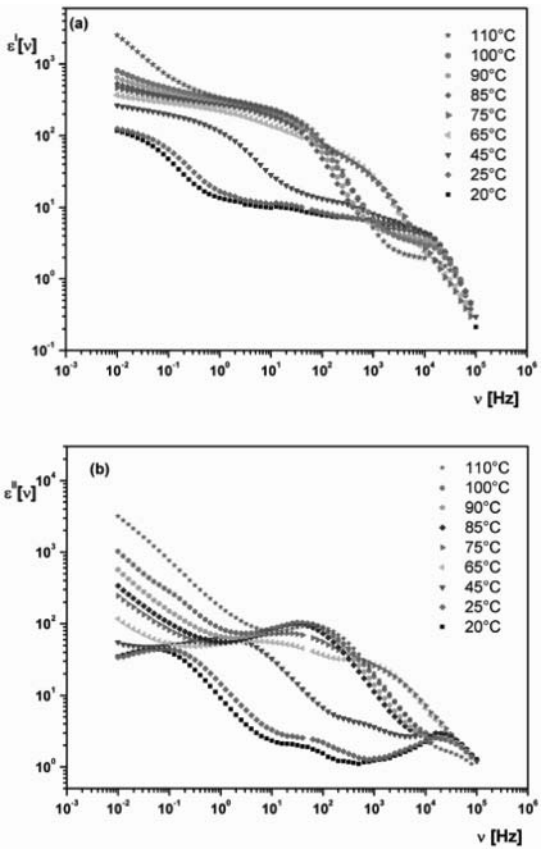

Figure 2. Dispersion (a) and absorption (b) curves of the dielectric spectra acquired for W-129 at different temperatures.

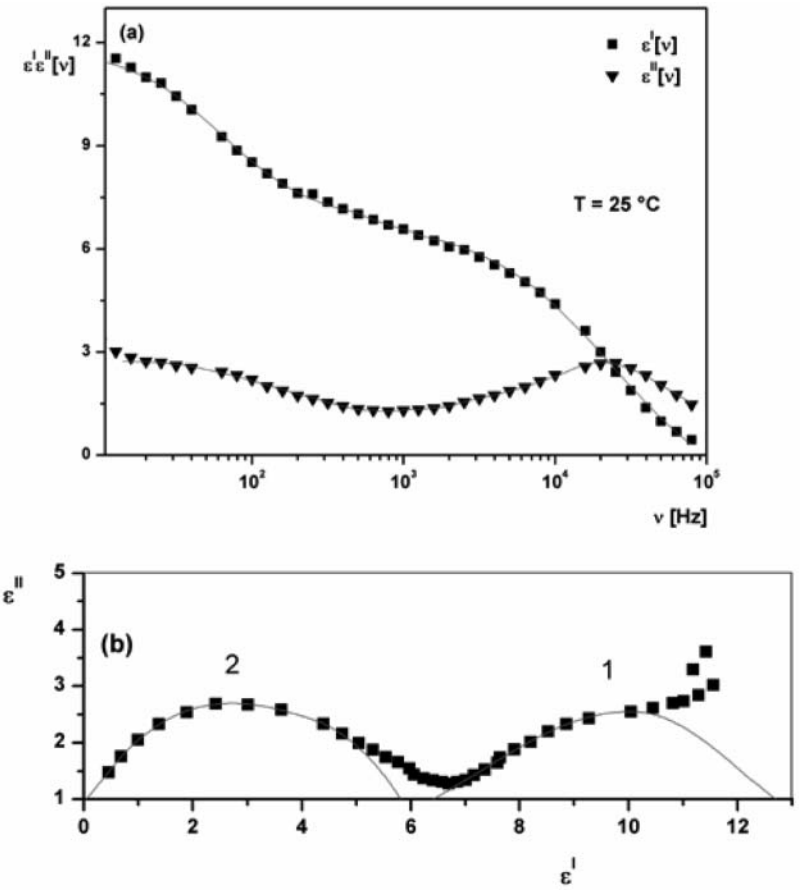

Figure 3. Dispersion and absorption curves (a) and Cole-Cole plot (b) of the dielectric spectra acquired for W-129 at 25°C. The solid red line shows the best theoretical fit of the Cole–Cole equation into experimental data.

were obtained from fitting the experimental dielectric constant data with the Cole-Cole modification of the Debye equation [10],

$$\varepsilon^* = \varepsilon_\infty + \frac{\varepsilon(0) - \varepsilon_\infty}{1 + (i2\pi\upsilon\tau)^{1-\alpha}} \tag{1}$$

Table 1. Fitting parameters for the two relaxation processes shown in Fig. 3 for SmCa* phase of W-129

T = 25°C						
Process	f_a	ε (0)	τ [s]	α	ε (∞)	$\Delta\varepsilon$
1	63.47	11.84	2.51 · E ^−3	0.31	6.78	5.06
2	2.38 · E ^+4	6.79	6.68 · E ^−6	0.49	1.59	5.20

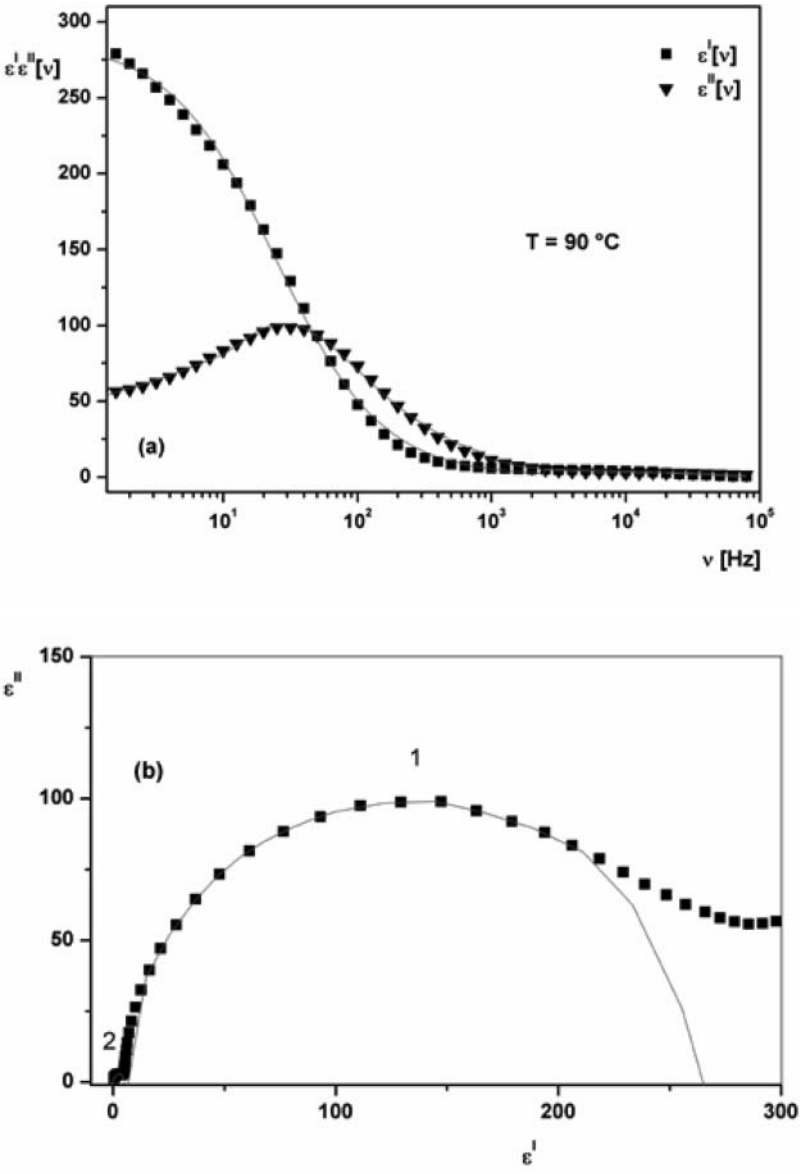

Figure 4. Dispersion and absorption curves (a) and Cole-Cole plot (b) of the dielectric spectra acquired for W-129 at 90°C. The solid red line shows the best theoretical fit of the Cole–Cole equation into experimental data.

where ν is the frequency, $\varepsilon(0)$ is the static dielectric constant, ε_∞ is the high frequency dielectric constant, $\tau(=1/(2\pi\nu_a))$ is the dielectric relaxation time, ν_a is the absorption peak frequency and α is the distribution parameter for a particular relaxation process that varies between 0 and 1. If α is very small (eq. 1), it satisfies the Debye equation while if α is more than 0.5 there could be more than one relaxation process.

Table 2. Fitting parameters for the two relaxation processes shown in Fig. 4 for SmC* phase of W-129

T = 90°C						
Process	f_a	ε (0)	τ [s]	α	ε (∞)	$\Delta\varepsilon_i$
1	24.42	287.42	6.52 · E ^−3	0.45	0.67	286.75
2	2.28 · E ^+4	5.05	6.98 · E ^−6	0.08	0.12	4.93

The real and imaginary part of the dielectric constant are shown together with the Cole-Cole plots at 25°C and 90°C respectively (see Fig. 3 and Fig. 4).

The relaxation response of W-129 at 25°C (Fig. 3(b)) is typical of the antiferroelectric phase. Two relaxation processes are evident: the relaxation process (2) corresponds to Anti-phase mode (PHM), the other process (1) corresponds to In-phase mode (PLM). In the Cole-Cole plot, obtained at 90°C (Fig. 4(b)), the Goldstone mode is well clear (1), while the Soft mode (2) is weakly detected.

The large value of distribution parameters evalueted for both processes at 25°C (see Table 1) makes the Cole-Cole plot far from being a overlapping of two semi-circles. The same result has been obtained for process (1) at 90°C (see Table 2) where an unusually large value of dielectric increment has been revealed. The very small value of the distribution parameter for process (2) (Table 2) makes the Cole-Cole mode very close to be a semi-circle, reducing it to a Debye response.

Conclusions

The basic physical parameters (i.e. relaxation frequencies, relaxation times, dielectric increments and distribution parameters) of an antiferroelectric liquid crystalline mixture have been determined for SmCa* and SmC* phases.

From dielectric spectra a great variety of relaxation responses that could indicate the presence of different SmCa* subphases is observed. Contributions to permittivity arise principally from the Goldstone mode and, in particular, dielectric increment is very large (∼287). A very high relaxation peak, probably due to the ionization diffusion in the limit of zero mobility of slow ions, is also present at low temperatures (20/25°C) and at low frequencies (∼0.1 Hz).

Acknowledgments

The authors acknowledge Professor Dabrowski for providing the W-129 liquid crystal, Dr M. Sposato for providing the necessary experimental facilities and for the interesting discussions and Mrs. Francesca Misasi for critical reading of the manuscript.

References

[1] Maltese, P. (1992). *Mol. Cryst. Liq. Cryst.*, *215*, 57–72.
[2] Koen D'havé. (2002). *Application of Antiferroelectric Liquid Crystals with High Tilt*, PhD Thesis, University of Gent: Belgium.
[3] Perkowski, P., Lada, D., Ogrodnik, K., Rutkowska, J., Piecek W., & Raszewski, Z. (2008). *Opto-Electron. Rev.*, *16*(3), 271–276.

[4] Filipic, C., Carlsson, T., Levstik, A., Zeks, B., Gouda, F., Lagerwall, S. T., & Skarp, K. (1988). *Phys. Rev. E*, *38*, 5833–5839.
[5] Gouda, F., Skarp, K., & Lagerwall, S. T. (1991). *Ferroelectrics*, *113*, 165–206.
[6] Hiller, S., Biradar, A. M., Wrobel, S., & Haase, W. (1998). *Phys. Rev. E*, *53*, 641–649.
[7] Rajiv, M., Abhishek Kumar, M., Abhishek Kumar, S., Purna Bahadur, C., & Shukla, J. P. (2007). *Soft Materials*, *5*(4), 207–218.
[8] Dabrowski, R. (2004). *Mol. Cryst. Liq. Cryst.*, *421*, 1.
[9] Perez Jubindo, M. A., Ezucer, A., Etxebarria, J., Remon, A., Tello, M. J., Marcos, M., & Serrano, J. L. (1988). *Mol. Cryst. Liq. Cryst.*, *159*, 137.
[10] Cole, K. S., & Cole, R. H. (1941). *J. Chem. Phys.*, *9*, 341.

J_ID: JAP DOI: 10.1063/1.4767915 Date: 10-November-12 Stage: Page: 1 Total Pages: 9

JOURNAL OF APPLIED PHYSICS **112**, 000000 (2012)

Dielectric investigations on a bent-core liquid crystal

Lucia Marino,[1,2] Andrei Th. Ionescu,[2,3] Salvatore Marino,[2] and Nicola Scaramuzza[1,2,a)]
[1]*Dipartimento di Fisica, Università della Calabria, Via Pietro Bucci, Cubo 31C, 87036 Rende (Cosenza), Italy*
[2]*CNR-IPCF UoS di Cosenza, Licryl Laboratory, and Centro di Eccellenza CEMIF.CAL, Università della Calabria, 87036 Rende (Cosenza), Italy*
[3]*Faculty of Physics, University of Bucharest, P.O. Box MG-11, RO-077125 Bucharest, Romania*

(Received 5 August 2012; accepted 31 October 2012; published online xx xx xxxx)

Dielectric measurements on a bent-core liquid crystal were carried out in the frequency range from 10 MHz to 100 kHz in planar aligned cells. Four relaxation ranges were detected during heating condition: two in a low frequency range of a few hertz probably due to conductivity and interface relaxation phenomena, another between 10 and 20 Hz, and another one in a range between 10 kHz and 100 kHz in smectic as in nematic and isotropic phases. The third relaxation response is no more visible during cooling conditions. Dielectric increments, distribution parameters, and relaxation frequencies have been evaluated at different temperatures by fitting data with Havriliak-Negami (H-N) relaxation function, which is an empirical modification of the Debye relaxation model. The presence of a relaxation response between 10 and 20 Hz and the relatively great values of the permittivity could suggest the presence of a ferroelectric response due to the presence of cybotactic clusters. © *2012 American Institute of Physics*. [http://dx.doi.org/10.1063/1.4767915]

I. INTRODUCTION

The discovery of the mesogenic properties of bent-core molecules has opened another exciting dimension in the field of thermotropic liquid crystals (LCs). Different aspects, for instance, the observation of ferroelectricity due to a spontaneous chiral symmetry breaking in smectic phases composed of non-chiral molecules,[1] make this kind of liquid crystals very interesting and useful for a great number of applications. Up today, most of the research effort has focused on bent-core smectics, because liquid phases exhibiting mainly orientational order (nematic (N) phases) are less common.

However, there has been a sudden increase in the theoretical studies[2–7] predicting bent-core nematic (BCN) and isotropic structures with interesting properties, such as biaxiality and spontaneous chirality. In this context, the experimental evidence of a ferroelectric response to a switching electric field in a low molar mass nematic bent-core liquid crystal can be placed.[8]

This kind of response could be explained by considering the effect of the molecules' kinked shape; while rod-shaped molecules can translate during shear flow, bent-shaped molecules experience a steric barrier caused by neighboring molecules and this may promote the formation of temporary clusters even in isotropic phase. For the same reason, the BCN structure is much less common than the N phase of the calamitics. This is mainly because of the kinked shape that is not really compatible with the translational freedom of the calamitic nematics. For this reason, BCNs exhibit some unusual physical properties compared to calamitic ones. These include giant flexoelectricity,[9] unprecedented scenarios in electroconvection,[10–12] as well as an unusual behavior found by light scattering[13] and ^{2}H NMR measurements[8] indicating the presence of clusters with higher ordering.

Dielectric spectroscopy (DS) is a widespread tool for studying liquid crystals which is based on determining the frequency (f) dependent complex permittivity of the substance. It provides not only important material parameters like the static dielectric permittivity and dc electrical conductivity, but it also provides information on the molecular dynamics. The number of relaxation modes is characteristic of the phase and can be associated with certain molecular rotations; the characteristic frequencies reflect how those motions are hindered.

In this work, the DS technique is used to investigate the smectic, nematic, and isotropic phases of bent-shaped liquid crystal ODA-9, and in order to find the parameters of observed phenomenon (relaxation time, conductivity, dielectric increment, etc.), it is necessary to fit the data with generalized relaxation functions. Nowadays, the phenomenological Havriliak-Negami (HN) equation is most frequently used to determine the frequency and temperature dependence of the dielectric parameters.

A low frequency relaxation response seen even in the nematic and isotropic phases probably could be explained by the formation of SmC-type cybotactic clusters, regarded as strongly fragmented SmC phases. Such clustering effect has been suggested by several studies,[14–19] though the exact size, shape, and temporal behavior of the clusters are not known.

II. EXPERIMENTAL

The material used for this study is ODA-9 (Manufacturers: S. Torgova, Lebedev Physical Institute, Russian Academy of Sciences). The phase sequence of this sample is

$$\mathrm{Cr} \underset{68.0\,^\circ\mathrm{C}}{\overset{73.6\,^\circ\mathrm{C}}{\rightleftharpoons}} \mathrm{SmC} \underset{98.2\,^\circ\mathrm{C}}{\overset{98.0\,^\circ\mathrm{C}}{\rightleftharpoons}} \mathrm{N} \underset{109.5\,^\circ\mathrm{C}}{\overset{110.3\,^\circ\mathrm{C}}{\rightleftharpoons}} \mathrm{I}$$

obtained from DSC measurements.

a)Author to whom correspondence should be addressed. Electronic mail: nicola.scaramuzza@fis.unical.it.

ID: sarathyo Time: 11:32 I Path: Q:/3b2/JAP#/Vol00000/123508/APPFile/AI-JAP#123508

J_ID: JAP DOI: 10.1063/1.4767915 Date: 10-November-12 Stage: Page: 2 Total Pages: 9

A Japanese planar aligned commercial cell (EHC Ltd, Tokyo, Japan) with a thickness of (2.0 ± 0.2) μm and an ITO resistance of 100 Ω/□ has been used. The material was introduced into the cells using capillary suction in its isotropic state. The dielectric measurements have been carried out using an EG&G 273A galvanostat-potentiostat/impedentiometer controlled by the impedance software M398 in order to acquire the real and imaginary parts of impedance in the frequency range of 10 MHz–100 kHz with a maximum applied voltage of 1.0 V (RMS) below the Freedericksz threshold. No bias field was applied. In order to perform dielectric measurements as a function of temperature, the sample has been placed in a CaLCTec FB150 programmable temperature hot stage with temperature stability within the range of 0.1 °C.

The measurements have been done at different constant temperatures starting from the smectic to isotropic phases and then slowly cooled from isotropic to crystalline phases.

III. RESULTS AND DISCUSSION

In the specified conditions, real and imaginary parts of the perpendicular component of the complex dielectric

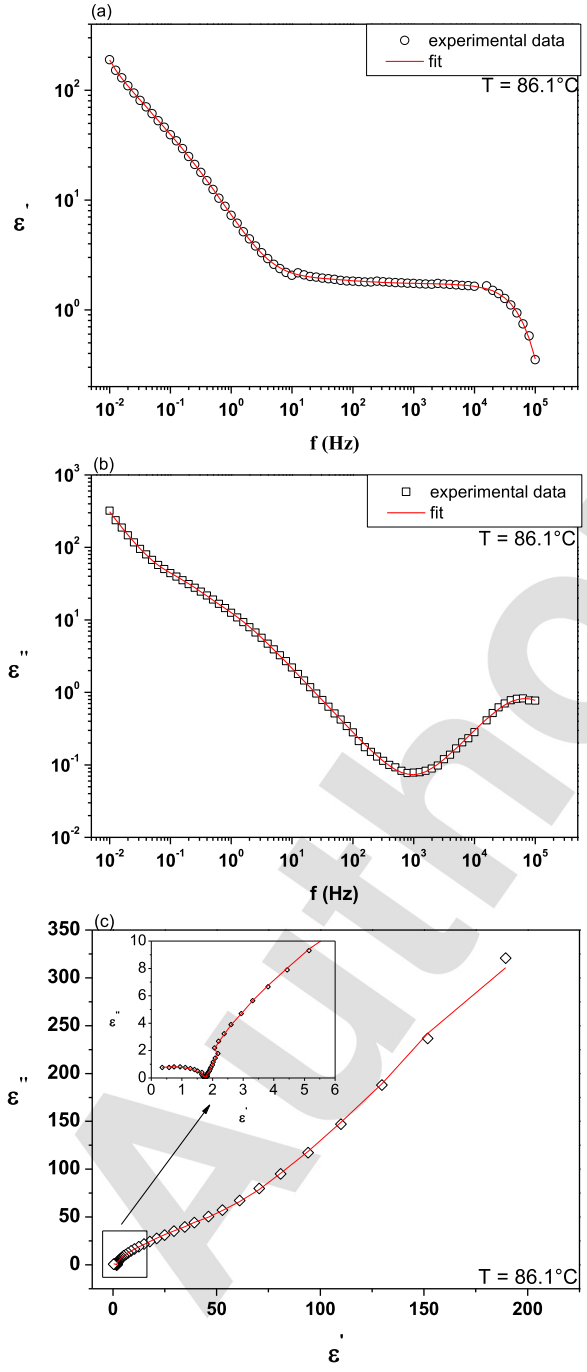

FIG. 1. Dielectric spectrum of ODA-9 acquired at T = 86.1 °C in heating conditions: (a) real part, (b) imaginary part, and (c) Cole-Cole plot. The inset shows a magnification of the selected region. Symbols: experiment; solid lines: fitting.

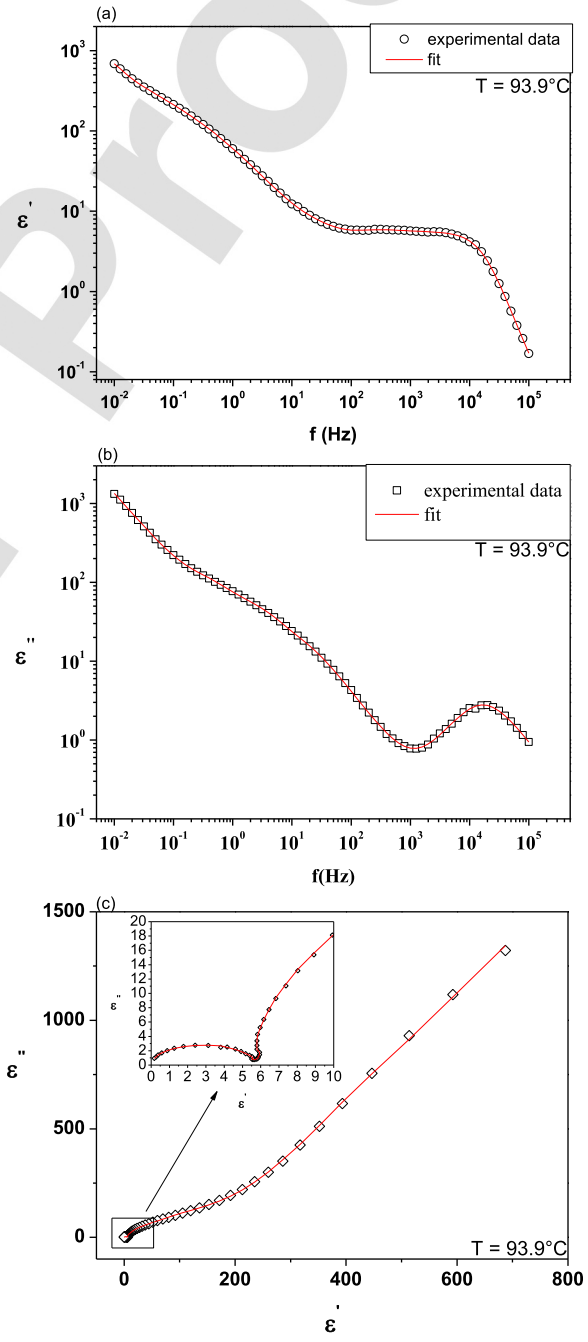

FIG. 2. Dielectric spectrum of ODA-9 acquired at T = 93.9 °C in heating conditions: (a) real part, (b) imaginary part, and (c) Cole-Cole plot. The inset shows a magnification of the selected region. Symbols: experiment; solid lines: fitting.

J_ID: JAP DOI: 10.1063/1.4767915 Date: 10-November-12 Stage: Page: 3 Total Pages: 9

permittivity have been measured in function of frequency at fixed temperatures.

The director relaxation can be described in terms of the complex dielectric permittivity, which is given by

$$\varepsilon^*_\perp(f) = \varepsilon^I(f) - i\varepsilon^{II}(f), \tag{1}$$

where ε^I gives the real part of dielectric permittivity and its spectrum is called the dispersion curve, ε^{II} gives the imaginary part of the complex permittivity and its spectrum is called the absorption or dielectric loss curve, and f being the frequency of the applied electric field. In order to understand the temperature dependence of measured dielectric relaxation, $\varepsilon^*_\perp(f)$ can be described by the Havriliak-Negami function[20] with the addition of a conductivity contribution (third term) present at lower frequencies

$$\varepsilon^*_\perp(f) = \varepsilon_\infty + \sum_j \frac{\Delta\varepsilon_j}{[1+(if\tau_j)^{a_j}]^{b_j}} - \frac{i\sigma}{\varepsilon_0(2\pi f)^n}, \tag{2}$$

where $\Delta\varepsilon_j$ is the dielectric strength, ε_∞ is the high-frequency limit of permittivity, $\tau_j = 1/f_{rj}$ is the relaxation time, f_{rj} is the corresponding relaxation frequency, a_j and b_j are shape parameters describing the asymmetry and broadness of the

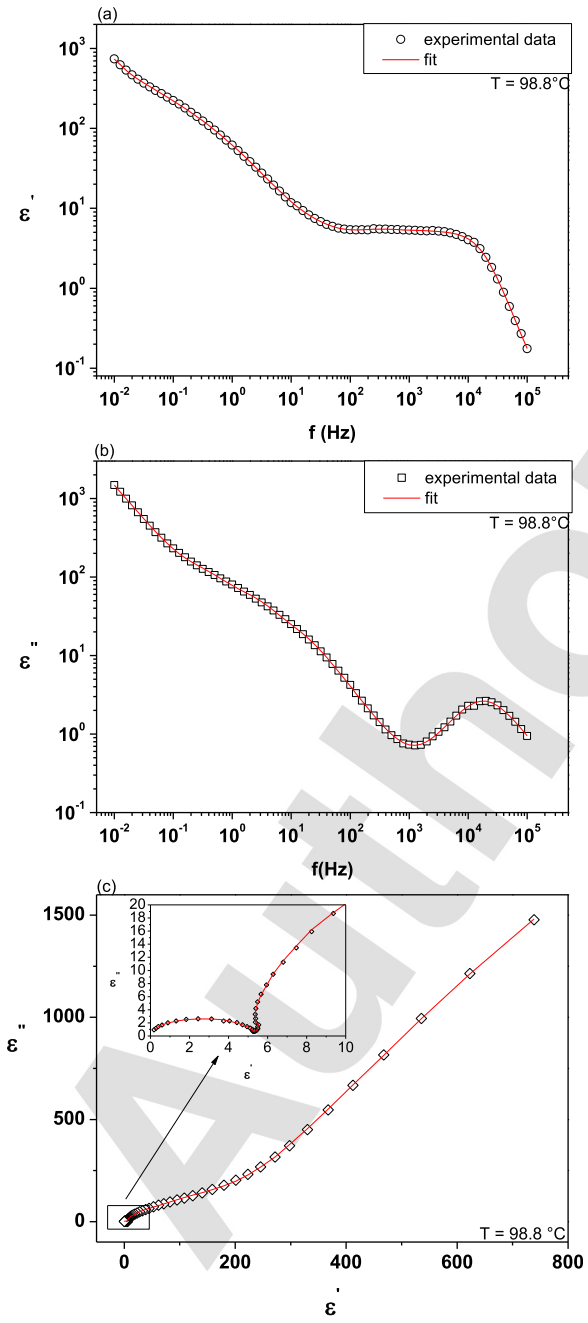

FIG. 3. Dielectric spectrum of ODA-9 acquired at T = 98.8 °C in heating conditions: (a) real part, (b) imaginary part, and (c) Cole-Cole plot. The inset shows a magnification of the selected region. Symbols: experiment; solid lines: fitting.

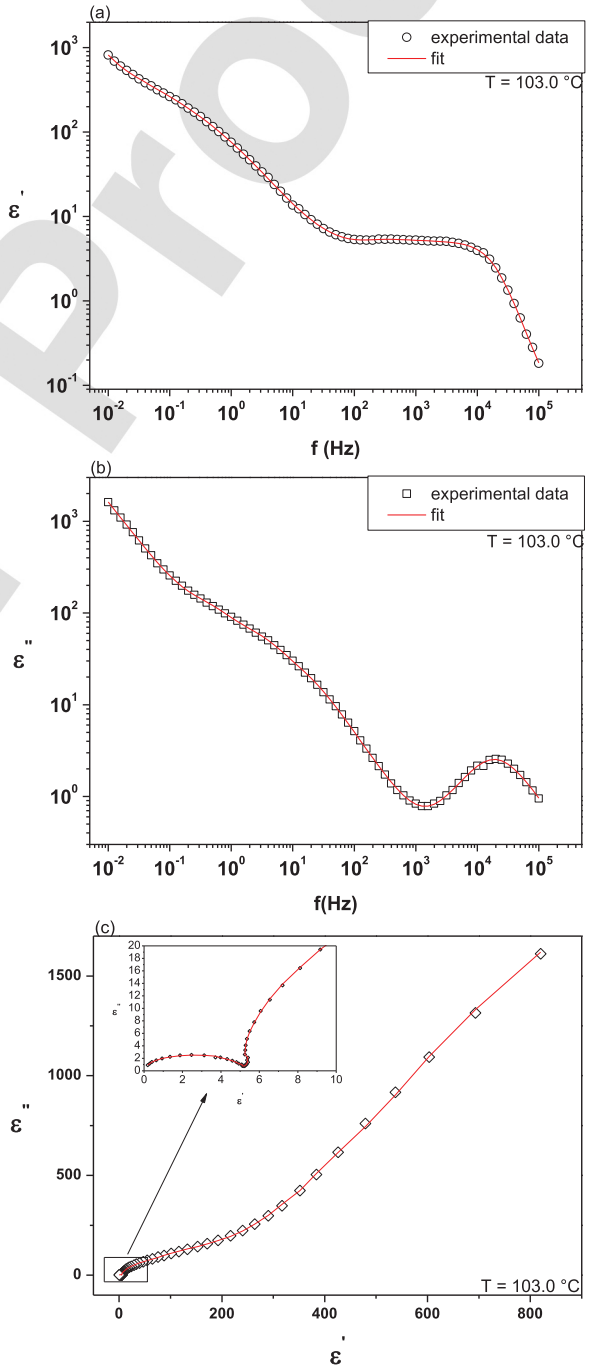

FIG. 4. Dielectric spectrum of ODA-9 acquired at T = 103.0 °C in heating conditions: (a) real part, (b) imaginary part, and (c) Cole-Cole plot. The inset shows a magnification of the selected region. Symbols: experiment; solid lines: fitting.

J_ID: JAP DOI: 10.1063/1.4767915 Date: 10-November-12 Stage: Page: 4 Total Pages: 9

dielectric dispersion curve, ranging between 0 and 1, and j is the number of the relaxation processes. In the last term, σ is related to the conductivity, and n is a fitting parameter responsible for the slope of the conductivity. In the case of pure Ohmic conductivity, $n = 1$, while the decrease of n, $n < 1$ could be observed if, in addition to the contribution to ε^{II} from conductivity, there is an influence of electrode polarization. The HN response reduces to Cole-Davidson[21] response when $a = 1$, and to Cole-Cole response[22] when $b = 1$.

It has to be noticed that the real part $\varepsilon^{I}(f)$ of the complex dielectric permittivity is proportional to the imaginary part $\sigma^{II}(f)$, $\varepsilon^{I}(f) \propto -\sigma^{II}(f)/f$, and the dielectric losses $\varepsilon^{II}(f)$ are proportional to the real part $\sigma^{I}(f)$ of the ac-conductivity, $\varepsilon^{II}(f) \propto \sigma^{I}(f)/f$.[23]

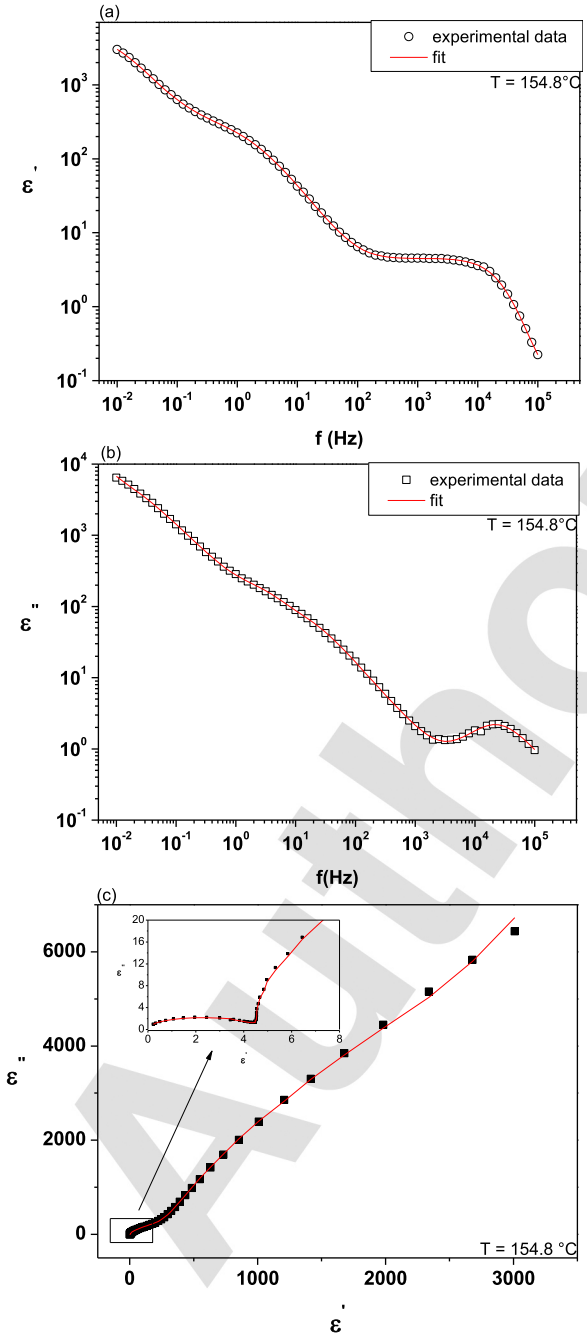

FIG. 5. Dielectric spectrum of ODA-9 acquired at T = 154.8 °C in heating conditions: (a) real part, (b) imaginary part, and (c) Cole-Cole plot. The inset shows a magnification of the selected region. Symbols: experiment; solid lines: fitting.

TABLE I. Fitting parameters for the first relaxation process (HN1) of ODA-9 at different temperatures in heating and cooling conditions.

T (°C)	f_r (Hz)	$\Delta\varepsilon$	a	b	f_r_err	$\Delta\varepsilon$_err	a_err	b_err
86.1	0.12	0.46×10^2	0.93	1.00	1.22	0.30×10^2	0.22	0.00
93.9	0.39	0.11×10^3	0.93	1.00	1.09	0.14×10^2	0.04	0.00
98.8	0.35	0.11×10^3	0.95	1.00	1.09	0.16×10^2	0.05	0.00
103.0	0.43	0.12×10^3	0.93	1.00	1.08	0.14×10^2	0.04	0.00
154.8	0.02	0.21×10^4	1.00	0.85	1.49	0.14×10^4	0.00	0.19
137.9	0.85	0.17×10^3	0.93	1.00	1.11	0.23×10^2	0.05	0.00
103.0	1.04	0.20×10^3	0.90	1.00	1.08	0.20×10^2	0.04	0.00
93.9	0.91	0.19×10^3	0.97	1.00	1.08	0.17×10^2	0.03	0.00
86.1	1.09	0.25×10^3	0.89	1.00	1.03	0.58×10^1	0.01	0.00

Dielectric spectra for smectic C (see Figures 1 and 2), nematic (see Figures 3 and 4), and isotropic phases (see Figure 5) are reported in function of frequency and collected at the augmenting of temperature. At the temperature of 86.1 °C, there are composite dispersions consisting of different molecular processes with their characteristic frequencies not so distant to each other; a sum of two different overlapping modes results from the fit, the first and the second related, respectively, to the ions diffusion and to the interfacial polarization relaxation at the liquid crystal-electrode interface. In fact, the processes are too slow (10^{-2}–1 Hz) to predict the presence of other physical phenomena.[23,24]

In the other spectra, from 93.9 to 154.8 °C, another loss peak is present (10–20 Hz). It is not so improbable that this low frequency peak represents a collective process connected with the formation of antiferroelectric order as just be seen in smectic bent-core phases.[25–27] In this perspective, the large relative permittivity is perhaps justified from the formation of (anti)ferroelectric clusters.

The resulting distribution parameters *a* and *b*, derived from fitting the experimental points (see Table I) are more or less equal to one for all phases, reducing the HN equation to a Cole-Cole or a Debye equation. Only the second process at 86.1 °C exhibits an asymmetrical relaxation peak broadening ($a \approx 0.93$, $b \approx 0.92$), and the first at 154.8 °C that is of Cole-Davidson kind ($a \approx 1.0$, $b \approx 0.85$).

TABLE II. Fitting parameters for DC conductivity of ODA-9 at different temperatures in heating and cooling conditions.

T (°C)	σ (S/cm)	n	σ_err	n_err
86.1	1.739	1.12	1.27	0.09
93.9	26.97	0.85	1.03	0.02
98.8	26.10	0.88	1.04	0.02
103.0	31.65	0.85	1.03	0.01
154.8	140.7	0.82	1.47	0.11
103.0	19.71	0.60	1.04	0.02
93.9	19.50	0.55	1.03	0.01
86.1	12.44	0.62	1.03	0.02

J_ID: JAP DOI: 10.1063/1.4767915 Date: 10-November-12 Stage: Page: 5 Total Pages: 9

Data analysis shows that the strong frequency dependence of ε^{II} for f < 0.1 Hz is due to Ohmic conductivity at 86.1 °C (see Table II), and at increasing temperature (from 93.9 to 154.8 °C), there is a small contribution from the electrode polarization that becomes increasingly important during the cooling process (from 137.9 to 86.1 °C).

The results obtained in the cooling down conditions appear very different from those obtained at heating up. The third mode (HN3) disappears decreasing the temperature and from 103.0 °C to 86.1 °C is not more visible. In Figures 6–9, it is shown that the Cole-Cole plots obtained in cooling conditions appear very different from those obtained in heating conditions. The last peak at higher frequencies (10^4 Hz) is a very clear process measured for all phases which is visible without detailed analysis. It suggests a reorientation around the molecular long axis probably shifted to lower frequencies for the high viscosity of the sample.[28] The nematic phase of ODA-9 has been compared with the nematic phase of E7, a typical rod-like liquid crystal. Real and imaginary parts of E7 are plotted in Figure 10 with Cole-Cole plot. Even in this

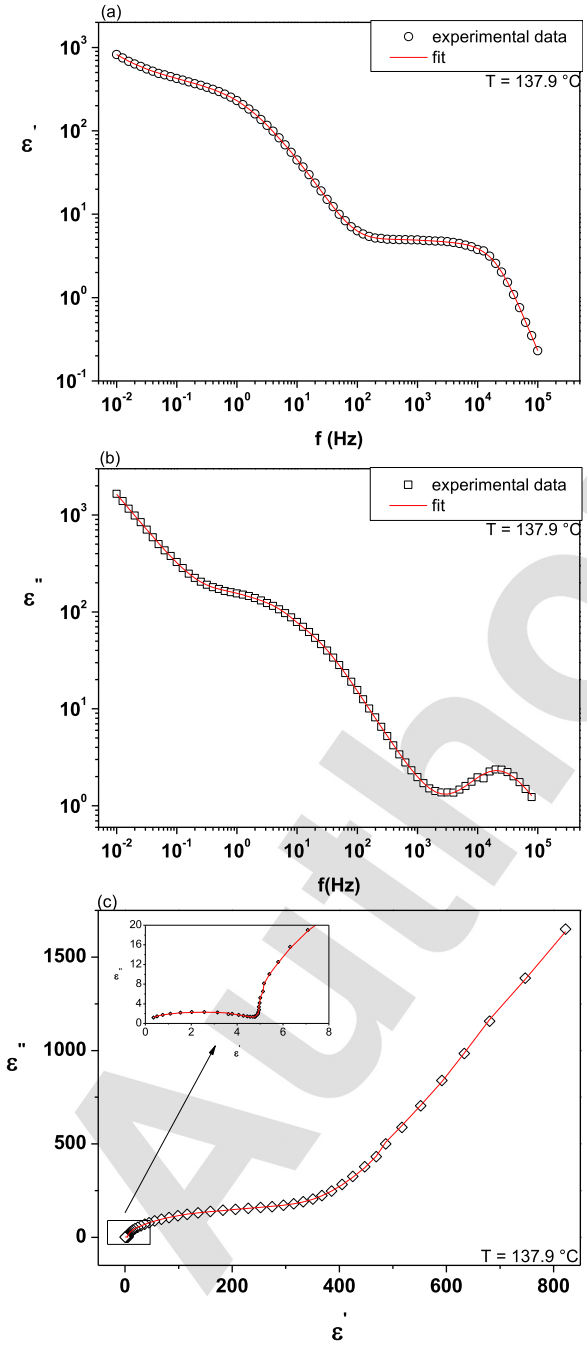

FIG. 6. Dielectric spectrum of ODA-9 acquired at T = 137.9 °C in cooling conditions: (a) real part, (b) imaginary part, and (c) Cole-Cole plot. The inset shows a magnification of the selected region. Symbols: experimental; solid lines: fitting.

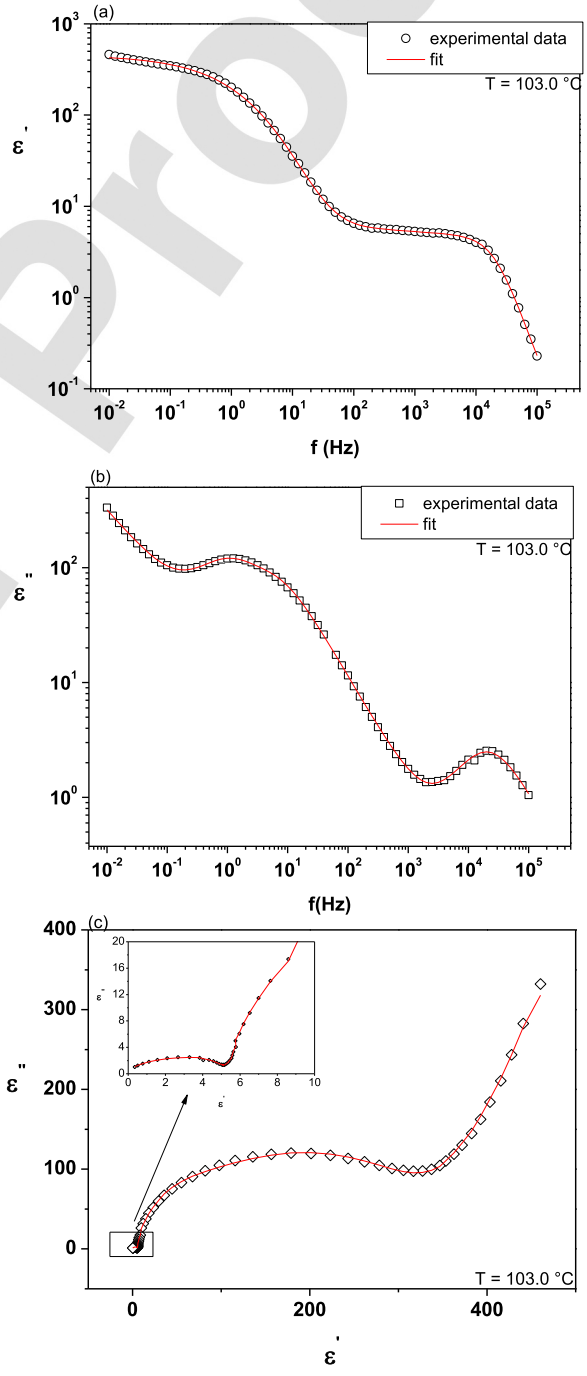

FIG. 7. Dielectric spectrum of ODA-9 acquired at T = 103.0 °C in cooling conditions: (a) real part, (b) imaginary part, and (c) Cole-Cole plot. The inset shows a magnification of the selected region. Symbols: experiment; solid lines: fitting.

J_ID: JAP DOI: 10.1063/1.4767915 Date: 10-November-12 Stage: Page: 6 Total Pages: 9

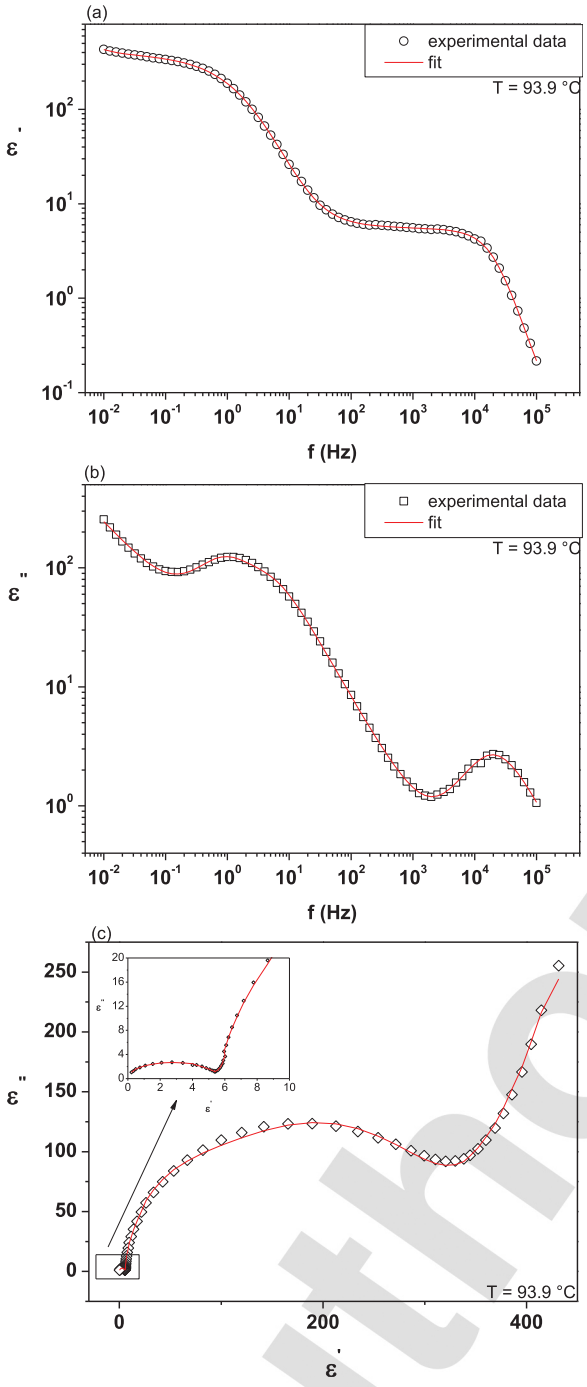

FIG. 8. Dielectric spectrum of ODA-9 acquired at T = 93.9 °C in cooling conditions: (a) real part, (b) imaginary part, and (c) Cole-Cole plot. The inset shows a magnification of the selected region. Symbols: experiment; solid lines: fitting.

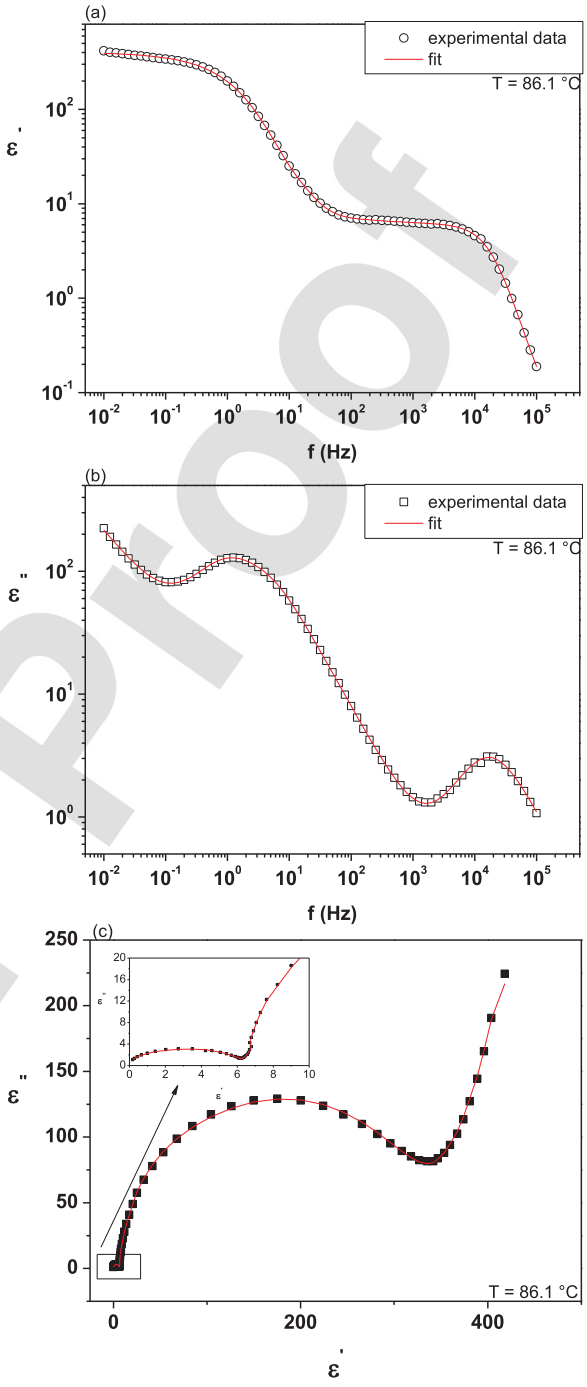

FIG. 9. Dielectric spectrum of ODA-9 acquired at T = 86.1 °C in cooling conditions: (a) real part, (b) imaginary part, and (c) Cole-Cole plot. The inset shows a magnification of the selected region. Symbols: experiment; solid lines: fitting.

case, the dielectric response at low frequencies is due to a combination of ions diffusion and interfacial polarization at the liquid crystal-electrode interface. The peak at higher frequencies is instead due to a reorientation around the molecular long axis. The corresponding fitting parameters are synthesised in Table VI.

Finally, in Figures 11 and 12, 3D graphs are represented in order to visualize the variation of the imaginary part of permittivity in function of frequency and temperature. The differences between heating and cooling conditions are evident. The results are displayed in a smaller range of frequencies in order to better appreciate the contribution of the third dielectric mode. The formation of temporary clusters could be an explanation for the presence of the low frequency relaxation process even in nematic and isotropic phases. In order to verify the presence of ferroelectricity or antiferroelectricity, measurements of the polarization reversal current should be done. All the parameters resulting from fitting are synthesised in Tables II–VI.

J_ID: JAP DOI: 10.1063/1.4767915 Date: 10-November-12 Stage: Page: 7 Total Pages: 9

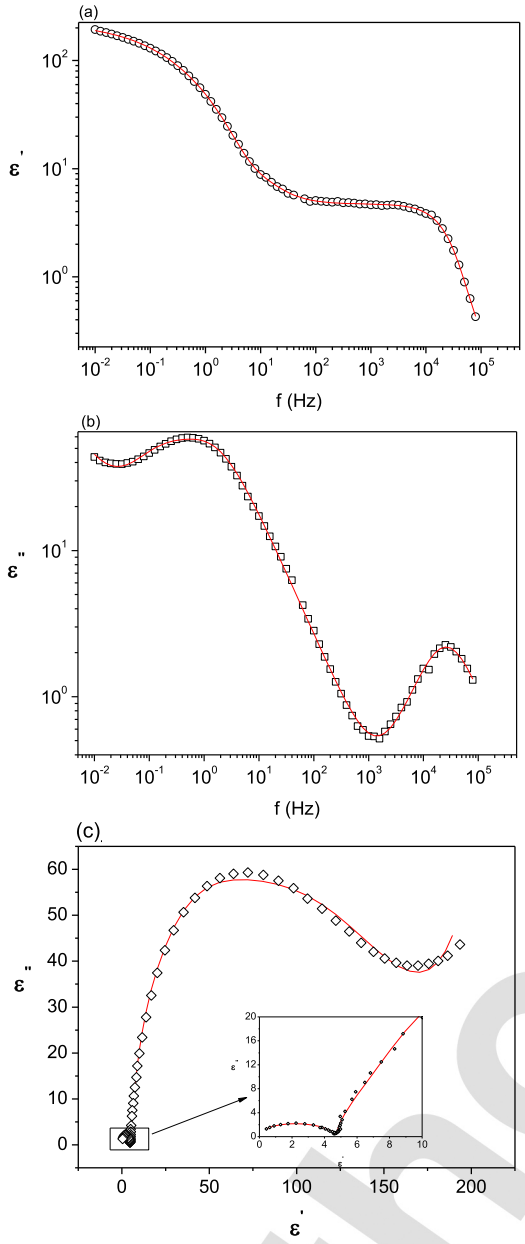

FIG. 10. Dielectric spectrum of E7 acquired at T = 27.0 °C: (a) real part, (b) imaginary part, and (c) Cole-Cole plot. The inset shows a magnification of the selected region. Symbols: experiment; solid lines: fitting.

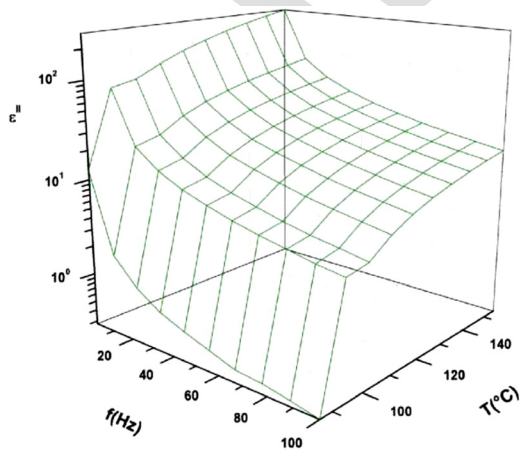

FIG. 11. Imaginary part of complex permittivity in function of frequency and temperature in heating conditions.

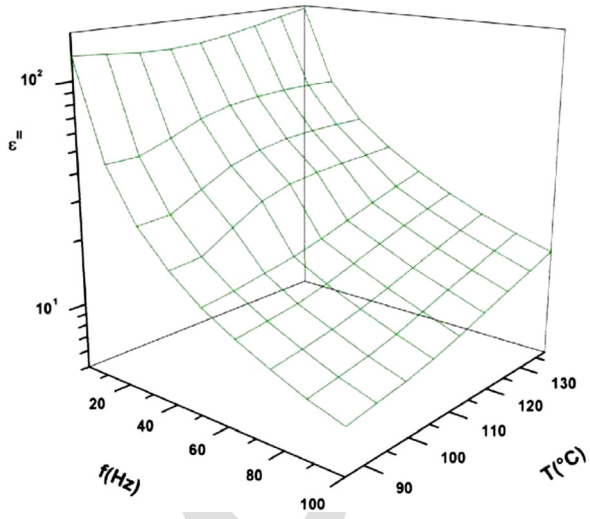

FIG. 12. Imaginary part of complex permittivity in function of frequency and temperature in cooling conditions.

TABLE III. Fitting parameters for the second relaxation process (HN2) of ODA-9 at different temperatures in heating and cooling conditions.

T (°C)	f_r (Hz)	$\Delta\varepsilon$	a	b	f_r _err	$\Delta\varepsilon$ _err	a_err	b_err
86.1	0.86	0.11×10^2	0.93	0.93	1.84	0.15×10^2	0.20	0.18
93.9	2.76	0.40×10^2	1.00	1.00	1.09	0.46×10^1	0.00	0.00
98.8	2.36	0.47×10^2	1.00	1.00	1.09	0.56×10^1	0.00	0.00
103.0	3.11	0.47×10^2	1.00	1.00	1.09	0.47×10^1	0.00	0.00
154.8	2.41	0.17×10^3	0.96	1.00	1.12	0.44×10^2	0.09	0.00
137.9	3.90	0.11×10^3	1.00	1.00	1.12	0.15×10^2	0.00	0.00
103.0	6.68	0.92×10^2	0.95	1.00	1.10	0.16×10^2	0.01	0.00
93.9	5.15	0.89×10^2	0.98	1.00	1.11	0.15×10^2	0.02	0.00
86.1	4.76	0.61×10^2	1.00	1.00	1.06	0.50×10^1	0.00	0.00

TABLE IV. Fitting parameters for the third relaxation process (HN3) of ODA-9 at different temperatures in heating and cooling conditions.

T (°C)	f_r (Hz)	$\Delta\varepsilon$	a	b	f_r_err	$\Delta\varepsilon$_err	a_err	b_err
93.9	17.95	10.62	1.00	1.00	1.07	0.96	0.00	0.00
98.8	14.89	13.35	1.00	1.00	1.06	1.20	0.00	0.00
103.0	17.27	12.85	1.00	1.00	1.08	1.42	0.00	0.00
154.8	18.51	39.49	1.00	1.00	1.11	9.51	0.00	0.00
137.9	19.57	38.87	1.00	1.00	1.08	4.54	0.00	0.00

TABLE V. Fitting parameters for the fourth relaxation process (HN4) of ODA-9 at different temperatures in heating and cooling conditions.

T (°C)	f_r (Hz)	$\Delta\varepsilon$	a	b	f_r_err	$\Delta\varepsilon$_err	a_err	b_err
86.1	6.75×10^4	1.85	0.92	1.00	1.04	0.04	0.01	0.00
93.9	1.68×10^4	5.61	0.99	0.99	1.04	0.03	0.01	0.04
98.8	1.82×10^4	5.30	0.99	1.00	1.01	0.03	0.01	0.00
103.0	1.91×10^4	5.12	0.99	1.00	1.01	0.03	0.01	0.00
154.8	2.28×10^4	4.30	0.98	1.00	1.02	0.08	0.01	0.00
137.9	2.18×10^4	4.79	0.95	1.00	1.01	0.05	0.01	0.00
103.0	2.09×10^4	5.05	0.96	1.00	1.01	0.06	0.01	0.00
93.9	2.03×10^4	5.22	0.99	1.00	1.01	0.07	0.01	0.00
86.1	1.73×10^4	6.22	0.97	1.00	1.01	0.04	0.01	0.00

TABLE VI. Fitting parameters for DC conductivity of E7 at T = 27.0 °C.

σ (S/cm)		n			σ_err			n_err
1.75		0.66			0.53			0.38
HN_mode	f_r (Hz)	$\Delta\varepsilon$	a	b	f_r_err	$\Delta\varepsilon$_err	a_err	b_err
1	0.19	0.90×10^{2}	0.81	1.00	1.62	0.90×10^{2}	0.26	0.00
2	1.30	0.92×10^{2}	0.86	1.00	1.38	0.58×10^{2}	0.05	0.00
3	2.61×10^{4}	0.44×10^{1}	0.98	1.00	1.02	0.07	0.01	0.00

IV. CONCLUSIONS

The relaxation behavior of dielectric permittivity has been determined with some basic physical parameters in the frequency range from 10 MHz to 100 kHz and during the different phases of a bent-core liquid crystalline material. Dielectric spectra emerge the presence of four distinct modes during heating conditions that are unusual for this kind of liquid crystals, and the third mode (HN3), a Debye type response, could indicate the formation of temporary polarized clusters even in fluid phases. The large permittivity at low frequencies is also unusual for this kind of liquid crystals and could be seen as another proof of the presence of cybotactic clusters. Other measurements, like reversal current method or XRD could be carried out to verify the presence of polar clusters with ferroelectric or antiferroelectric properties.

[1]T. Niori, T. Sekine, J. Watanabe, T. Furukawa, and H. Takezoe, J. Mater. Chem. **6**(7), 1231–1233 (1996).
[2]T. Sekine, T. Niori, M. Sone, J. Watanabe, S. W. Choi, Y. Takanishi, and H. Takezoe, Jpn. J. Appl. Phys., Part I **36**, 6455 (1997).
[3]D. R. Link, G. Natale, R. Shao, J. E. Maclennan, N. A. Clark, E. Körblova, and D. M. Walba, Science **278**, 1924–1927 (1997).
[4]H. R. Brand, P. E. Cladis, and H. Pleiner, Eur. Phys. J. B **6**, 347–352 (1998).
[5]T. C. Lubensky and L. Radzihovsky, Phys. Rev. E **66**, 031704 (2002).
[6]L. Radzihovsky and T. C. Lubensky, Europhys. Lett. **54**, 206–212 (2001).
[7]H. R. Brand, H. Pleiner, and P. E. Cladis, Eur. Phys. J. E **7**, 163–166 (2002).
[8]O. Francescangeli, V. Stanic, S. I. Torgova, A. Strigazzi, N. Scaramuzza, C. Ferrero, I. P. Dolbnya, T. M. Weiss, R. Berardi, L. Muccioli, S. Orlandi, and C. Zannoni, Adv. Funct. Mater. **19**, 2592–2600 (2009).
[9]J. Harden, B. Mbanga, N. Éber, K. Fodor-Csorba, S. Sprunt, J. T. Gleeson, and A. Jákli, Phys. Rev. Lett. **97**, 157802 (2006).
[10]D. B. Wiant, J. T. Gleeson, N. Éber, K. Fodor-Csorba, A. Jákli, and T. Tóth-Katona, Phys. Rev. E **72**, 041712 (2005).
[11]S. Tanaka, H. Takezoe, N. Éber, K. Fodor-Csorba, A. Vajda, and Á. Buka, Phys. Rev. E **80**, 021702 (2009).
[12]P. Tadapatri, U. S. Hiremath, C. V. Yelamaggad, and K. S. Krishnamurthy, J. Phys. Chem. B **114**, 10 (2010).
[13]M. Majumdar, K. Neupane, J. T. Gleeson, A. Jakli, and S. Sprunt, "Flexoelectric effect in a bent-core liquid crystal measured by dynamic light scattering," in *APS March meeting, New Orleans*, 2008, Abstract No. W8.00006.
[14]D. B. Wiant, J. T. Gleeson, N. Éber, K. Fodor-Csorba, A. Jákli, and T. Tóth-Katona, Phys. Rev. E **72**, 041712 (2005).
[15]D. Wiant, S. Stojadinovic, K. Neupane, S. Sharma, K. Fodor-Csorba, A. Jákli, J. T. Gleeson, and S. Sprunt, Phys. Rev. E **73**, 030703 (R) (2006).
[16]J. Harden, B. Mbanga, N. Éber, K. Fodor-Csorba, S. Sprunt, J. T. Gleeson, and A. Jákli, Phys. Rev. Lett. **97**, 157802 (2006).
[17]A. Jákli, M. Chambers, J. Harden, M. Majumbar, R. Teeling, J. Kim, Q. Li, G. G. Nair, N. Éber, K. Fodor-Csorba, J. T. Gleeson, and S. Sprunt, Proc. SPIE **6911**, 691105 (2008).
[18]V. Domenici, C. A. Veracini, and B. Zalar, Soft Matter **1**, 408 (2005).
[19]G. Cinacchi and V. Domenici, Phys. Rev. E **74**, 030701 (2006).
[20]S. Havriliak and S. Negami, Polymer **8**, 101 (1967).
[21]D. W. Davidson and R. H. Cole, J. Chem. Phys. **19**, 1484–1490 (1951).
[22]K. S. Cole and R. H. Cole, J. Chem. Phys **9**, 341–351 (1941).
[23]Y. Feldman, A. Puzenko, and Y. Ryabov, *Fractals, Diffusion, and Relaxation in Disordered Complex Systems: A Special Volume of Advances in Chemical Physics* (John Wiley & Sons, Inc., Hoboken, 2006), Vol. 133.
[24]F. Kremer and A. Schonhals, *Broadband Dielectric Spectroscopy* (Springer-Verlag, Berlin, 2003).
[25]G. P. Sinha and F. M. Aliev, Phys. Rev. E **58**, 2001 (1998).
[26]T. Salfetnikova, G. Zhuchkova, C. Dantlgraber, C. Tschierske, and H. Kresse, Liq. Cryst. **29**, 155–158 (2002).
[27]H. Schlacken, P. Schiller, and H. Kresse, Liq. Cryst. **28**, 1235 (2001).
[28]F. Kremer, S. U. Vallerien, and R. Zentel, Adv. Mater. **2**, 145 (1990).

CONTRIBUTIONS TO INTERNATIONAL SCHOOLS AND CONFERENCES

International School of Liquid Crystals
18th Course

"Liquid crystal nanostructures and self-assembling: from organic electronics to metamaterials"

2nd School of the Italian Liquid Crystal Society

***E. Majorana* Centre for Scientific Culture, Erice (Italy)**
Erice, 3 -10 July 2011

Lecturers

P. Barois (France)
V. Domenici (Italy)
B. Donnio (France)
J. Emsley (UK)
D. Evans (USA)
D. Finotello (USA)
A. Golemme (Italy)
R. Kamien (USA)
I-C. Khoo (USA)
G. Mehl (UK)
M. O'Neill (UK)
G. Strangi (Italy)
E. Virga (Italy)
C. Zannoni (Italy)
S. Žumer (Slovenia)

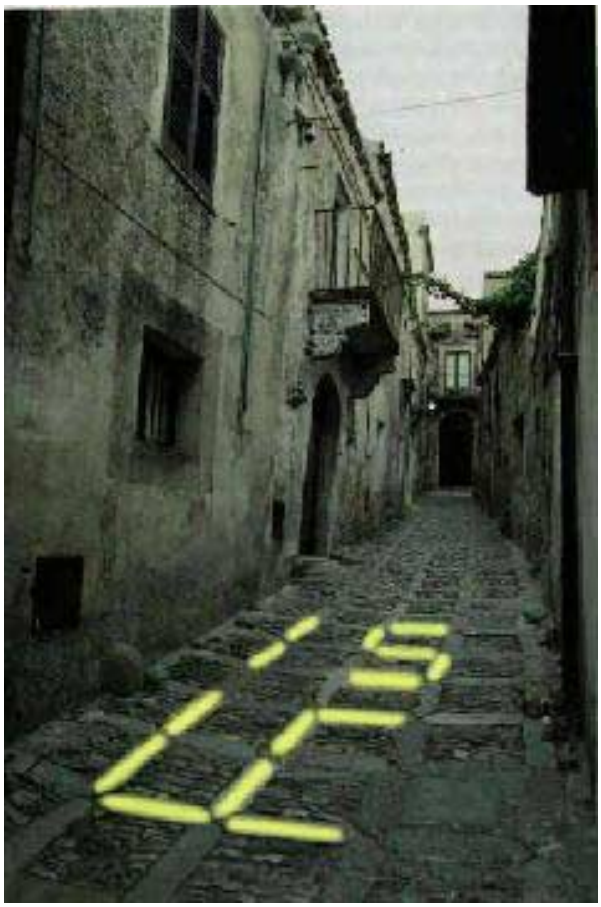

Scientific committee

G. Assanto
A. d'Alessandro
G. De Luca
P. Pasini
G. Strangi
E. Virga
C. Zannoni

Directors of the Course:
A.d'Alessandro, P. Pasini, C. Zannoni

Director of the School:
C. Zannoni

Dielectric characterisation of a ferroelectric and antiferroelectric liquid crystal

***L. Marino*, E. Bruno, M. P. De Santo and N. Scaramuzza**

IPCF-CNR UOS Cosenza c/o Physics Department, University of Calabria 87036 Arcavacata di Rende (CS) Italy

Liquid crystals exhibiting both a ferroelectric and an antiferroelectric phase are interesting for a great number of applications in electro-optical devices. In particular, for their fast response time they can be employed in visual display applications [1].
We present our recent investigations on the electric properties of W129, an orthoconic smectic liquid crystal which presents both ferroelectric and antiferroelectric smectic C phases. In particular, W129 is a very interesting material since it is able to exhibit an high spontaneous polarization (> 300 nC/cm^2 at room temperature) in virtue of its tilted chiral structure. This liquid crystal has been synthesised by professor Dabrowski at the Military University of Technology, Warsaw, Poland.
In the present study, dielectric relaxation of W129 has been studied as a function of the frequency of an applied electric field through Dielectric Spectroscopy technique. For this purpose the Cole-Cole function [2] has been used to determine the distribution parameter, the dielectric strength and the relaxation frequency as a function of temperature.
Finally, we present a first attempt to study the morphological and ferroelectric properties of a thin layer of W129 deposited on ITO using Atomic Force Microscopy techniques.

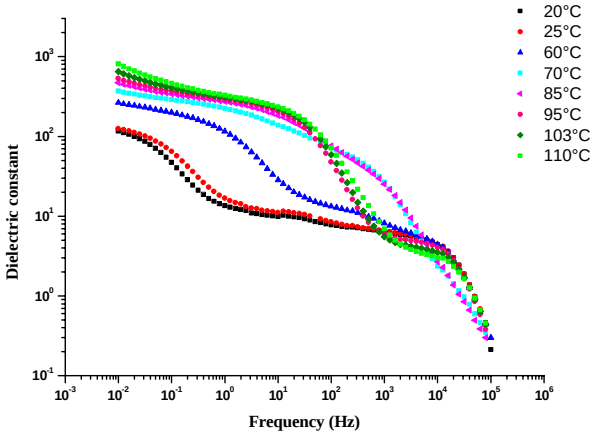

Frequency dependence of the real part of the dielectric constant at different fixed temperatures.

References

[1] Koen D'havé, PhD Thesis, University of Gent, Belgium, "Application of Antiferroelectric Liquid Crystals with High Tilt", 2002.
[2] Cole K. S. and Cole R. H., J. Chem. Phys. **9**, 341 (1941).

Broadband Dielectric Spectroscopy and its Applications

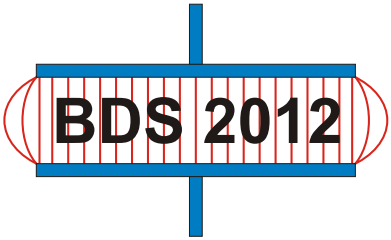

Leipzig - 2012
3rd- 7th September

UNIVERSITÄT LEIPZIG

The conference is a joint meeting of the 7th “Conference of the International Dielectric Society” and the 13th “Conference on Dielectric & Related Phenomena”.

18: Dielectric characterization of gold nanoparticles / antiferroelectric liquid crystal composites

L. Marino[1,2], E. Bruno[1,2], S. Marino[2], A.Th. Ionescu[3] and N. Scaramuzza[1,2]

[1] *Department of Physics, University of Calabria, Via P. Bucci, CUBO 33B, 87036 Rende (CS), Italy*
[2] *IPCF-CNR UOS Cosenza c/o Department of Physics, University of Calabria, Rende (CS), Italy*
[3] *Faculty of Physics, University of Bucharest, Magurele, P.O. Box MG-11, R-76900, Bucharest, Romania*
Poster M: Mon 18:00, Chem

By its very nature, nanotechnology is of immense academic and industrial interest as it involves the creation and exploitation of materials with structural features in between those of atoms and bulk materials, with at least one dimension limited to between 1 and 100 nm. Most importantly, the properties of materials with nanometric dimensions are, in most instances, significantly different from those of atoms or bulk materials. An important subset of nano-structured materials is represented by the so-called nano-composites which consist of nano-particles dispersed in a continuous three-dimensional matrix. In this context the nano-composites obtained by dispersing metallic nano-particles in liquid crystal materials are of particular interest. Liquid crystals by their very nature are suitable candidates for matrix-guided synthesis and self-assembly of nanoscale materials [1]. Since liquid crystals are anisotropic materials they provide an excellent support for self assembling of nano-particles into larger ordered superstructures. Moreover, as the liquid crystals responds to small external forces (electric, magnetic, mechanical stress), dispersed nano-particles can be forced to follow the molecular order of the hosting medium effectively controlling the order of the superstructure. Interesting results has been obtained by dispersing ferroelectric nano-particles [2] in nematic liquid crystals (NLCs). Low concentration of such nano-particles increase the orientational order of the hosting NLCs, the nematic-isotropic transition temperature and decrease the Frederiks transition threshold voltage. We present our recent investigations on the electric properties of W-129, an orthoconic smectic liquid crystal mixture, and on the same liquid crystal mixture doped with gold nanoparticles. W-129 presents both ferroelectric and antiferroelectric smectic C phases and an high spontaneous polarization (> 300 nC/ cm^2 at room temperature) in virtue of its tilted chiral structure. The gold nanoparticles are functionalised with a polymer which presents both hydrophilic and hydrophobic properties in dependence of temperature. In the present study, dielectric relaxation of W-129 and W-129 doped with gold nanoparticles has been studied in a planar aligned cell as a function of the frequency of an applied electric field and as a function of temperature through Dielectric Spectroscopy technique. For this purpose the Havriliak-Negami function [3] has been used to determine the distribution parameters, the dielectric strengths and the relaxation frequencies as a function of temperature. In addition to that, we present a first attempt to study the morphological and ferroelectric properties of a thin layer

of W-129 and W-129 doped with gold nanoparticles deposited on ITO using Atomic Force Microscopy techniques. The differences found in the dielectric spectra are evidence of the influence of gold nanoparticles. They represent an interesting result from the theoretical and experimental point of view. These results are relevant for fundamental nano-science because they show how nano-sized particles can be coupled with the orientational order of macroscopic systems. Of course potential applications are envisioned in the field of soft nanotechnology and optical materials.

[1] T. Hegmann, H. Qi and V. M. Marx, Journal of Inorganic and Organometallic Polymers and Materials,2007, 17, 3, 483-508.

[2] L. M. Lopatina, J. V. Selinger, Physical review letters, 2009, 102(19),197802.

[3] S. Havriliak, and S. Negami, Polymer, 1967, 8, 101.